Mechanistic Contributions of the p10 FAST Protein Ectodomains to Membrane Fusion and Syncytiogenesis

by

Timothy Key

Submitted in partial fulfilment of the requirements
for the degree of Doctor of Philosophy

at

Dalhousie University
Halifax, Nova Scotia
December 2013

TABLE OF CONTENTS

LIST OF FIGURES

ABSTRACT

The homologous p10 fusion-associated small transmembrane (FAST) proteins of the fusogenic avian (ARV) and Nelson Bay (NBV) reoviruses are the smallest known proteins capable of mediating syncytiogenesis. Their extremely small size precludes them from following the paradigmatic membrane fusion pathway proposed for enveloped viral fusion proteins. I exploited the sequence conservation/divergence and differential syncytiogenic rates between ARV and NBV to define functional motifs in the p10 ectodomains. Using chimeric p10 constructs, I determined the 40-residue ectodomain (sizes refer to ARV) comprises two distinct functional motifs essential for syncytiogenesis. Cellular syncytiogenic and surface biotinylation assays identified an indivisible, 25-residue, N-terminal ectodomain motif required for cystine loop fusion peptide formation. I further determined the roles of this cystine loop in promoting lipid binding and cholesterol-dependent lipid destabilization. Immunofluorescence staining, FRET analysis and cholesterol depletion/repletion studies identified a second motif comprising the 13 membrane-proximal ectodomain residues (MPER). This motif governs the reversible, cholesterol-dependent assembly of p10 multimers in the plasma membrane. I demonstrate that ARV and NBV homomultimers segregate to separate foci in the plasma membrane, and the four juxtamembrane residues present in the multimerization motif dictate species-specific homomultimerization. I also discovered the novel codependency of p10 multimerization and cholesterol-dependent microdomain localization. The majority of enveloped virus membrane fusion proteins function as stable multimers, which nonetheless must undergo dramatic, irreversible, tertiary structure rearrangements to mediate membrane fusion. Cholesterol-rich membrane microdomains have also been implicated in the function of several enveloped virus fusion proteins, and a limited number of studies have investigated the role of cholesterol in multimerization. My results reveal cholesterol-dependent p10 homomultimerization is an essential aspect of p10-mediated syncytium formation, and I identify the motifs responsible for this process. The reversible nature of p10 cholesterol-dependent multimerization at the plasma membrane is in line with several other studies suggesting that the dynamic clustering and dispersion of cholesterol microdomains, as well as protein transitioning from multimeric to monomeric intermediates, are essential phenomena of protein mediated membrane fusion.

LIST OF ABBREVIATIONS AND SYMBOLS USED

ARV	avian reovirus
ASLV	avian sarcoma/leukosis virus
BPB	bromophenol blue
BroV	Broome reovirus
BRV	baboon reovirus
CCD	charge coupled device
CD	circular dichroism
CH	cholesterol
CM	conserved motif
CRAC	cholesterol recognition amino acid consensus
DAG	diacylglycerol
DMSO	dimethylsulfoxide
DPC	dodecylphosphocholine
DRM	detergent resistant membrane
DTT	dithiothreitol
EDTA	ethylenediaminetetraacetic acid
EFF	epitheilial fusion failure
EGFP	enhanced green fluorescent protein
EM	electron microscopy
ER	endoplasmic reticulum
FACS	fluorescence activated cell sorting
FAST	fusion associated small transmembrane
FBS	fetal bovine serum
FF	fusion failure
FP	fusion peptide
FRET	fluorescence resonance energy transfer
gB	glycoprotein B
HA	hemagglutinin
HBSS	Hank’s balanced salt solution

HCl	hydrochloric acid
hET	human endothelin
HFIP	hexafluoro-2-propanol
HII	hexagonal II
HIV	human immunodeficiency virus
HP	hydrophobic patch
hpt	hours post transfection
HSV	herpes simplex virus
Ld	liquid disordered
Lo	liquid ordered
LPC	lysophosphatidylcholine
LUV	large unilamellar vesicle
MAS	magic angle spinning
mNFRET	mean NFRET
MPER	membrane proximal ectodomain region
MβCD	methyl-ß-cyclodextrin
NaCl	sodium chloride
NaDOC	sodium deoxycholate
NaF	sodium fluoride
NBD-DOPE	1,2-dioleoyl-sn- glycero-3-phosphoethanolamine-N-(7-nitro-2-1,3- benzoxadiazol-4-yl)
NBV	Nelson Bay reovirus
NFRET	normalized FRET
NMR	nuclear magnetic resonance
NOESY	nuclear Overhauser effect spectroscopy
NSF	N-ethylmaleimide-sensitive factor
OA	oleic acid
OD	optical density
PA	phosphatidic acid
PB	polybasic
PBS	phosphate-buffered saline
PC	phosphatidylcholine
PE	phosphatidylethanolamine

PEG	polyethylene glycol
PRV	pteropine reoviruses
PS	phosphatidylserine
PSB	protein sample buffer
PtdIns	phosphatidylinositol
PVDF	polyvinylidene difluoride
Rho-DOPE	1,2- dioleoyl-sn-glycero-3-phosphoethanolamine-N-4-(lissamine rhodamine B sulfonyl)
RIPA	radio-immunoprecipitation assay
RRV	reptilian reovirus
RSV	respiratory syncytial virus
SBT	spectral bleed-through
SDS	sodium dodecyl sulfate
SDS-PAGE	sodium dodecyl sulphate-polyacrylamide gel electrophoresis
SFV	Semliki forest virus
SM	sphingomylein
SNARE	soluble N-ethylmaleimide-sensitive factor attachment protein receptor
TBEV	tick-borne encephalitis virus
TBS-T	Tris-buffered saline with Tween-20
TMD	transmembrane domain
TOCSY	total correlation spectroscopy
TRAP	tartrate-resistant acid phosphatase
VAMP	vesicle-associated membrane protein
VSV	vesicular stomatitis virus
$\Delta\delta$	secondary chemical shifts
θ	mean residue ellipticity
λ	wavelength

CHAPTER 1

Introduction

1.1 Overview

After the evolution of self-replicating organic molecules, an essential development in the advancement of life was the spatial organization of these molecules by lipidic membranes. The formation of such membranes provided two main advantages: i) various genetic constituents could be kept in close proximity, and ii) the internal environment could be different from the external environment. Membranes have since evolved to become intricate three-dimensional structures, which spatially and temporally regulate essential cellular functions. However, the benefits of cellular compartmentalization would all be for naught if it were not for the ability to selectively merge membrane compartments. The importance of biological membrane fusion is illustrated by the diversity of membrane fusion events, including fusion of intracellular components during protein trafficking, vesicle fusion during endo- and exocytosis (Ungermann and Lanosch, 2005), cell-cell fusion during fertilization, placenta formation (Benirschke, 2003), muscle development (Taylor, 2002), and bone maintenance (Vignery, 2005), as well as enveloped viral infections (Earp et al., 2004). The merger of two membranes is an energetically unfavorable process (Kozlovsky and Kozlov, 2002; Malinin and Lentz, 2004), which prevents spontaneous incidences. Consequently, specific membrane fusion proteins are employed to overcome these large thermodynamic barriers. Although specific membrane fusion proteins are employed to mediate each of the processes noted above, those involved in cellular fusion events have remained elusive. Our current understanding of membrane fusion is modeled from studies on the soluble N-ethylmaleimide-sensitive factor attachment protein receptor (SNARE) vesicle fusion proteins and enveloped viral fusion proteins (Rothman, 1994; Sapir et al., 2008; White et al., 2008). The only proteins identified as dedicated cell-cell fusogens are the reovirus fusion associated small transmembrane (FAST) proteins encoded by non-enveloped reoviruses (Duncan, 1999; Duncan et al., 1996; Duncan et al., 2004; Duncan et

al., 1995; Shmulevitz, 2000), the fusion failure (FF) proteins from nematodes (Kontani and Rothman, 2005), and the syncytin proteins found in the syncytiotrophoblast (Huppertz and Borges, 2008).

The FAST proteins exist exclusively to fuse virus-infected cells to neighboring uninfected cells. These proteins are able to delegate elements of the fusion reaction to cellular co-factors involved in pre-fusion events, such as close membrane apposition (Salsman et al., 2008a), and possibly post-fusion events, such as pore expansion, retaining within their rudimentary structures what is required for membrane deformation, lipid mixing, and pore formation. While certain similarities exist between the FAST proteins and other fusogens (as discussed below), they do not structurally or functionally resemble any previously identified membrane fusion protein, and therefore are likely to induce membrane merger through a novel, unidentified mechanism. An understanding of the fusion reaction elements influenced or mediated by the FAST proteins would provide considerable insight into the minimal requirements for protein mediated cell-cell fusion, while potentially providing a framework for the identification of cell-encoded fusogens. This thesis describes novel research providing mechanistic insights into the membrane fusion and syncytiogenic activity of the smallest known membrane fusion proteins: the homologous 10 kDa (p10) FAST proteins of the avian (ARV) and Nelson Bay (NBV) reoviruses.

The first chapter introduces membrane fusion and provides rationales for the study of membrane fusion during viral infections. The initial sections introduce the main themes of membrane fusion, including the predominant membrane components, steps of a membrane fusion reaction, and membrane parameters that influence native fusogenicity. The following sections describe proteins known to induce membrane fusion, including descriptions of functional motifs and proposed mechanisms. The final section provides an overview of the FAST proteins, including what was known about them prior to this study.

1.2 Biological Membranes

1.2.1 Components

Biological membranes are complex mixtures of various proteins and lipids. Lipids are naturally occurring, amphipathic molecules consisting of hydrophilic head groups and one or more hydrophobic fatty acid tails. Under aqueous conditions, the amphipathic nature of these molecules favors self-assembly into lipid bilayers, with the hydrophilic head groups aligned towards the aqueous medium, sequestering the hydrophobic tails from the external hydrophilic environment. Membranes in this state are said to be in the lamellar phase. While several forces contribute to the formation of lipid bilayers, such as Van der Waals, electrostatic, hydrogen bonding, and noncovalent interactions, the main driving forces are from hydrophobic interactions.

Generally, eukaryotic membranes consist of three major lipid classes: phospholipids, sphingolipids and sterols. Phospholipids are the major component of biological membranes. In higher plants and animals, the diglyceride tails are predominantly 16 or 18 carbon atoms (i.e. palmitic, oleic, linoleic acids) and vary in their levels of saturation (Weinstein, 1968). The nomenclature of the most common phospholipid species reflects the nature of their hydrophilic head group. Such species include phosphatidylcholine (PC), phosphatidylserine (PS), phosphatidylethanolamine (PE), phosphatidylinositol (PtdIns), diacylglycerol (DAG), and phosphatidic acid (PA) (Weinstein, 1968). Sphingolipids, another major lipid component, are derivatives of sphingosine and dihydrophingosine (and their homologs). They consist of fatty acid chains connected to various head groups, such as phosphocholine or phosphoethanolamine, through their sphingosine groups. The most common sphingolipid in eukaryotic cells is sphingomylein (SM) (Voet and Voet, 2004b). Sterols are the third major lipid component of biological membranes. Cholesterol (CH) is the most abundant sterol in animal plasma membranes (25-40%), however it is present in lesser amounts in intracellular membranes (Meer et al., 2008). CH consists of a bulky steroid structure of four linked hydrocarbon rings with a hydrocarbon tail at one end and a small hydroxyl head group on the other.

1.2.2 Properties of Membranes

The lipid compositions of biological membranes are quite complex and vary across cellular locations. In many biological membranes, lipids are asymmetrically distributed between the inner and outer leaflets. The inner leaflets are commonly composed of lipids such as PE, PS, and several forms of PtdIns, while the outer leaflets contain primarily PC, SM and various glycolipids (Bretscher, 1972). CH is unique in that it has a propensity to migrate between the inner and outer leaflets of a biological membrane. This allows it to establish an equilibrium, with approximately 50% of the total CH in each membrane leaflet (Muller and Herrmann, 2002; Steck et al., 2002). While the biological functions of asymmetrically distributed lipids are widely unknown, it is clear that the cell can exploit this feature. For example, inner leaflet-localized PS is transferred to the outer leaflet during apoptosis, where it can be recognized by macrophages and recycled (Fadok et al., 1992). The overall spherical shape of a cell requires net positive curvature in the outer leaflet and net negative curvature in the inner leaflet. The asymmetric distribution of lipids may be a necessary consequence of the three-dimensional structures of the lipid molecules in each membrane. The relative cross sectional area between head groups and hydrocarbon tails can induce a natural, spontaneous curvature in the membrane (Figure 1.1A). For example, inner leaflet-localized PE has a relatively higher head group-tail ratio, resulting in a cone-shaped molecular structure that imparts negative spontaneous curvature in membranes (Chernomordik, 1996).

Different lipid compositions can have dramatic effects on membrane functions by influencing membrane elasticity, flexibility and fluidity through influencing the long-range order and phase behavior of membranes (Campelo et al., 2008; Haque et al., 2001; Kasson and Pande, 2007; Kozlov et al., 2010). The main determinant of membrane phase behavior is the strength of Van der Waals interactions between adjacent lipid molecules. For example, the hydroxyl group of CH can form hydrogen bonds with nearby carbonyl oxygens of phospholipid and sphingolipid head groups, while the hydrocarbon tail situates in the hydrophobic core of the membrane. These interactions increase lipid packing, which adds rigidity, reduces permeability and restricts the lateral motions of

membranes (Ohvo-Rekila et al., 2002). Additionally, the length of hydrocarbon tails on phospholipid and sphingolipid species can affect their lipid packing, with longer tails allowing for more densely packed lipids, resulting in decreased membrane fluidity. Conversely, the presence of unsaturated hydrocarbon tails on these lipid species increases the overall membrane fluidity by interfering with interactions between neighboring tail groups (Szule et al., 2002).

While the hydrocarbon tails of lipids predominantly determine the phase behavior of membranes, the lipid head groups determine the bilayer surface chemistry. The most common lipid species, PC, has a positive charge on its amine group and a negative charge on its phosphate group, making it zwitterionic. Other lipid head groups, such as PA and PS, have a net negative charge. The surface charge density of a membrane has important implications for electrostatic interactions occurring on the membrane surface, which directly influences membrane function (Dickey and Faller, 2008).

1.2.3 Membrane Microdomains

In the 1970s, Singer and Nicholson proposed a concept for membrane structure called the fluid mosaic model (Singer and Nicolson, 1972). In this model, the membrane bilayer is viewed as a two-dimensional liquid that permits the free lateral diffusion of lipids and proteins. While this model still has merit, more recent observations have found that membranes can exist in several states, including liquid-disordered (L_d), liquid-ordered (L_o) and gel states. The majority of the plasma membrane, which contains hydrocarbon tails in an unsaturated state, exists in the L_d state (London, 2005), which is akin to the two-dimensional liquid proposed in the fluid mosaic model. The L_o state consists of phospholipids with saturated acyl chains, such as SM and other glycosphingolipids, and is relatively more rigid and less permeable than the L_d state (Almeida et al., 2005). In the gel state, lipids are semi-frozen. This state is only observed at low temperatures and will be omitted from further discussion.

The complex lipid compositions of biological membranes can lead to both L_d and L_o states coexisting in laterally segregated microdomains, which have been termed “lipid rafts”. Early descriptions of lipid rafts identified a strict requirement for CH and

sphingolipids for formation, and noted an inherent ability to resist solubilization by non-ionic detergents (Brown and Rose, 1992). The initial lipid raft proposal hypothesized that they were stable lipid structures of between 100 and 500 nm in diameter. However, more recent studies have observed quite the opposite; the consensus definition of lipid rafts, as developed at the 2006 Keystone Symposium of Lipid Rafts and Cell Function, is that they are transient, sterol- and sphingolipid-enriched domains of between 10 and 200 nm in diameter (Pike, 2006, 2009). This definition remains highly controversial due predominantly to difficulties in studying lipid rafts in living cells, which do not exist in thermodynamic equilibrium (Allen et al., 2006). Lipid rafts have proven very difficult to directly visualize because the proposed lipid raft diameter sits below the diffraction limit of light microscopes. For years, the most common method of determining the presence of rafts was their resistance to solubilization by cold, non-ionic detergents, such as Triton X-100 (Brown and Rose, 1992). During this process, most lipid-lipid interactions are disrupted, but a small fraction can be isolated as detergent resistant membranes (DRMs), which can be separated by sucrose density gradient fractionation. These DRMs were thought to arise specifically from the relatively tight packing of lipids in rafts (London and Brown, 2000; Schroeder et al., 1994). However, this technique has since been shown to be far from ideal; the isolation of DRMs depends on the type of detergent used (Triton X-100, lubrol, etc.), the ratio of detergent to lipid, as well as the cell type used. Additionally, the use of detergents can generate their own domains, cause mixing of domains and solubilize other L_o domains (Heerklotz, 2002; Heerklotz et al., 2003; Lichtenberg et al., 2005).

In the study of DRM-associated proteins, the distribution of membrane components in DRMs fractions is ambiguous, and the absence of a protein from DRM fractions does not necessarily indicate an absence from rafts in living cells. For example, epidermal growth factor is found in a subset raft domains by subcellular fractionation (Mineo et al., 1996), but is not detectable in Triton X-100 DRM fractions (Pike et al., 2002). The *in vivo* manipulation of membrane CH levels through sequestration, depletion/removal, and inhibition of synthesis are currently the most widely employed techniques to study lipid rafts and lipid raft-associated proteins (Zidovetzki and Levitan, 2007).

1.3. Biological Membrane Fusion

The extensive subdivision of eukaryotic cells by membranes necessitates mechanisms by which lipid bilayers can be selectively fused. Early studies on the mechanisms of membrane fusion created conflicts over what actually constituted fusion. Such conflicts primarily arose due to the methodologies employed to promote membrane fusion in these studies; calcium (and other divalent cations), detergents and bilayer phase transitions (Papahadjopoulos et al., 1976a; Papahadjopoulos et al., 1976b). While promoting fusion, these techniques also induced significant levels of content leakage. In this thesis, membrane fusion is defined as the process by which two individual lipid bilayers merge both the outer and inner membrane leaflets to form a continuous structure, allowing mixing between previously separated aqueous contents. The study of membrane fusion in diverse systems has identified a common pathway of membrane merger, progressing from close membrane apposition, to outer leaflet mixing and hemifusion stalk formation, then inner leaflet mixing and fusion pore formation, and finally fusion pore stabilization and expansion (Figure 1.1B) (Basanez, 2002; Cohen and Melikyan, 2004; Sollner, 2004). This process is energetically unfavorable, and requires the use of specific membrane fusion proteins to overcome the large, thermodynamic barriers imposed at various stages. The following subsections will describe a common pathway of membrane merger in terms of membrane rearrangements and energy requirements. The influence of proteins on this process will be discussed in subsequent sections.

1.3.1. Apposition

The first step of a membrane fusion reaction occurs prior to any membrane remodeling. The outer leaflets of two membranes destined to undergo fusion must be brought into close apposition. While cellular adhesion proteins, such as cadherins or nectins can bring two cells within 28 to 38 nm of one another (Irie et al., 2004; Koch et al., 2004; Leckband and Sivasankar, 2000; Zhu et al., 2003), cells must approach within 2 to 3 nm prior to fusion. To accomplish this, the adherent proteins are first removed from the intermembrane space (Martens and McMahon, 2008). However, at these short

separation distances, repulsive "hydration forces" dominate (Chernomordik and Kozlov, 2003; Leikin et al., 1993). Several processes have been proposed to overcome this force: 1) one or both of the apposed membranes are deformed into point-like protrusions, which minimize the contact area and the accompanying repulsive hydration force (Chernomordik and Kozlov, 2003, 2008); 2) larger-scale membrane bending, which creates a highly fusogenic "dimple" that overcomes the repulsive hydration force by inducing localized membrane curvature in the outer leaflet, making fusion a more energetically favorable process by reducing the energy barrier (Chernomordik and Kozlov, 2003; Kozlov and Chernomordik, 1998; Martens and McMahon, 2008); Such curvature has been experimentally observed in both cells and synthetic liposome systems (Frolov et al., 2000; Kanaseki et al., 1997; Martens et al., 2007; Vaidya et al., 2007); and 3) reduction of the free energy of hydrophobic interstices by volume exclusion-induced aggregation and membrane dehydration, such as is observed for polyethylene glycol (PEG)-mediated fusion (Arnold et al., 1985; Arnold et al., 1990; Lentz, 2007).

1.3.2. Hemifusion

Merger of the proximal outer leaflets of two closely apposed membranes results in the formation of a hemifusion stalk structure. This hourglass structure requires sufficient negative curvature in the outer leaflets to reduce the energy costs for formation (Kozlovsky and Kozlov, 2002; Kuzmin et al., 2001b; Markin and Albanesi, 2002). The necessity for this curvature has been determined both experimentally and mathematically. In the experimental observations, it was found that the presence of negative curvature-inducing lipids in membranes, such as oleic acid (OA) and PE, was able to enhance hemifusion stalk formation, while positive curvature-inducing lipids, such as lysophosphatidylcholine (LPC), dramatically inhibited formation (Chernomordik et al., 1998; Chernomordik and Kozlov, 2003; Fuller and Rand, 2001; Russell et al., 2001). The mathematical calculations were based on the elastic free energy of curved monolayers, and their preference for downstream progression along the fusion pathway versus abortion of the fusion process and regression to separate bilayers (Katsov et al., 2004; Markin et al., 1984). However, the mathematical models encountered a significant difficulty; the amount of curvature required to store enough elastic free energy to

favorably progress the fusion reaction was so high that it would theoretically create void spaces between the hydrocarbon tails in the area of curvature, resulting in astronomically high activation energies to induce such curvature (Siegel, 1993). Attempts to resolve this problem led to the inclusion of hydrocarbon tail tilt and splay into calculations in an attempt to reduce activation energies (Kozlovsky and Kozlov, 2002; Kuzmin et al., 2001b; Markin and Albanesi, 2002). However, the underlying basis of such mathematical models involves physical discontinuities. Additionally, these elastic models assume that the membrane maintains a high degree of order during the structural transitions that result in hemifusion. It is possible that this entire step is substantially more disordered, and small perturbations of the bilayer that induce local fluctuations in the hydrophobic boundary or phospholipid packing may suffice. This is evidenced by the ability of small molecules, such as PEG and annexins (Hung et al., 1996; Lentz, 2007), to induce membrane fusion. The disordered intermediate hypothesis, as with the elastic membrane hypothesis, has been shown to be mathematically viable through the use of course-grained molecular simulations (Noguchi and Takasu, 2001) and atomistic models (Jahn and Grubmuller, 2002).

1.3.3. Fusion Pore Formation and Expansion

Whatever structure the hemifusion intermediates adopts, the inner leaflets must be successively merged to form an aqueous connection across fusing bilayers, known as a fusion pore. It was initially hypothesized that in order for fusion pore formation to be energetically favorable, the hemifusion stalk must first radially expand in all directions, creating a bilayer from the extended area of contact between inner leaflets (Markin et al., 1984). However, this model has since been shown to be energetically unfavorable, and would more likely result in reversion of the hemifusion stalk to separate bilayers (Kuzmin et al., 2001b; Siegel, 1993). Further studies on the progression of a hemifusion stalk into a fusion pore have suggested it is, in fact, more energetically favorable to progress directly from the initial stalk structure into a fusion pore (Katsov et al., 2004; Kuzmin et al., 2001b; Siegel, 1993).

Fusion pores are predicted to open very quickly after the initiation of fusion, although some of these events may be transient and lead to rapid closure of nascent pores,

resulting in very brief "flickering" observations during pore formation (Chanturiya et al., 1997; Chernomordik et al., 1998; Fernandez et al., 1984; Frolov et al., 2000). However, most fusion pore formation events are stabilized and radially expand (Lindau and Almers, 1995). This stage, known as fusion pore expansion, is irreversible and has been indicated as the most energetically demanding step of the entire fusion pathway (Chernomordik et al., 1998; Leikina and Chernomordik, 2000; Lindau and Almers, 1995). This is, perhaps, the least well-understood stage of membrane fusion because it is influenced by several factors outside of the immediate fusion site. The membrane lipid composition, which influences lateral membrane tension, bending elasticity, fluidity and curvature, has direct effects on the efficiency of fusion pore expansion (Chizmadzhev et al., 1995; Leikina et al., 2004).

1.4. Factors Effecting Membrane Fusion

The mechanism of bilayer merger involves major rearrangements of membrane lipids in a very limited contact area. Many aspects of lipid bilayer structure and the physical properties of lipids directly influence the membrane fusion process. The following sections will outline the key influential factors.

1.4.1. Bilayer Dehydration

Water ordering at membrane interfaces plays important roles in many membrane functions (Berne et al., 2009; Chandler, 2005; Mittal and Hummer, 2008). Spectroscopic studies have revealed that water forms distinct, ordered structures on membrane surfaces (Cheng et al., 2003; Fukuma et al., 2007; Higgins et al., 2006), and that the hydration level of a membrane is directly influenced by its lipid composition. Lipid molecules such as PC and SM are relatively strongly hydrated (Steinbauer et al., 2003), while PE and CH have limited head group hydration (Aeffner et al., 2012; Marra and Israelachvili, 1985). As mentioned above, the presence of ordered water molecules in the intermembrane region during close membrane apposition produces strong hydration repulsion between the two membranes (Rand and Parsegian, 1989). One method of reducing the hydration

repulsion is to diminish the concentration of water at the interface by dehydrating the membrane (Burgess et al., 1992). Such dehydration also results in the generation of a strong osmotic force, which drives membranes into close contact, lowers the free energy barrier for lipid mixing and fusion stalk formation, and likely stabilizes the ensuing fusion intermediates (Malinin and Lentz, 2002).

Interestingly, recent studies employing atomic-resolution simulations of vesicle fusion have identified a dual role for interfacial water in membrane fusion: The interfacial water layer initially stabilizes contact between membranes, slowing lipid dynamics and prolonging the average time in which hydrophobic tails are able to encounter each other to form a fusion stalk. However, the same interfacial water layer in the contact site is a major part of the overall free energy barrier to stalk formation and fusion (Kasson et al., 2011). Thus, interfacial water acts as "molecular flypaper", increasing the time in which membranes stick together, but slowing the final lipid rearrangements required for fusion.

1.4.2. Imperfect Lipid Packing

The two-dimensional organization of lipids in a bilayer can have dramatic effects on fusogenicity. Lipids will spontaneously conform to the lowest energy packing conformation; however, the composition of a membrane can influence the overall organization and packing proficiency of lipids due to variations in head group hydrophobicity and charge, as well as hydrocarbon tail length and saturation (Risselada and Marrink, 2009; Wu et al., 1996). Loose lipid packing in the outer leaflets during close apposition can lead to significant exposure of hydrocarbon tails within the hydrophobic core of the membrane to the outer aqueous environment, which can reduce the energy penalties for stalk formation (Lee and Lentz, 1998; Pabst et al., 2012; Wu et al., 1996; Yang et al., 1997).

1.4.3. Local Alterations in Bilayer Curvature

As mentioned above, different lipids have differently propensities for spontaneously inducing positive or negative curvature when present in membranes due to

the relative ratio of head group-to-tail cross-sectional area. The induction of negative curvature in the outer leaflets is an absolute requirement for the formation of a hemifusion stalk (Kozlovsky and Kozlov, 2002; Kuzmin et al., 2001b; Markin and Albanesi, 2002). Similarly, the induction of positive curvature in the inner leaflets is predicted to be essential for transitioning from a hemifusion stalk to a fusion pore (Katsov et al., 2004). From an elementary standpoint, curvature generation can adequately reduce the free energy barriers to fusion, providing the driving force for progression through the fusion reaction (Cevc and Richardsen, 1999).

1.4.4. Elastic Free Energy

A major result of membrane deformations during the membrane fusion reaction is the generation of elastic free energy, which arises from membrane bending, membrane stretching and hydrocarbon tail tilting (Chernomordik and Kozlov, 2003; Zimmerberg and Kozlov, 2006). The amount of elastic free energy in a membrane is mainly contributed by the degree of curvature in the membrane, and thus is the main energy constituent in membrane fusion. However, lateral tension generated by stretching the membrane can have important implications for the fusion pore expansion stage of membrane fusion (Shillcock and Lipowsky, 2005). Generation of lateral membrane tension requires the input of energy, and results in the radial expansion of the membrane area. The final contributor to elastic free energy, the respective tilting of hydrocarbon tails relative to the membrane plane, specifically arises during the hemifusion stalk formation stage of membrane fusion (Hamm and Kozlov, 1998, 2000). This type of deformation is required to avoid the generation of voids in the hydrophobic core of the membrane, which would result in unrealistically high activation energies.

1.4.5. Changes in Membrane Fluidity

The strength of the inter-lipid van der Waals interactions is a major determinant of the two-dimensional molecular motions within a bilayer. As mentioned above, lipid composition plays a very important role in this process; membranes containing lipids with short hydrocarbon tails are more fluid because of the smaller surface area over which stabilizing interactions occur. Similarly, membranes containing lipids with

unsaturated hydrocarbon tails are more fluid due to decreased lipid packing, which stems from kinks in the hydrocarbon tails. Additionally, incorporation of lipids with higher or lower melting temperatures will influence the overall fluidity of the membrane. Membrane fusion is directly influenced by membrane fluidity (Wilschut et al., 1985). Intuitively, a more rigid membrane, in which lipids are more tightly packed, will require more energy input to induce bending, making membrane fusion less favorable. Experimentally, it has been observed that an increase in membrane fluidity precedes the fusion of muscle cells (Prives and Shinitzky, 1977).

1.4.6. Locally-Induced Non-Bilayer Phases

Certain lipids species, such as PE and CH, can promote transitioning of the membrane from the lamellar phase (described above) to the hexagonal II (H_{II}) phase (Chen and Rand, 1997; Chernomordik, 1996). Lipid molecules in the H_{II} phase are oriented inversely to those in the lamellar phase; the hydrocarbon tails orient outwards, while the hydrophilic head groups pack tightly together on the inside. This type of phase behavior tends to form extended tubules due to the nature of hydrophilic head group packing (Siegel and Epand, 1997). The outward orientation of the hydrophobic tails seems as though it would be energetically unfavorable in an aqueous environment, however the energetically favorable head group packing seems to provide overall stability to this phase. It is possible that an outer layer of lipid surrounds H_{II} phase tubules to shield the hydrophobic tails from the external aqueous environment. It has been hypothesized that during membrane fusion, a considerable number of lipids undergo lamellar-to-H_{II} phase transition, which is required for progression from lipid mixing to fusion pore formation (Kinnunen, 1996).

1.4.7. Summary

The energetics of membrane fusion have been studied using numerous different mathematical models and computer simulations (Aeffner et al., 2012; Basanez, 2002; Chizmadzhev et al., 1995; Cohen and Melikyan, 2004; Fernandez et al., 1984; Hamm and Kozlov, 2000; Kasson et al., 2011; Kasson and Pande, 2007; Katsov et al., 2004; Kozlov et al., 2010; Kuzmin et al., 2001b; Malinin and Lentz, 2004; Markin et al., 1984; Pabst et

al., 2012; Risselada and Marrink, 2009; Siegel, 1993). While these models vary slightly in their assumptions and interpretations, the energy contributors and influential factors are shared. Several of the factors affecting membrane fusion are very closely intertwined. For example, the elastic free energy is mainly contributed by the induction of curvature in the membrane, which is influenced by the fluidity of the membrane and also has a direct effect on lipid packing and hydrocarbon tail tilt. Perhaps the most universal effector of all energy contributors is the lipid composition of the membrane. Successful membrane fusion depends on favorable free energy contributions from all of the above processes.

1.5. Examples of Cell-Cell Fusion and Syncytiogenesis

Biological membrane fusion is an essential cellular process involved in numerous intracellular and extracellular events. The following subsections will provide examples and instances of cellular processes involving membrane fusion.

1.5.1. Fertilization

Our lives begin with the fusion of a sperm to an ovum. This is a very demanding process involving sperm-egg cellular adhesion and signaling and penetration of the sperm through several protective layers of the egg prior to even initiating membrane contact (Talbot et al., 2003). Once the sperm reaches the egg plasma membrane, a binding event signals the sperm to exocytose the acrosome; its single secretory vesicle (Bleil and Wassarman, 1983). This exocytosis event activates the sperm by remodeling its cell surface, allowing it to become fusion competent. The actual membrane fusion event is localized to a small region of contact between the sperm and the egg, which has been suggested to reflect a unique protein population or membrane feature within this region (Stein et al., 2004). There have been a number of proteins identified to be involved in the membrane fusion reaction between sperm and egg, including egg tetraspanin CD9 and IZUMO1 (Inoue et al., 2005; Kaji et al., 2000; Le Naour et al., 2000; Miyado et al., 2000), however none have been identified as the specific fusion protein.

1.5.2. Syncytiotrophoblast

A successful pregnancy requires formation of a protective barrier at the maternal-fetal interface. This cover is of epithelial origin and is organized into two distinct layers; the multinucleated syncytiotrophoblast on the maternal side, and the mononucleated cytotrophoblast on the fetal side. Throughout pregnancy, the syncytiotrophoblast is maintained via the continuous fusion of the underlying, mononucleated cytotrophoblasts. This fusion process is absolutely required for a successful pregnancy, and supplies the syncytiotrophoblast with proteins, nucleic acids, lipids and organelles (Pidoux et al., 2012). The membrane fusion reaction has been shown to be dependent on multiple factors, however one protein, syncytin, has stood out above all others as being absolutely indispensible (Pötgens et al., 2004). Current efforts are attempting to identify the mechanism of syncytin fusion, and if it is indeed a bona fide membrane fusion protein (Chang et al., 2004; Ruebner et al., 2013).

1.5.3. Muscle Development

Membrane fusion is an essential step in the formation of skeletal muscle fibers. These multinucleated syncytia are generated via the fusion of mononucleated myoblast cells. The myoblast cells have the ability to fuse to each other during fetal development, or with an existing multinucleated muscle fiber during muscle growth and repair (Wakelam, 1985). The membrane fusion reaction of myogenic cells is a multi-step process, beginning with myoblast-myoblast contact, recognition, adhesion and finally membrane fusion (Chen and Olson, 2004; Knudsen et al., 1989; Wakelam, 1985). Similar to sperm-egg fusion, the fusion of myoblasts is initiated from a restricted area of membrane contact, suggesting that specific proteins or plasma membrane properties are responsible for the fusion events (Fumagalli et al., 1981; Mukai and Hashimoto, 2008). However, specific membrane fusion proteins have yet to be discovered for this process.

1.5.4. Macrophage Fusion

During our lives there is a requirement for continual bone maintenance. This task is performed by specialized multinucleated cells known as osteoclasts, which originate

from mononuclear hematopoetic cells known as macrophages (Boyle et al., 2003). The formation of osteoclasts is a multi-step process involving: 1) recruitment of mononuclear monocytes from bone marrow or peripheral blood, 2) localization of these cells in the bone to the site requiring resorption, 3) attachment to the bone lining cells (Perez-Amodio et al., 2009), 4) differentiation of precursor monocyte cells into tartrate-resistant acid phosphatase (TRAP)-positive polarized cells (Boyle et al., 2003), 5) migration of TRAP-positive cells to the mineralized surface, and finally 6) fusion of the progenitor cells to form multinucleated osteoclasts (Jansen et al., 2012). Similar to myogenic cells of skeletal muscle, the osteoclasts have the ability to fuse with both mononuclear cells and multinuclear cells.

In addition to formation of multinuclear osteoclasts, macrophages can also fuse to form giant cells during chronic inflammatory reactions. In this case, the membrane fusion reaction occurs after one macrophage entirely engulfs another, producing a syncytium in a process referred to as cellocytosis (Vignery, 2000). Several proteins have been discovered that are required for various stages of syncytiogenesis during both osteoclast and giant cell formation (Cui et al., 2006; de Vries et al., 2005; Han et al., 2000; Saginario et al., 1998), however, the protein(s) that specifically mediate the fusion reaction remain elusive.

1.5.5. Nematode Developmental Fusion

A very interesting instance of membrane fusion is mediated by the FF proteins in nematodes. The best characterized is the epithelial fusion failure (EFF)-1 protein, which has been shown to be essential for cell fusion during the development of *Caenorhabditis elegans* (Mohler et al., 2002). This protein was initially identified as a candidate fusogen using genetic screens, and has since been shown to be necessary for most cell fusion events in *C. elegans* (del Campo et al., 2005; Mohler et al., 2002; Shemer and Podbilewicz, 2002; Shemer et al., 2004). The EFF-1 protein has also been shown to induce fusion of cells that are not normally fusion competent (del Campo et al., 2005; Podbilewicz et al., 2006; Shemer et al., 2004).

1.6. Enveloped Virus Membrane Fusion Proteins

As exemplified in the previous section, cellular membrane fusion is an indispensible process involved in numerous aspects of our lives. However, outside of the EFF nematode fusogens and the putative syncytin fusogens, we have yet to discover specific cellular membrane fusion proteins. Our current understanding of membrane fusion has been pioneered by the study of enveloped viral fusion proteins, which have evolved to specifically mediate virus-to-cell fusion. Further insight into membrane fusion has since been garnered through the study of the SNARE vesicle fusion proteins.

The entry of all enveloped viruses into host cells requires fusion of the viral envelope to the host membrane. This reaction is mediated by specific glycoproteins that are expressed on the viral particle surface. These are single-pass transmembrane domain (TMD) proteins generally consisting of relatively short endodomains in comparison to their large, complex ectodomains (Figure 1.2). To promote the membrane fusion reaction, the ectodomains of these glycoproteins undergo large structural rearrangements that drive membrane merger. There are three classes of enveloped viral fusion proteins, which are defined based on differences in their pre- and post-fusion structures. Despite these differences, a common sequence of structural rearrangements occurs for each class. All viral membrane fusion glycoproteins are present on the virion surface in a metastable, pre-fusion state. In this metastable state, a sequence of moderate hydrophobicity, known as the fusion peptide (FP), is embedded within the pre-fusion structure (Carr et al., 1997; Earp et al., 2004; Hernandez et al., 1996; Skehel and Wiley, 2000). The fusion proteins are activated by either a low pH trigger or binding to a cellular receptor, which induces conformational changes resulting in exposure of the FP, allowing for interaction with the cellular target membrane, the virus membrane or both membranes. These interactions are accompanied by further structural transitions, which result in membrane merger (Figure 1.3). The similarities and differences of the three enveloped viral fusion protein classes will be described using the most comprehensively characterized example of each class.

1.6.1. Class I Enveloped Viral Fusion Proteins

The very first structure solved of an enveloped viral fusion protein component was that of the avian influenza virus hemagglutinin (HA) ectodomain in its pre-fusion conformation (Figure 1.2A) (Wilson et al., 1981). The avian HA protein is synthesized as a HA_0 precursor, which undergoes proteolytic cleavage by a cellular protease, resulting in HA_1, the sialic-acid binding domain, and HA_2, the membrane-bound fusion domain (Stieneke-Grober et al., 1992). These two HA subunits are linked in the final conformation via a disulfide bond. The proteolytic cleavage of a single precursor molecule is a hallmark of the class I enveloped viral fusion proteins (Lamb and Jardetzky, 2007; Pager and Dutch, 2005; Pager et al., 2006; Stieneke-Grober et al., 1992).

The class I fusion proteins exists as homotrimeric spikes in both their pre-fusion and activated states. In HA, the HA_2 subunit forms a triple coiled coil, with the HA_1 subunit attached to the top. The amino-terminus (~20 amino acids) of the HA_2 subunit constitutes the hydrophobic FP motif, which is buried in the homotrimeric structure of the metastable pre-fusion state (Chen et al., 1998; Wiley and Skehel, 1987). Influenza virus particles bound to the cell surface are internalized into endocytic vesicles, which fuse to lysosomes, resulting in a dramatic drop in the endosomal pH. This pH reduction acts as the trigger for HA activation: key histidine residues become protonated, resulting in the dissociation of HA_1 subunits (Huang et al., 2002). This dissociation induces a dramatic conformational change of the HA_2 subunit, resulting in exposure of the hydrophobic FP motif, as well as its localization to the distal tip of the protein structure (Figure 1.2A) (Bullough et al., 1994; Skehel et al., 1982a). During this conformational change, an unstructured loop in the pre-fusion HA_2 subunit becomes an extended α-helix, resulting in a length increase of the coiled coil domain. The associated FP translocation places this motif in proximity to the target membrane, potentiating interaction. The characteristics and membrane interactions of FP motifs are discussed in further detail in section 1.7.1.

Following the extended intermediate conformation described above, the HA homotrimer undergoes an additional conformational change into its lowest energy structure. During this conformational change, the carboxyl-terminus of the HA folds towards the amino-terminal end, resulting in a hairpin structure with the FP and

transmembrane domain in close proximity (Figure 1.2A). This structure is stabilized through tight associations between the heptad repeats located C-terminal to the FP and N-terminal to the TMD (Dutch et al., 2000; Madhusoodanan and Lazaridis, 2003; Reuven et al., 2012). The central N-terminal trimeric coiled coils pack tightly with the C-terminal helices to form a six-helix bundle (Bullough et al., 1994; Dutch et al., 2000). Due to this structure, the post-fusion conformation of class I enveloped viral fusion proteins is sometimes referred to as "a trimer of hairpins" (Eckert and Kim, 2001).

The influenza HA protein was the first structurally characterized enveloped viral fusion protein, and has served as the basis of class I fusion protein discussion thus far. Indeed, the final six-helix bundle structure is encountered in the fusion proteins of coronaviruses (Duquerroy et al., 2005; Supekar et al., 2004; Xu et al., 2004), filoviruses (Weissenhorn et al., 1998), paramyxoviruses (Baker et al., 1999; Dutch et al., 1999; Yin et al., 2005) and retroviruses (Buzon et al., 2010; Weissenhorn et al., 1997), all of which are class I fusion proteins. However, outside of this common post-fusion structure, there is considerable variability across the class I fusion proteins. First, the resulting subunits of proteolytic cleavage are not always disulfide linked in the final conformation. For example, the human immunodeficiency virus (HIV) gp160 protein consists of the gp120 subunit non-covalently bound to the gp41 subunit (Veronese et al., 1985). Second, recent determination of the pre-fusion structures of other class I fusion proteins, such as parainfluenza virus type 5 fusion protein (Yin et al., 2006) and Ebola virus GP (Lee et al., 2008), have revealed that outside of a common heptad repeat region adjacent to the FPs, there are significant variations in the three-dimensional structures. Finally, the activation mechanisms of the class I enveloped viral fusion proteins are quite varied. While low pH activation, as observed for HA, is required for some class I proteins, many other members are activated via receptor binding events (Earp et al., 2004), which can either be through direct interactions with the fusion protein (Melikyan, 2008), or through indirect interactions with a viral attachment protein (Lamb and Jardetzky, 2007).

1.6.2. Class II Enveloped Viral Fusion Proteins

The *Bunyaviridae*, *Flaviviridae* and *Togaviridae* families encode class II enveloped viral fusion proteins (Garry and Garry, 2004; Kanai et al., 2006; Krey et al.,

2010; Lescar et al., 2001; Modis et al., 2003; Nybakken et al., 2006; Rey et al., 1995b). A common feature of these proteins is their co-translational folding with specific chaperone proteins (Heinz et al., 1994; Wahlberg et al., 1989). This interaction is absolutely required for the correct folding and transportation of the class II proteins (Sanchez-San Martin et al., 2009). The chaperone proteins undergo a cleavage event late in the secretory pathway, which is required to prime the fusion protein, leaving it in the pre-fusion metastable conformation (Sanchez-San Martin et al., 2009; Stadler et al., 1997; Zhang et al., 2003).

In contrast to the predominantly α-helical structures observed for the class I fusion proteins, the class II fusion proteins are mostly composed of β-sheet secondary structures that lie parallel with the membrane plane (Figure 1.2B) (Kielian, 2006). These proteins are comprised of three globular domains: the N-terminal domain I, the FP-containing domain II, and the TMD-containing domain III (Allison et al., 2001; Heinz and Allison, 2001; Kielian and Rey, 2006; Lescar et al., 2001). Unlike the class I fusion proteins, which mostly contain N-terminal FPs, the class II fusion proteins all contain internal FPs stabilized as extended looped structures (Kielian, 2006; White et al., 2008). Additionally, while class I proteins are activated by various mechanisms, all class II proteins are activated by a low pH trigger (Kielian, 2006; Stiasny et al., 2001). The structural rearrangements undertaken during the fusion reaction also differ between the class I and class II fusion proteins. As mentioned above, the class I proteins are trimeric in both the pre-fusion and post-fusion conformations. The class II fusion proteins, in contrast, are dimeric in the metastable pre-fusion conformation, and undergo structural rearrangements to become trimeric in their stable post-fusion conformation (Bressanelli et al., 2004; Gibbons et al., 2004; Modis et al., 2003). However, reminiscent of the post-fusion hairpin of the class I fusion proteins, the post-fusion trimeric conformation of the class II proteins has the TMD and FP motif in very close proximity (Figure 1.2B).

1.6.3. Class III Enveloped Viral Fusion Proteins

The class III enveloped viral fusion proteins are the most recent addition to the fusion protein classes. This class consists of the vesicular stomatitis virus (VSV) G

protein (Roche et al., 2006), herpes simplex virus (HSV)-1 glycoprotein B (gB) (Heldwein et al., 2006), Epstein Barr virus gB (Backovic and Jardetzky, 2009), baculovirus gp64 (Kadlec et al., 2008), G proteins from animal rhabdoviruses (Roche et al., 2006), as well as the glycoprotein from Borna disease virus (Garry and Garry, 2009). However, VSV G is the only class III protein for which both the pre-fusion and post-fusion crystal structures have been determined (Figure 1.2C) (Roche et al., 2007). Further discussion will focus on VSV G as a model for the class III enveloped viral fusion proteins.

The pre-fusion structure of VSV G consists of four globular domains: 1) Domain I, which is composed primarily of β-sheets, 2) Domain II, which is responsible for trimerization, 3) Domain III, which is a pleckstrin homology domain, and 4) Domain IV, which contains the FP motif (Roche et al., 2007). The overall structural features of the class III enveloped viral fusion proteins contain similarities with both the class I and class II proteins, with some additional, unique properties. The class III proteins contain both α-helical and β-sheet secondary structures, however they contain a central α-helical coiled-coil domain in the post-fusion conformation, which is a signature characteristic of class I proteins (Backovic and Jardetzky, 2009; Roche et al., 2007). They also contain internal FP motifs that are stabilized as loop structures, similar to the class II proteins. However, unlike the class II FPs, the class III FP loops are made of two separate domains, rather than one extended loop structure (Backovic and Jardetzky, 2009; Roche et al., 2006; Roche et al., 2007). Also, the FPs are not buried in the pre-fusion structure, but point toward the viral membrane (Figure 1.2C) (Roche et al., 2007). While the class III proteins share a similar trimeric conformation in the pre- and post-fusion conformation to the class I and II proteins, they do not undergo any proteolytic processing prior to arriving at their metastable pre-fusion state (Backovic and Jardetzky, 2009).

Regardless of their overall structural characteristics, the class I, II and III enveloped viral fusion proteins have remarkable similarities in the conformational changes undertaken while inducing membrane fusion. Proteins of each class are multimeric in nature, and rely upon triggered conformational changes to expose

hydrophobic FPs, followed by overall folding back to drive membrane merger (Figure 1.3).

1.7. SNARE Vesicle Fusion Proteins

Outside of the enveloped viral fusion proteins, the most well-studied proteins known to induce membrane fusion are the SNARE vesicle fusion proteins. These proteins are the core of the cellular vesicle-transport machinery and are responsible for mediating fusion of transport vesicles with their correct subcellular compartments (Bonifacino and Glick, 2004). They are responsible for such essential cellular activities as hormone secretion, enzyme release and neurotransmission. The coordination of these events requires a concerted effort from tethering factors, which promote vesicle targeting, Rab-GTPases, which determine the site of fusion, the SNARE proteins, which mediate the membrane fusion reaction, and N-ethylmaleimide-sensitive factor (NSF) with cofactors, which are responsible for activation and recycling of the fusion complex (Ungermann and Lanosch, 2005).

The SNARE proteins are characterized by sequences called SNARE motifs, which are heptad repeats that predominantly form coiled coil structures (Bock et al., 2001). There are two broad categories of SNARE proteins: the vesicular or v-SNAREs, which are present in the membranes of transport vesicles, and the target or t-SNAREs, which are present in the membranes of target compartments (Rothman, 1994; Sollner et al., 1993). In order to avoid ambiguity during homotypic SNARE-mediated fusion, these two categories have since been redefined as R-SNAREs and Q-SNAREs, respectively. These names reflect the identify of highly conserved, functionally essential residues (Fasshauer et al., 1998). In the example of synaptic vesicle exocytosis, the R-SNARE component synaptobrevin, which is part of the vesicle-associated membrane protein (VAMP) family (Baumert et al., 1989), and the Q-SNARE components syntaxin-1 and SNAP-25 form a highly stable SNARE complex comprising a parallel four-helix bundle (Sutton et al., 1999). This complex bridges the vesicle membrane and target membrane, bringing them into close proximity, and is referred to as the trans-SNARE complex. An

influx of calcium ions triggers completion of the fusion process, which is mediated by synaptotagmin association with the trans-SNARE complex (O'Connor and Lee, 2002; Pang et al., 2006). This reaction results in formation of the cis-SNARE complex, which is significantly more structurally stable than the trans-SNARE complex. It has been suggested that structural transitioning from trans- to cis-SNARE complexes provides the necessary free energy to drive membrane fusion (Chen and Scheller, 2001; Hanson et al., 1997; Weber et al., 1998). Completion of the fusion process requires at least one SNARE-complex protein associated with each membrane possess a TMD. This is likely required to induce membrane tension to promote the pore formation and expansion stages of membrane fusion (McNew et al., 2000). Control and specificity of vesicle fusion is controlled by the variety of R- and Q-SNARE proteins able to form trans-complexes (Ungar and Hughson, 2003).

1.8. Functional Motifs of Fusion Proteins

Several stages of the membrane fusion reaction require energy input to overcome thermodynamic barriers. In order for membrane fusion proteins to transmit free energy into the membrane, several membrane-interacting functional motifs are employed. The following subsections will describe these motifs and how they may function to impart or relieve membrane stresses during fusion.

1.8.1. Fusion Peptides

All enveloped viral fusion proteins contain a series of hydrophobic amino acids in their ectodomains, termed FPs (White et al., 2008). These functional motifs are generally less than 25 amino acids in length, overall moderately hydrophobic, frequently enriched in alanine and glycine residues, and are highly conserved across fusion proteins from different isolates of the same virus (Cross et al., 2009; Earp et al., 2004; Martin et al., 1999; Martin and Ruysschaert, 2000). These motifs are extremely sensitive to mutation, and are absolutely required for membrane fusion activity (Smith et al., 2012b). As noted above, FPs are usually sequestered in the complex pre-fusion structure of enveloped viral

fusion proteins, and become exposed in response to an external trigger. After exposure, FPs insert into the target membrane (Durrer et al., 1996), which plays an important role in bridging the viral and target membranes.

1.8.2. Membrane Proximal Ectodomain Regions

For many enveloped viral fusion proteins, the membrane-proximal ectodomain regions (MPERs) play important roles in the membrane fusion reaction (Howard et al., 2008; Vishwanathan and Hunter, 2008). These regions frequently contain hydrophobic amino acids, and are specifically enriched in tryptophan. Mutation of tryptophan residues within the MPER of HIV gp41 completely abrogated membrane fusion activity (Salzwedel et al., 1999). MPERs are predicted to partition into the viral membrane water-phospholipid interface to promote fusion (Apellaniz et al., 2011; Ivankin et al., 2012; Jeetendra et al., 2003; Suarez et al., 2000; Vishwanathan and Hunter, 2008).

1.8.3 Transmembrane Domain Regions

The TMDs of several enveloped viral fusion proteins and the SNARE proteins have been shown to play active roles in membrane fusion (Giraudo et al., 2005; Kemble et al., 1994; McNew et al., 2000; Nussler et al., 1997; Odell et al., 1997; Sjoberg and Garoff, 2003; Smith et al., 2012a). While the exact mechanistic roles of these domains remain poorly understood, several possibilities have been proposed. For example, it has been suggested that the energy released during the proposed structural rearrangements of the enveloped viral fusogen ectodomains can be transmitted through the TMD to generate membrane stresses, which could drive pore formation (McNew et al., 2000; Melikyan et al., 1995). This model is also feasible for the SNARE complex proteins; the structure of this complex revealed a continuous helical bundle from the extracellular complex, through a short linker sequence, into the TMD sequence (Ellena et al., 2009; Stein et al., 2009). Alternatively, the TMDs of fusogenic proteins frequently contain an abundance of glycine and β-branched residues, prompting the theory that α-helical flexibility within TMDs is required for fusion activity (Neumann and Langosch, 2011; Poschner et al., 2010).

1.9. Energy Generation During Fusion

The membrane deformations that must occur throughout the proposed membrane fusion reaction can only occur if the overall reaction is energetically favorable, and the progression through high-energy intermediate structures is able to occur in a biologically relevant time-frame. Membrane fusion proteins must make membrane fusion energetically feasible by supplying energy into the system, or lowering the energy of intermediate structures. Enveloped viral and vesicle fusion proteins are predicted to input energy into the membrane system by generation of elastic stress. The relaxation of this stress thus provides the driving force for membrane fusion. Energy input of this sort has been predicted to manifest as the induction of membrane curvature in the fusing region of the membrane (Kozlov and Chernomordik, 1998; Martens et al., 2007; Martens and McMahon, 2008; McMahon et al., 2010).

One mechanism by which membrane fusion proteins have been suggested to induce membrane curvature is via the shallow insertion of hydrophobic peptides (Campelo et al., 2008; Martens et al., 2007; McMahon and Gallop, 2005; Zimmerberg and Kozlov, 2006). Synthetic versions of the FPs and MPERS of enveloped viral fusion proteins have been shown to induce merger between lipid bilayers, in the absence of the rest of their respective fusion proteins, by obliquely inserting into membranes, which induces positive curvature via the expansion of polar lipid head groups (Epand, 1998, 2003; Siegel and Epand, 2000; White et al., 2008) (Campelo et al., 2008; Charloteaux et al., 2009; Lai et al., 2012). The FPs and MPERs induce curvature and membrane destabilization in the target and viral membrane, respectively, to mediate membrane merger (Apellaniz et al., 2011; Ivankin et al., 2012; Jeetendra et al., 2003; Saez-Cirion et al., 2003; Saez-Cirion et al., 2002; Schibli et al., 2001; Suarez et al., 2000; Vishwanathan and Hunter, 2008). Interestingly, the energy provided through the insertion of FPs from a single HA trimer is theoretically sufficient to induce hemifusion stalk formation (Gunther-Ausborn et al., 2000).

The membrane fusion activity of the SNARE vesicle fusion proteins also seems to depend on the induction of curvature by synaptotagmin-1 and DOC2, which are SNARE cofactors involved in calcium sensing (Hui et al., 2009; Martens et al., 2007; Martens and

McMahon, 2008). Upon calcium binding, these proteins shallowly insert their small, relatively hydrophobic C2 domains into the membrane, which induces a highly curved (~9nm radius) tubule with a highly fusogenic end cap (Groffen et al., 2010; Hui et al., 2009; Martens et al., 2007).

Alternatively, FPs have been suggested to displace the hydration layer at the lipid-water interface, which reduces the hydration-repulsion force, allowing membranes to come into closer contact (Tamm and Han, 2000). This effectively reduces the energy barrier to stalk formation. In fact, the free energy generated by the dehydration of lipid membranes through volume exclusion may be an ample driving force for membrane fusion. Small molecules, such as PEG and annexins, induce membrane fusion via this method (Hung et al., 1996; Lentz, 2007). This works by excluding water between the areas of membrane contact, which creates a positive osmotic pressure that helps stabilize membrane intermediates (Malinin and Lentz, 2004). This highlights the fact that there are several mechanisms by which membrane fusion can be induced, and that energy input via membrane bending is not a universal requirement to induce membrane fusion.

1.10. Emerging Pathogens

On average, more than two new species of human-infecting viruses are reported worldwide each year. All newly discovered, uncharacterized viruses pose substantial threats of becoming emerging human infections (Woolhouse et al., 2008). While there are over 20 virus families that contain pathogens able to infect humans, over half of the known, as well as half of newly discovered human-infecting viruses emerge from just four virus families: the *Bunyaviridae*, *Flaviviridae*, *Togaviridae* and *Reoviridae* (Woolhouse and Gowtage-Sequeria, 2005). An overwhelming majority of these emerging and reemerging pathogens are viruses containing RNA genomes. Such genomes are associated with very high mutation rates (Drake, 1993; Drake and Holland, 1999), which drastically increases their risk of evolving into emerging pathogens (Woolhouse and Gowtage-Sequeria, 2005; Woolhouse et al., 2008). Whether causing massive progressive pandemic diseases, such as HIV, or more transient events, such as the coronavirus

associated with severe acute respiratory syndrome (SARS) or the Ebola virus, novel emerging viruses pose a major public health concern.

The study of emerging pathogens has largely focused on the variety of pathogens, the basis and reasons for emergence, and intervention plans to control and prevent emergence. Designing disease control systems using this approach are impractical due to the potentially vast number, geographic range, potential for rapid circulation, as well as numerous ecological and societal factors that influence emergence (Morse, 1991, 1995; Satcher, 1995). This makes it very difficult to predict and prevent the emergence of only the most harmful pathogens. Rather, a more feasible approach to curbing pathogen emergence is to understand the evolution and function of virulence factors, which would identify pathogens that are of potentially higher threat and allow for early prevention and control measures to be taken.

1.10.1. Bats as Reservoirs for Emerging Pathogens

A considerable number of studies have examined bat populations as reservoirs and sources of potential emerging viral pathogens, as they are the sources of such well-known viruses as Hendra, Nipah and coronaviruses (Chua et al., 2000; Halpin et al., 2000; Lau et al., 2010; Li et al., 2005; Wong et al., 2007). Bats are the second largest order within the mammal clade, accounting for about 20% of all known mammalian species. Several different bat species inhabit all human-populated continents, and their unique biological and ecological features result in them hosting a large number of infectious agents (Wong et al., 2007). Bat colonies are found to reside in several man-made habitats, such as buildings, bridges, tombs, mines, etc., which results in a closer association and increased contact with humans and livestock. Such contact directly results in increased zoonotic transmission of bat-borne viruses, such as bat rabies viruses, to humans.

Recently, several novel *Orthoreovirus* species of bat origin have been isolated from humans suffering from severe respiratory illnesses (Cheng et al., 2009; Chua et al., 2007; Chua et al., 2008; Chua et al., 2011; Ouattara et al., 2011), though very little is known about the transmission and pathogenicity of these bat-borne reoviruses. The

orthoreoviruses are non-enveloped viruses with segmented, double-stranded RNA genomes. Monitoring agencies have recommended close monitoring of orthoreoviral evolution, as well as a necessity for further research to allow for prevention and control measures to be taken in the event of increased virulence (Wong et al., 2012).

1.10.2. Fusogenic Reoviruses

The *Orthoreovirus* genus is divided into two subgroups based on the ability to induce cell-cell fusion and syncytium formation (Duncan, 1999). The infection of humans by orthoreoviruses is not uncommon; the non-fusogenic mammalian reoviruses (MRV's) are often found to infect humans. These viruses are mainly asymptomatic, although in rare cases have been shown to cause mild respiratory or gastrointestinal illnesses (Schriff et al., 2007). In contrast, infections of fusogenic orthoreoviruses often result in very severe consequences, ranging from encephalitis and neurological disease caused by baboon reovirus (BRV) and reptilian reovirus (RRV), to pneumonia and death caused by the avian reoviruses (ARVs) (Chen et al., 2012; Leland et al., 2000; Ni and Kemp., 1995; Vieler et al., 1994). While syncytia formation is not essential for virus replication (Duncan et al., 1996) the degree of syncytiogenesis directly correlates with viral pathogenicity (Duncan and Sullivan, 1998).

1.10.3. The FAST Proteins

Members of the fusogenic reoviruses encode unique, non-structural proteins termed the fusion-associated small transmembrane (FAST) proteins. The FAST proteins are a family of membrane fusion proteins that function as dedicated cell-cell fusogens. In the absence of a lipid envelope surrounding the viral nucleocapsid, reoviruses do not require membrane fusion for host-cell entry and infectivity. Thus, the FAST proteins are not involved in viral entry or exit, but promote viral dissemination and pathogenesis during infection. This is accomplished in two ways: first, by inducing fusion of virus-infected cells with neighboring uninfected cells, resulting in localized cell-cell transmission of the virus (Duncan et al., 1996), and second by inducing apoptotic disruption of late-stage syncytia resulting in enhanced progeny virus release (Salsman et al., 2005). When placed in the context of a heterologous virus, members of the FAST

protein family act as virulence factors to enhance neuropathogenesis, which is a direct result of FAST-induced syncytiogenesis (Brown et al., 2009). Very little is known of the relationship between syncytiogenesis and pathogenicity, however it is likely that syncytiogenesis allows for viral spread without coming in direct contact with the immunological factors outside of the cell.

The evolutionary origin of the FAST proteins remains unknown. It is unlikely that they evolved from the large, complex enveloped viral fusion proteins. While these proteins have been shown to induce cell-cell fusion, the process of virus-cell fusion drove their evolution. As such, these proteins preform many other functions in addition to the membrane fusion reaction, including receptor-binding, close membrane apposition, virus particle assembly, maturation and egress (Loving et al., 2008; Merten et al., 2005; Nayak et al., 2004; Skehel and Wiley, 2000). Unlike their enveloped viral fusion protein counterparts, the FAST proteins are promiscuous fusogens that do not require a low-pH, receptor binding or proteolysis trigger to induce membrane fusion (Salsman et al., 2008a; Shmulevitz, 2000; Top et al., 2005). Also, they are non-structural proteins that are not involved in receptor-binding, virus particle assembly, maturation or egress (Salsman et al., 2008a). Phylogenetic analysis suggests the ancestral reovirus was non-fusogenic and at least 2, and possibly 3 or more, gain of function events led to the fusogenic aqua- and orthoreoviruses, possibly by adaptation of small, membrane-interactive non-structural viral proteins (Nibert and Duncan, 2013).

There are currently six confirmed members of the FAST protein family, named according to their size in kilodaltons (kDa, Figure 1.4). The homologous 10 kDa (p10) proteins from ARV and pteropine reoviruses (PRVs), the p13, p14 and p15 proteins from Broome reovirus (BroV), RRV and BRV, respectively (Duncan et al., 2004; Duncan et al., 1995; Shmulevitz, 2000; Thalmann et al., 2010), and the p16 and p22 proteins of aquareoviruses (Mohd Jaafar et al., 2008; Racine et al., 2009). The FAST proteins share no identifiable sequence similarity with each other, or with any other known membrane fusion protein. However, some defining features are common across the group, including: their small size (95-140 amino acids), a single-pass transmembrane domain with $N_{exoplasmic}/C_{endoplasmic}$ membrane topology, a fatty-acid modification and various linear

motifs (hydrophobic patches, poly-basic regions) (Corcoran and Duncan, 2004; Dawe, 2002; Shmulevitz, 2000).

1.10.4. The Avian and Pteropine Reovirus p10 FAST Proteins

The p10 FAST proteins from the ARV and PRV lineages provide an ideal system to study FAST-mediated syncytiogenesis; they are the only FAST proteins with numerous homologous isolates within and across host ranges (Figure 1.5). Additionally, the induced rate of syncytiogenesis varies across p10 isolates, providing a functional measure for protein comparison (Salsman et al., 2005). At 95-98 residues, p10 FAST proteins are the smallest known viral or cellular fusion proteins. They comprise a central transmembrane domain, which separates approximately equal sized (about 40 residue) ecto and endodomains. The ectodomain contains intramolecular disulfide-bonded cysteine residues flanking a moderately hydrophobic region, termed the hydrophobic patch (HP) (Barry et al., 2010). The HPs function similarly to enveloped viral FPs in fluorescent lipid mixing assays (Sackett et al., 2010; Shmulevitz et al., 2004b). Additionally, the ectodomain contains a stretch of nine residues that are absolutely conserved across all p10 isolates, termed the conserved motif (CM). The endodomain contains two palmitoylated cysteine residues immediately adjacent to the TM domains, which are followed by a stretch of moderately conserved basic residues, known as the polybasic (PB) motif. Mutation of the palmitoylated cysteines or PB motif impairs or eliminates syncytium formation (Shmulevitz et al., 2003).

1.11. Objectives

As the smallest known membrane fusion proteins, the FAST proteins provide a unique model system to study the minimal requirements for protein-mediated membrane fusion. Additionally, a comprehensive mechanistic understanding of FAST protein-mediated syncytiogenesis would shed light on the role of this process in viral pathogenicity. The homologous p10 FAST proteins encoded by ARV and PRV isolates offer a powerful system in which to compare and contrast the fusogenic capabilities of

these proteins. Matching this with the sequence conservation and divergence would further define the mechanistic roles of functional motifs comprising the p10 proteins. This thesis describes how structural and functional motifs contained with the p10 ectodomains contribute to p10-mediated syncytiogenesis. This work provides novel insight into how such diminutive proteins are able to accomplish the energetically unfavorable task of membrane fusion.

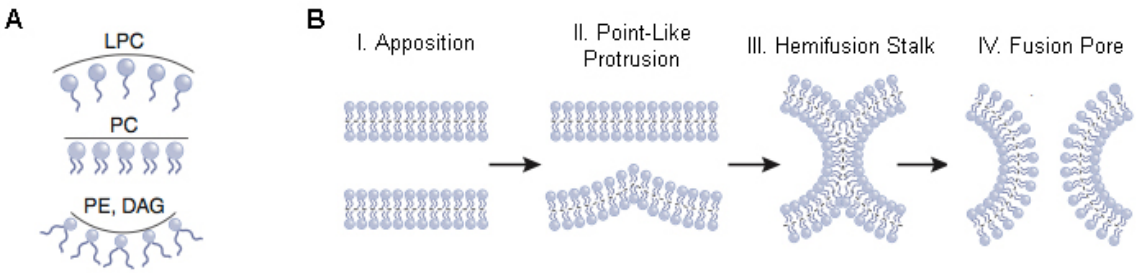

Figure 1.1- Membrane curvature dynamics during bilayer merger. (A) Based on the relative cross-sectional area ratio of lipid head groups to hydrocarbon tails, different lipid species have different propensities to induce positive (LPC), negative (PE, DAG) or neutral (PC) natural curvature. (B) The membrane fusion reaction is predicted to progress from close membrane apposition (I), to contact via a point-like protrusion (II), to outer leaflet mixing and hemifusion stalk formation (III), and finally fusion pore formation (IV). Adapted from (Chernomordik and Kozlov, 2008) with permission.

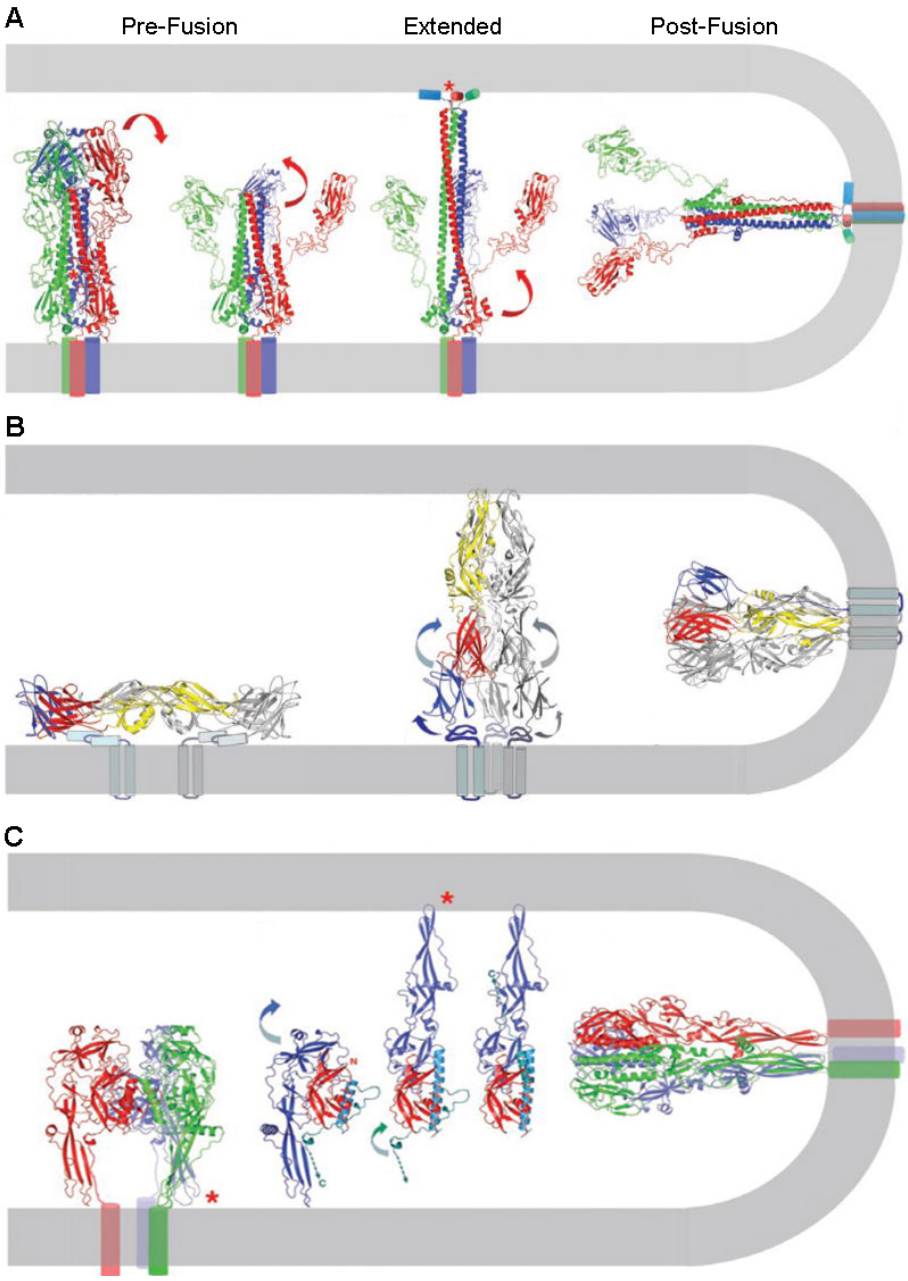

Figure 1.2- Enveloped Viral Fusion Protein Structures. (A) Influenza virus HA as a model of the class I fusion proteins. Each subunit is represented as a different color. The red asterisk identifies the FP of the red subunit in the pre-fusion and extended conformations. (B) Flavivirus E as a model of the class II fusion proteins. The red, yellow and blue colors correspond to domains I, II and III of each subunit, respectively. (C) VSV-G as a model for the class III fusion proteins. Each color represents a different subunit in the pre-fusion (left) and post-fusion (right) conformations. The red asterisk indicates the location of the fusion loop in the pre-fusion conformation (right) and in a single subunit of the predicted extended intermediate conformation (middle-right). Adapted from (Harrison, 2008) with permission.

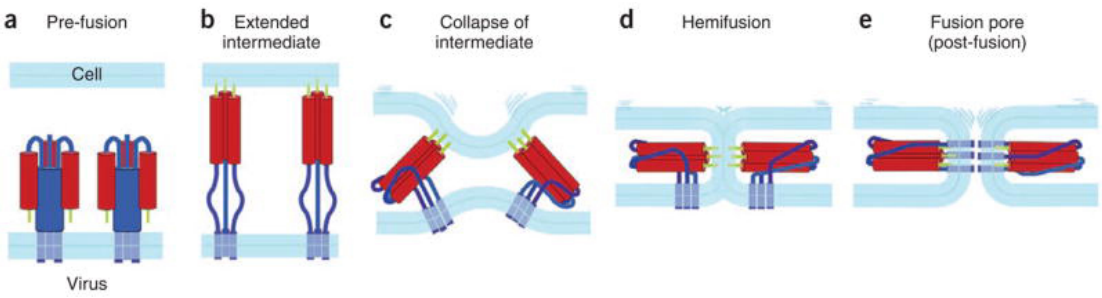

Figure 1.3- Structural rearrangements during mechanically driven membrane fusion. (A) The protein in its pre-fusion conformation, with the hydrophobic FP sequestered in the complex ectodomain structure. (B) Upon an external trigger, the ectodomain undergoes conformational changes that result in exposure of the FP and translocation to the distal tip of the protein, which ends in the extended intermediate conformation. (C) Collapse of the extended intermediate structure pulls the target and donor membranes together, driving (D) hemifusion, where the proximal leaflets are united, but the inner leaflets remain separate. (E) The inner leaflets of hemifused bilayers open into a fusion pore, resulting in a continuous membrane bilayer. Reprinted from (Harrison, 2008) with permission.

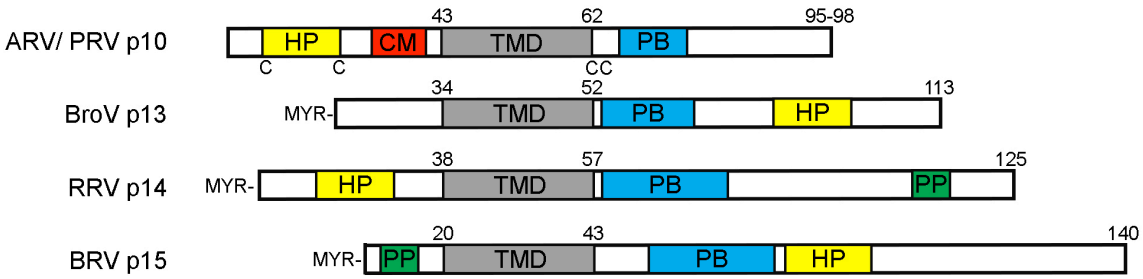

Figure 1.4- Domain organization of orthoreovirus FAST proteins. Schematic of the known orthoreovirus-encoded FAST proteins with linear motif locations indicated. Sizes are relative and drawn approximately to scale. All proteins contain single-pass TMDs with N_{ecto}/C_{endo} membrane topology and with an endodomain membrane-proximal polybasic motif (PB). Each of the FAST proteins contains an ecto- or endodomain localized stretch of moderately hydrophobic amino acids, termed the hydrophobic patch (HP). Two cysteine residues flank the HPs of the p10 proteins. C-terminal to the HP, the p10 ectodomains contain a stretch of absolutely conserved amino acids, referred to as the conserved motif (CM). The endodomains contain two palmitoylated, membrane proximal cysteine residues. The p13, p14 and p15 proteins are all N-terminally myristolated (MYR), while the p14 and p15 proteins contain polyproline (PP) motifs. The residue number of the beginning and end of each TMD, as well as the total length of the proteins are indicated.

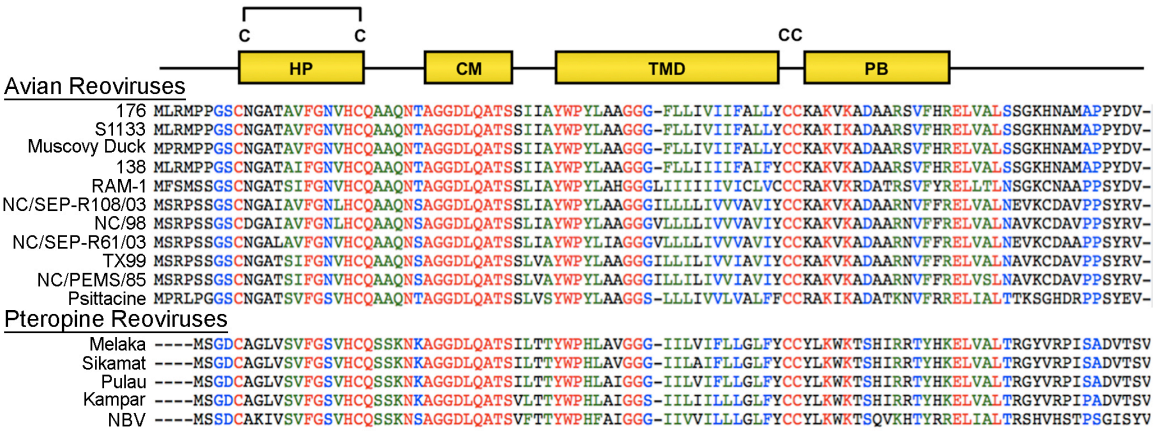

Figure 1.5- The p10 FAST protein have multiple, homologous isolates from avian and pteropine Reoviruses. Selected, representative isolates are shown for each host range., The domain organization includes a central TMD separating approximately equal sized (~40 residue) ecto- and endodomains. Each isolate contains the same repertoire and arrangement of linear motifs, including the hydrophobic patch (HP) fusion peptide and conserved motif (CM) in the ectodomain, as well as the polybasic motif (PB) in the endodomain. Red residues are absolutely conserved, blue are highly conserved, green are moderately conserved, and black are not conserved.

CHAPTER 2

Materials and Methods

2.1. Plasmids and Cloning

2.1.1. Vectors

All parental FAST protein constructs were subcloned into pcDNA3 mammalian expression vectors (Invitrogen) as previously described (Shmulevitz et al., 2004a). All FAST protein mutant constructs, as well as all epitope- and fluorescent protein-tagged versions, were also subcloned into pcDNA vectors.

2.1.2. Site-Directed Mutagenesis

The QuikChange site-directed mutagenesis kit (Agilent Technologies) was used, according to the manufacturer's instructions, to generate point mutations for all CM and neck region constructs, as well as putative cholesterol recognition amino acid consensus (CRAC) motif knock-out constructs. Custom oligonucleotide primers were purchased from IDT. All constructs were confirmed by sequencing.

2.1.3. Chimeric p10 Constructs

ARV and NBV p10 chimeric constructs were created via PCR using sequential, partially overlapping oligonucleotide primers (IDT). Primers for first round PCR were designed with 20-25 nucleotides overlapping with the parental protein, which was used as the template. An additional 20-30 non-annealing nucleotides of the domain intended to be exchanged were added to the end of the primer. Primers in following rounds were designed with 20-25 nucleotides overlapping with the PCR product of the previous round, which was used as the template, plus 20-30 additional nucleotides of the domain intended to be exchanged. This process was repeated until the entire domain was reconstructed. Vent polymerase (New England Biolabs) was used according to the manufacturer’s instructions for each PCR reaction. PCR products were gel purified

between each round, and final products were subcloned into pcDNA3 expression vectors. Sequences were verified by sequencing.

2.1.4. Glycerol Stocks

All parental, tagged and mutant constructs in pcDNA3 expression vectors were transformed into $CaCl_2$ competent DH5α E.coli cells (Green and Sambrook, 2012). Transformed cells were streaked onto ampicillin-containing agar plates. Single colonies were picked and grown up in fresh ampicillin-containing LB media for ~16 hours. Suspension cultures were mixed with an equivalent volume of LB media containing 50% glycerol and stored at -80º C. Plasmid DNA was obtained using Qiagen miniprep or midiprep kits from glycerol stock E.coli cultures grown overnight in ampicillin-containing LB media. DNA concentration was measured via spectroscopy.

2.2. Cells and Cell Culture

Quail muscle fibroblast (QM5) and monkey kidney epithelial (Vero) cell lines were maintained in 175 cm^2 at 37º C in a 5% CO_2 environment, as previously described (Corcoran and Duncan, 2004). QM5 cells were grown in Earle's 199 growth media (Gibco) supplemented with 10% fetal bovine serum (FBS, Sigma-Aldrich) and Vero cells were grown in the same medium with 5% FBS. Every 2-3 days, cells were subcultured using trypsin to prevent overcrowding and cell death. Cells were maintained in the absence of antibiotics.

2.3. Transfections and Syncytial Indexing

QM5 or Vero cells were transfected using polyethylimine (PEI, Polysciences Inc.) as per manufacturer's instructions. Syncytial indexing was performed on 50% confluent monolayers (using low passage numbers cells) in 12-well plates transfected with 0.5µg of plasmid DNA (unless otherwise stated). At 4 h post transfection (hpt), the transfection mix was replaced with Earle's 199 growth media supplemented with 10% FBS. At

indicated times post-transfection the cells were fixed with methanol and Wright-Giemsa stained (Siemens Healthcare Diagnostics). Stained monolayers were imaged using a Nikon DIAPHOT-TMD under 200x magnification. The numbers of syncytial nuclei were counted from 5 random fields per well, in 3 separate experiments. Error was calculated within each replicate, and propagated across replicates. Final values are reported as standard error of the mean.

2.4. Surface Protein Expression by Flow Cytometry

Transfected QM5 monolayers were incubated for 24 h in Earle's 199 growth media supplemented with 10% FBS. Live cells were labeled with 1:200 dilution of mouse anti-FLAG primary antibody, followed by 1:2000 dilution of Alexa 647-conjugated goat anti-mouse antibody, as previously described (Barry et al., 2010; Clancy and Duncan, 2009). Cells were suspended with 50 mM EDTA in PBS, fixed in 3.7% formaldehyde, and surface expression was measured using FACSCalibur (Becton Dickinson) by counting 20,000 cells. The fluorescence was analyzed using FCS Express 2.0 (De Novo Software).

2.5. Western Blotting

Protein samples were heated to 70º C for 5 min, then loaded into 15% acrylamide gels and electrophoresed at 170V for 55 min using the mini-protean III electrophoresis cell (Biorad). The proteins were then transferred to PVDF membranes using the Biorad wet transfer system. The membranes were blocked overnight in tris-buffered saline with tween-20 (TBS-T) containing 4% skim milk and 10% normal goat serum. Rabbit α-p10 1º antibody (1:10,000 dilution) was bound for 1 h, and then the excess was removed by extensive washing. Bound 1º antibody was then detected with HRP-conjugated goat α-rabbit 2º antibody (1:10,000 dilution) (Jackson Immunoresearch) for 1 h. After further washing, membranes were developed using ECLplus western blotting reagent (GE Healthcare) and imaged on the Kodak 4000 mm Pro CCD imager.

2.6. Cell-Surface Biotinylation

QM5 cells were seeded into 10 cm tissue culture dishes (Corning) and grown overnight to ~50% confluency, at which point the cells were transfected using 0.5 µg of plasmid DNA and PEI transfection reagent. At 6 hpt, the medium was replaced with fresh growth medium. At 24 hpt, cells were washed twice with Hank's balanced salt solution (HBSS) before being incubated in 0.1 mM DTT (+DTT) or HBSS (-DTT) for 5 min. This respectively cleaved disulfide bonds or allowed them to remain intact. Cells were then washed three times with HBSS before being incubated in 1 µg/ml maliemide-PEG_2-biotin for 25 min at 4º C (with shaking every 5 min) in order to biotinylate any free sulphydryl groups. Cells were then washed four times with HBSS to remove excess biotinylation reagent, then once with 1% BSA (in HBSS) to quench DTT. Following this, cells were washed twice with PBS, then incubated in 50 mM EDTA (in PBS) for 5 min to resuspend cells. Cells were then transferred to 1.5 mL eppendorf tubes and centrifuged at 700 x g for 7 min. The pellet was then lysed with RIPA buffer (50 mM Tris pH 8.0, 150 mM NaCl, 1 mM EDTA, 1% NP-40, 0.5% NaDOC) for 45 min on ice. The lysate was then centrifuged at maximum speed for 10 min in a benchtop microcentrifuge, and the supernatant was incubated overnight at 4º C with neutravidin beads (Invitrogen) to pull down biotinylated proteins. After incubation, the samples were washed three times with RIPA buffer to remove non-biotinylated proteins. Final pellets were then boiled in 2X protein solubilization buffer (PSB, 0.08 M Stacking buffer Tris pH 6.8, 2% SDS, 20% glycerol, 0.2% bromophenol blue (BPB), 0.6% Resolving buffer Tris pH 8.8 and 100mM DTT) to release biotinylated proteins into the supernatant, which was collected and frozen at -20º C.

2.7. Immunofluorescence Microscopy

QM5 cells grown on coverslips at approximately 50% confluence were transfected with FLAG- or c-myc-tagged versions of the indicated ARV or NBV p10

constructs as described above. At 24 hpt, cells were fixed with paraformaldehyde. Cells were then blocked with 1% BSA in PBS for 30 min, and then incubated with 1:1000 dilutions of mouse anti-FLAG and rabbit anti-c-myc monoclonal antibodies for 1 h at room temperature. After thoroughly washing with PBS, the cells were incubated with 1:1000 dilutions of Alexa 488-conjugated goat anti-mouse antibodies and Alexa 647-conjugated goat anti-rabbit antibodies for 1 h at room temperature. Coverslips were then mounted and sealed on slides using prolong gold anti-fade reagent (Invirogen), then imaged using an Axiovert 200M inverted microscope (Zeiss).

2.8. Cholesterol Chelation

QM5 cell monolayers transfected with FLAG-tagged ARV p10 were treated with 2, 5, 10 or 20 mM MβCD for 20 min, then fixed with 3.7% paraformaldehyde. Immunofluorescence staining for surface-localized proteins was performed as described above. For cholesterol repletion experiments, QM5 cell monolayers transfected with FLAG-tagged ARV p10 or c-myc-tagged NBV p10 were treated with 20 mM MβCD for 20 min, then either immediately fixed, or treated with cholesterol-loaded MβCD for 30 min at 37º C, then fixed with 3.7% paraformaldehyde. Cholesterol-loaded MβCD was prepared by dissolving cholesterol (6 mg/ml) in 20 mM MβCD in serum-free medium by vigorous vortexing and heating at 37° C for 30 min, then filtering to remove insolubile cholesterol. Immunofluorescence staining for surface-localized proteins was performed as described above.

2.9. Spinning Disc Confocal Microscopy

QM5 cell monolayers grown on glass coverslips were transfected with EGFP-tagged NBV p10. At 24 hpt, live cells were imaged using a spinning-disc confocal microscope (3i Intelligent Imaging Innovations, Denver, CO) consisting of a Cell Observer Z1 microscope (Zeiss), an Evolve EMCCD camera (Photometric), and a CSU-X1 spinning disk head (Yokagawa) and live-cell imaging capability. Images were

captured at 1 min intervals to monitor the movement of fluorescently-tagged proteins. At t=100 sec, 20 mM MβCD in HBSS was circulated into the cell chamber to chelate cholesterol. The diffusion of p10 proteins was followed for an additional 800 seconds. Images were acquired using the Slidebook imaging software (Version 5.0).

2.10. FRET-Based Multimerization Assay

2.10.1. Image Acquisition

Sensitized emission FRET provides a sensitive, minimally disruptive tool to examine protein-protein interactions. We developed a multimerization assay using the EGFP/mCherry FRET pair. This pair was selected because it shows good spectral overlap, yet has low crosstalk between donor and acceptor channels and the emission spectra are independent from pH and halide ion concentration (Albertini et al., 2012). Since the efficiency of energy transfer between fluorophores varies inversely to the power of 6 with the distance between the donor and acceptor, EGFP emission will only induce mCherry excitation if the average spatial separation of the fluorophores does not exceed 5-10nm, which is a distance only stably observed during a direct interaction of tagged proteins (Ahn et al., 2002). We co-transfected C-terminally EGFP-tagged and C-terminally mCherry-tagged p10 FAST proteins, as well as indicated mutants, into QM5 monolayers. Formaldehyde-fixed cells were imaged at 100x in widefield mode using the Zeiss LSM 510 META confocal microscope. Cells were imaged under a 100x oil immersion, 1.4 NA Plan Apochromat objective. EGFP was excited and detected using a 40 mW Argon 458/477/488/514 nm laser, a BP450-490 excitation filter and a BP515-565 barrier emission filter. mCherry was excited and detected using a HeNe 548 nm laser and LP590 emission filter. The PixFRET Image-J plug-in was used to calculate donor and acceptor spectral bleed-through (SBT) values, as well as normalized FRET (NFRET) levels in each pixel.

2.10.2. Spectral Bleed-Through Determination

Donor and acceptor SBT were determined by acquiring one stack of two images (the FRET and the donor/acceptor images) of cells expressing either EGFP-only or mCherry-only. For each stack, the SBT ratios were mathematically modeled after background subtraction. While SBT and fluorophore intensity are theoretically linearly related, in practice it is often observed that SBT ratios vary as a function of fluorophore intensity. This may be caused by the use of different photomultiplier tubes for the donor and FRET images (Ahn et al., 2002). To deal with this issue, donor and acceptor SBT ratios were modeled using exponential relationships with fluorophore intensity after exclusion of aberrant background values at low intensities and the application of a Gaussian blur.

2.10.3. Background Subtraction and FRET Normailization

With the SBT values determined, the NFRET for the p10-p10 interaction was calculated. A stack of three images was acquired for each cell imaged: I) the sensitized emission FRET image (donor excitation, acceptor emission), II) the donor image (donor excitation, donor emission), and III) the acceptor image (acceptor excitation, acceptor emission). Background subtraction and Gaussian blur of the donor, acceptor and FRET channels were performed on each image of the stack prior to analysis. The FRET signal was normalized to the square root of the product of the donor and acceptor fluorescence intensities for each pixel of each image using equation (1).

$$\mathbf{NFRET} = \frac{\mathbf{I_{FRET} - I_{EGFP} \times BT_{EGFP} - I_{mCherry} \times BT_{mCherry}}}{\sqrt{\mathbf{I_{EGFP} \times I_{mCherry}}}} \quad (1)$$

This normalization controlled for variations in fluorophore expression levels between images and provided a quantification of FRET intensity that is comparable between different samples (Apellaniz et al., 2011).

2.10.4. Data Summary and Presentation

Pixel amplitude distributions of the 8-bit NFRET images generated by the PixFRET software were summarized as histograms using a bin width of 0.03906 NFRET

units. Each histogram was fit with four Gaussian distributions, and that with the highest calculated R^2 value was used for further analysis. Ten images were acquired for each condition in duplicate (a total of twenty images). The mean NFRET (mNFRET) was determined for each image from the best-fit Gaussian distribution. The grey box highlights the standard deviation of mNFRETs, the + indicates the mean mNFRET, the line is the median mNFRET and the whisker ends indicate the absolute min and max mNFRETs for each condition. The Gaussian-fitted NFRET histograms were also used to calculate the average pixel amplitude from each condition. Error bars represent standard error propagated within and across experiments.

2.11. Synthetic Peptides and Aggregation Studies

Peptides corresponding to the ectodomain (residues 1-40) of the ARV p10 protein were synthesized by Genscript to contain a disulfide bond between residues 9 and 21. Peptides corresponding to residues 4-36 of the ARV p10 ectodomain, as well as those corresponding to the NBV p10 ectodomain (residues 1-35) were synthesized by United Peptide to contain a disulfide bond between residues 6 and 18, and 5 and 17 respectively. Aggregation of the ARV p10 ectodomain peptide (0.5 mM), with and without DTT (5 mM), was followed by OD350 measurements using a Varian Cary 50 UV/Vis spectrophotometer.

2.12. Lipid Mixing Assay

A fluorescence resonance energy transfer (FRET)-based mixing assay was employed to monitor the lipid-mixing potential of synthetic p10 ectodomain peptides (Predescu et al., 2005). Large unilamellar vesicles composed of a 40:20:20:20 ratio of 1,2-dioleoyl-sn-glycero-3- phosphocholine (DOPC): 1,2-dioleoyl-sn-glycero- 3-phosphoethanolamine (DOPE):Cholesterol:Sphingomylein (Avanti Polar Lipids) in 10 mM phosphate buffer with 100 mM NaF, pH 7.4, were prepared as previously described (Corcoran et al., 2004) and extruded to 100 nm. A fluorescently-labeled liposome

population was similarly prepared to contain 2 mol% each of 1,2-dioleoyl-sn- glycero-3-phosphoethanolamine-N-(7-nitro-2-1,3- benzoxadiazol-4-yl) (NBD-DOPE) and 1,2-dioleoyl-sn-glycero-3-phosphoethanolamine-N-4-(lissamine rhodamine B sulfonyl) (Rho-DOPE). Non-labeled and labeled liposomes were incubated at 37º C in a 9:1 ratio at a concentration of 100 mM prior to addition of ARV or NBV p10 synthetic peptides at the indicated concentrations, or a buffer blank control. Fluorescence was recorded for up to ten minutes. The percent lipid mixing was calculated using the equation (2).

$$\% \, Lipid \, Mixing = \left[\frac{(F_t - F_0)}{F_{MAX} - F_0}\right] \times 100 \quad (2)$$

A third liposome population of 0.2 mol% each of NBD-DOPE and Rho-DOPE represented the theoretical maximum (F_{MAX}) level of lipid mixing. All experiments were performed in quadruplicate.

2.13. Circular Dichroism Spectroscopy

Far-UV (260-185 nm) CD spectra of p10ecto under indicated conditions were recorded using a Jasco J-810 spectropolarimeter (Easton, MD) with temperature control capability. CD data were collected at 37° C. Quartz cuvettes with path length of 0.01 cm (Hellma, Müllheim, Germany) were used. A total of 6 accumulations were acquired in 0.1 nm steps and the raw data was converted to mean residue ellipticity [θ]. The value of [θ] for a given wavelength (λ), averaged over all accumulations and blank subtracted followed by sliding-window averaging over 3 nm stretches using equation (3), was determined.

$$[\theta] = \frac{1}{4}x_{n-1} + \frac{1}{2}x_n + \frac{1}{4}x_{n+1} \quad (3)$$

2.14. Electron Microscopy

LUV's (100nm) composed of 50:20:20:10 of DOPC:DOPE:CH:SM (100 μM) were incubated with either buffer alone, ARV p10 or NBV p10 ectodomain peptides (10 μM) for 5 min at 37 ºC. Samples were settled on to a Formvar/Carbon coated grid and incubated with a 2% uranyl acetate stain. Samples were visualized using a JEOL JEM

1230 Transmission Electron Microscope (Tokyo, Japan). Liposome sizes were determined by measuring diameters of at least 900 liposomes present in 5 random fields from two separate experiments at 50000-80000x magnification using ImageJ. Liposome sizes were binned and presented as percent liposomes in each bin size, or as percent total liposome volume in each bin size, calculated by dividing the sum of liposome volumes in each bin by the total volume of all liposomes measured.

2.15. Liposome-Peptide Binding Assay

LUVs (100 nm) of a constant 20% DOPE and 10% SM composition, containing indicated amounts of CH and corresponding DOPC, were incubated in a 1:10 ratio with p10ecto peptide (125 μM) in 250 μl of 10 mM phosphate buffer with 100 mM NaF, pH 7.4, with or without 5 mM DTT. Samples were thoroughly mixed with an equivalent volume of 60% sucrose, and then overlaid with 800 μl of 20% sucrose and 100 μl of buffer, successively. Samples were subjected to centrifugation at 50K rpm for 45 min at 4º C in a Beckman SW60 Ti rotor (256,760 xg), and then the liposome-containing fraction was removed. Samples were mixed with 2x protein sample buffer (20% SDS, glycerol, Tris-HCl, pH 6.8) and separated by tricine gel SDS-PAGE at a constant 50 mA for 3.5 h. Gels were subjected to silver staining to visualize peptides. Silver-stained gels were images using a Kodak 4000mm Pro CCD imager.

CHAPTER 3

Results

3.1. The p10 Cystine Loop Fusion Peptide

3.1.1. NBV p10 is an Inherently Better Fusogen than ARV p10

As previously reported, the p10 FAST proteins of the ARV clade induce syncytiogenesis at a slower rate than those of the PRV clade (Salsman et al., 2005). To directly compare the induced syncytiogenic rates, I selected representative isolates from each clade: the ARV 176 isolate (referred to hereinafter as ARV) and the NBV isolate. First, I confirmed the previous observation that the p10 proteins from these two isolates qualitatively differ in the levels of syncytium formation at 24 hpt, as observed by Giemsa-stained QM5 monolayers (Figure 3.1A). Using a syncytiogenesis assay based on the average number of syncytial nuclei in five random microscopic fields across three replicates, this initial observation was quantified and expanded across a time-course in both QM5 and Vero cell monolayers (Figure 3.1B and C). These results confirmed that NBV p10 induces syncytiogenesis at a faster overall rate than ARV p10 with equivalent amounts of transfected DNA. This also demonstrated that the increased syncytiogenic activity of NBV is not a cell-specific result, as the overall trend of ARV- versus NBV p10-induced syncytiogenesis was consistent between cell types. The difference between static levels of ARV and NBV p10-induced syncytiogenesis was most apparent at ~24 hpt, with the number of syncytial nuclei in NBV-transfected monolayers being ~3-4 fold higher than that of ARV (Figure 3.1B). This time point represents the best indicator of the ARV/NBV syncytiogenic disparity, as it is in the middle of the exponential phase of ARV p10 transfected monolayers and just before the maximum observable level of NBV p10 transfected monolayers. The 24 h time point was used for further comparative analysis of the ARV and NBV p10 proteins.

It is possible that the observed difference in syncytiogenic activity between ARV and NBV p10 may be due to factors independent of the protein-specific syncytiogenic activity of these two proteins. It has previously been shown that ARV p10 is rapidly

degraded prior to reaching the cell surface, where it accumulates in a stable form (Shmulevitz et al., 2004a). If NBV p10 is synthesized more rapidly, degrades more slowly, or otherwise accumulates in the plasma membrane at a higher level than ARV p10, an increase in syncytiogenic activity would directly result. Surface-expression levels were determined for N-terminally triple FLAG-tagged versions of each protein using fluorescence activated cell sorting (FACS), normalizing fluorescence measurements to ARV p10 **(**Figure 3.2A**)**. There was no significant difference between the surface-localized levels of ARV and NBV p10 in transfected QM5 monolayers (p=0.9826). As an additional control, I performed western blots on the same FLAG-tagged constructs (Figure 3.2B). To determine if the N-terminal FLAG-tags had an influence on p10 expression levels, I also measured total protein levels of authentic ARV p10 and FLAG-tagged ARV p10 (Figure 3.2C)**.** These results revealed there were no detectable expression differences between un-tagged and tagged versions of the p10 proteins. The similarities in total protein and surface expression levels of ARV and NBV p10 indicated these homologs are synthesized, degraded and trafficked within the cell at comparable rates, resulting in approximately equivalent cell-surface expression levels. When taken together, these data suggest that the inherent syncytiogenic activity of NBV p10 is greater than that of ARV p10.

3.1.2. The Ectodomains Confer Syncytiogenic Efficiency

Similarities in the repertoire and arrangement of structural motifs, as well as the similarities and differences in amino acid identity, between ARV and NBV p10 were exploited to further characterize functional motifs involved in p10-mediated syncytiogenesis. Through sequential PCR reactions, we permutationally exchanged the ecto-, TMD and endodomains between ARV and NBV p10. This resulted in six p10 chimeras (Figure 3.3A), which were named according to the proportion of domains present from each parental p10 protein. For example, the p10 chimera composed of the ARV TMD and endodomain with the NBV ectodomain is termed ARV ecto-NBV (abbreviated AectoN), as two of three domains are from the ARV p10 protein. N-terminally FLAG-tagging each p10 chimera allowed for comparable detection of each construct. Using FACS and western blotting analysis of N-terminally FLAG-tagged

constructs, we determined that the cell surface and total expression levels were approximately equivalent for all chimeras ($p=0.26$, one-way ANOVA of cell surface expression) (Figure 3.3C).

Using the same syncytiogenesis assay as for the parental p10 proteins, we quantified the syncytiogenic progression induced by each untagged chimera in transfected QM5 cell monolayers, revealing the contribution of each domain to the overall syncytiogenic rate (Figure 3.3C). Exchanging the TMDs or endodomains of ARV and NBV did not influence the rate or extent of syncytium formation; AtmN and AendoN had identical syncytiogenic kinetics as parental ARV p10. The same situation applied for the NtmA and NendoA chimeras, both of which shared the fusogenic activity of parental NBV p10. The ectodomains were the only p10 domains that individually altered the syncytiogenic rate when exchanged; the NBV ectodomain substantially increased the syncytiogenic activity of ARV p10 (AectoN chimera) while an ARV ectodomain impaired the fusogenic activity of NBV p10 (NectoA chimera). However, this did not result in a complete exchange of syncytiogenic activity. Both the AectoN and NectoA chimeras induced intermediate levels of syncytiogenesis compared to the parental proteins, indicating that the ectodomains directly contribute to the differing fusion activities of ARV and NBV p10 but require a homotypic TMD or endodomain to confer the full parental syncytiogenic activity. Indeed, if either ectodomain was present with the TMD or endodomain from the same parental protein, the syncytiogenic activity was equivalent to that parental protein. For example, exchanging the NBV ectodomain onto ARV (AectoN) increased the syncytiogenic activity to an intermediate phenotype. If either the NBV TMD or endodomain were then inserted into this construct, creating NendoA or NtmA, the syncytiogenic activity became identical to that of parental NBV p10. The reciprocal was also true for ARV domain exchange chimeras. These results indicated the ectodomains are necessary but not sufficient for maximal syncytiogenic efficiency, and suggested the TMD and endodomains function downstream of the ectodomain in similar or overlapping roles that augment the overall syncytiogenic efficiency.

3.1.3. The p10 Ectodomains Form Essential Intramolecular Disulfide Bonds

The ARV and NBV p10 HPs play an important role in p10-induced syncytiogenesis, and the cysteine residues flanking these regions are absolutely essential for function (Cheng et al., 2005; Shmulevitz et al., 2004b), as shown by the effect of serine substitutions on syncytiogenesis (Figure 3.4A). A previous study using non-reducing SDS-PAGE detected no change in p10 migration, as would be expected if p10 formed disulfide-stabilized multimers, indicating the cysteine residues are not involved in intermolecular interactions (Shmulevitz et al., 2004b). To determine whether these cysteines formed an intramolecular disulfide bond, a membrane-impermeable biotinylation assay was developed to detect free thiol groups cell-surface localized p10. At 24 hpt, ARV p10-transfected QM5 monolayers were either left untreated, or treated with 0.1 mM dithiothreitol (DTT) to reduce disulfide bonds. Free thiol groups in both treated and untreated cells were labeled with maleimide-PEG2-biotin, which were then bound to neutravidin beads and detected via Western blotting using ARV p10-specific antiserum. In the absence of DTT treatment, no p10 was detected (Figure 3.4C), suggesting the cysteine residues do not contain free thiol groups. Additionally, when either of the two cysteine residues were substituted with serine (C9S and C21S, respectively) the remaining cysteine was available to react with the biotinylation reagent, resulting in a detectable band under both DTT-treated and untreated conditions. These results implied the p10 ectodomain cysteines form an intramolecular disulfide bond, suggesting the p10 HPs exist as disulfide-stabilized loops that are required for membrane fusion activity and syncytiogenesis.

3.1.4. Sequence Context of Cysteines Affects p10 Disulfide Bond Formation

In FPs of enveloped viral fusion proteins, the relative location of key residues can be critical for membrane fusion activity (Delos et al., 2000; Qiao et al., 1999; Steinhauer et al., 1995). Previous studies on the ARV and NBV p10 HPs indicate substitution of specific amino acids is detrimental to syncytiogenesis (Cheng et al., 2005; Shmulevitz et

al., 2004b), although it is unclear whether these substitutions have any influence on the disulfide bonding status of the p10 ectodomains. To examine the constraints on p10 disulfide bond formation, eight ARV p10 cysteine shift constructs (S1-S8) were created by varying the relative position of one or both cysteine residues, effectively altering the size of the loop and the position of residues within the loop (Figure 3.5A). All cysteine shift constructs failed to induce detectable syncytiogenesis in transfected QM5 monolayers (Figure 3.5B). The disulfide bonding status of each construct was determined using the cell-surface biotinylation assay, which revealed that all but the S5 construct failed to form the essential intramolecular disulfide bond (Figure 3.5C). The presence of bands in both the DTT-treated and untreated lanes indicates the proteins were accessible to the membrane-impermeable biotinylation reagent, implying they successfully trafficked to the plasma membrane through the oxidizing environment of the endoplasmic reticulum (ER) where disulfide bond formation usually occurs (Sevier and Kaiser, 2006). This suggests that the size of the cystine loop, the relative positioning of key amino acids within the loop, or the sequence context flanking the cysteine residues either alters the protein folding energy, making it no longer favorable to form a stable disulfide bond, or that the cysteines are no longer recognized by thiol oxidoreductases and thus disulfide bond formation is not catalyzed. It has been shown in the context of other proteins that formation and stability of disulfide bonds can be altered by the amino acid context of neighboring residues (Goldenberg et al., 1993; Goldenberg and Zhang, 1993; Zhang and Snyder, 1989).

Interestingly, the S5 construct (H20C/C21S), which shortened the loop by one residue from the C-terminus, retained its ability to form a disulfide bond but still did not induce syncytiogenesis, implying disulfide bond formation and the sequence or relative positioning of amino acids within the loop both influence p10 membrane fusion activity. Additionally, the histidine at position 20 that was replaced by cysteine in the S5 construct may play an important role in p10-mediated membrane fusion; this residue is absolutely conserved in all isolates of both ARV and NBV p10 (Figure 1.5), suggesting an evolutionary ion preference for this residue at this location in the loop. Substitution of histidine with alanine eliminated syncytiogenic activity (Figure 3.5D), further supporting

a role in mediating some aspect of membrane fusion. The disulfide-bonding status of this construct would need to be assessed to strengthen this conclusion.

Creation of the cysteine shift constructs involved a minimum of two amino acid substitutions (Figure 3.5A). Three additional constructs were created to vary the size of the loop and position of key residues within the loop without substituting or eliminating any authentic p10 sequence. This was accomplished by inserting alanine residues in the loop adjacent to one or both cysteine residues (Figure 3.6A). All alanine insertions effectively increased the size of the loop, while either conserving (C9/20+A) or changing (C9+A and C20+A) the relative position of key residues. All three of these constructs failed to induce syncytiogenesis in transfected QM5 cell monolayers (Figure 3.6B), and also were defective for intramolecular disulfide bond formation (Figure 3.6C). The acute sensitivity of p10 disulfide bond formation to even minor, conservative changes in and around the HP reflects the extremely high evolutionary constraints on the amino acid content of this region.

3.1.5. The N-terminal p10 Ectodomain Region Defines an Independent Motif Governing Cystine Loop Formation

To further define motifs within the ectodomain that contribute to fusion potential, six additional constructs were created that exchanged small segments between the ARV and NBV p10 ectodomains. These exchanges were guided by the presence of diverged p10 sequences between the avian and pteropine clades (Figure 1.5). Using sequential PCR reactions, constructs were made that exchanged the sequences bracketing the HP (constructs A1, A3, N1, and N3 in Figure 3.7A), the sequences within the cysteine-flanked HP (constructs A2 and N2), the non-conserved residue adjacent to the N-terminus of the CM (constructs A4 and N4), and the four membrane-proximal residues (constructs A5 and N5). Quantitative syncytiogenesis assays revealed that chimeras composed of residues exchanged within or flanking the HP were unable to induce syncytium formation in transfected QM5 monolayers (Figure 3.7B). The cell-surface biotinylation assay previously employed to identify the cysteine loop in ARV p10 also revealed that NBV p10 forms a cystine loop, as cells had to be treated with DTT before

plasma-membrane localized NBV p10 could react with the thiol-specific biotinylation reagent (Figure 3.7C). More notably, ARV and NBV constructs A1-A3 and N1-N3 constructs could all be biotinylated in the absence of DTT treatment, indicating the presence of free thiols and inability to form an intramolecular disulfide bond. Conversely, constructs A4, A5, N4 and N5, which contained substitutions flanking the CM, remained fusion-active (Figure 3.7B) and were able to form the essential intramolecular disulfide bond (Figure 3.7C). Thus, the N-terminal ~25 ectodomain residues of ARV and NBV p10 define a single motif required for species-specific formation and fusion activity of an essential cystine loop FP.

3.1.6. ARV and NBV p10 Syncytiogenic Efficiency Correlates with Ectodomain Fusion Peptide Activity

In the enveloped viral fusion proteins, triggered conformational changes expose the hydrophobic FPs, which partition into bilayers and are proposed to alter membrane curvature and/or destabilize lipid bilayers (Durell et al., 1997; Han et al., 2001; Martin et al., 1999; Pecheur et al., 1999 ; Tamm et al., 2002). The HP of the p10 ectodomain functions similarly to enveloped viral FPs in a fluorescent lipid mixing assay (Shmulevitz et al., 2004b), although the level of p10-induced lipid mixing was substantially lower than that of enveloped viral FPs (Pecheur et al., 1999 ; Sackett et al., 2010). However, the presence of the essential intramolecular disulfide bond in the peptides used in the lipid mixing assay was not confirmed. To determine the effect of disulfide bonding on the lipid destabilizing and mixing abilities of the p10 proteins, synthetic peptides of ARV and NBV p10 ectodomains were commercially synthesized to include the disulfide bond, as confirmed by mass spectrometry. Measuring the lipid mixing activity using a fluorescent lipid-mixing assay (Sackett et al., 2010; Struck et al., 1981) revealed the NBV p10 ectodomain consistently induced higher levels of lipid mixing than that of ARV p10 in a dose-dependent manner (Figure 3.8).

3.1.7. Cystine Loop Formation Causes p10 Peptide Aggregation

In collaboration with Muzaddid Sarker, a nuclear magnetic resonance (NMR) spectroscopist, we attempted to solve the structure of the ARV p10 ectodomain peptide in

aqueous and/or membrane mimetic environments. Unfortunately, although this peptide was initially soluble in aqueous solvents, it slowly aggregated over time (Figure 3.9B), precluding structural analysis under these conditions. Incubating the p10 peptide with 5 mM DTT prevented aggregation in aqueous conditions (Figure 3.9B), suggesting the intramolecular disulfide bond may force solvent exposure of hydrophobic residues located within the FP loop, resulting in peptide aggregation.

Using a truncated version of the p10 ectodomain peptide representing amino acids 4-36 (missing the N-terminal Met-Leu-Arg residues and the C-terminal Ser-Ile-Ile-Ala residues; Figure 3.9A), 2D ^{1}H-^{1}H TOCSY and 2D ^{1}H-^{1}H NOESY solution-state NMR data were acquired in sodium dodecyl sulfate (SDS), dodecylphosphocholine (DPC) lipid mimetic environments, as well as in dimethylsulfoxide (DMSO) and hexafluoroisopropanol (HFIP) organic solvents at 22 and 37 °C (Figure 3.9C). Unfortunately, the NMR spectra did not exhibit a sufficient number of spin systems to be consistent with the set of constituent amino acids in any of the conditions (data not shown). Despite this, assignment of the peaks and identification of the spin systems were attempted in DMSO, which displayed the maximum number of peaks with reasonable intensities among the four conditions. Out of 33 amino acids present in the peptide, only nine representing Ala28-Ser36 (numbers represent p10 sequence positions) could be identified unambiguously. Another 13 amino acids, scattered throughout the rest of the peptide, were also identified but were primarily ambiguous due to missing sequential correlations in the NOESY spectrum. Spin systems corresponding to the remaining 11 amino acids were completely lacking from the NMR spectra. Thus, <28% of the p10 residues were unambiguously assignable, making high-resolution structural determination impossible even in the best case environment of DMSO. The spectral features indicated the majority of the peptide was undergoing conformational exchange on the intermediate NMR time-scale (i.e., on the order of milliseconds) (Cavanagh et al., 2007) in all conditions. However, the unambiguously assigned peaks corresponding to the Ala28-Ser36 segment indicated this region was not undergoing such conformational exchange, but was homogeneously structured in DMSO. Presumably, the observable peaks in HFIP, SDS and DPC were also mostly from this region of the peptide. Interestingly, this region of the p10 protein corresponds to the conserved amino acids of the CM (Figure 1.5).

Given the poor overall solution-state NMR characteristics, we did not pursue full structural determination of this short, well-behaved segment of the p10 ectodomain.

3.1.8. Cystine Loop Formation is Required for p10 Lipid Binding and Lipid Mixing Activity

While a high-resolution, three-dimensional structure of the p10 ectodomain was unattainable, I reasoned that far-ultraviolet (UV) circular dichroism (CD) spectroscopy might provide insights into the functional implications of p10 disulfide bond formation. The global secondary structure characteristics of the ARV p10 ectodomain peptide under both oxidized and reduced conditions in aqueous and liposome environments were therefore determined by CD analysis. There was a dramatic change in the CD spectrum when the peptide was assessed in aqueous versus liposome environments, and this change only occurred when the disulfide bond was present (Figure 3.10A). Furthermore, ARV p10 ectodomain peptides containing the cystine loop induced ~40% lipid mixing in the fluorescent lipid mixing assays while reduced versions of this peptide displayed only ~5% lipid mixing using the same peptide:lipid ratio (Figure 3.10B). Disulfide bond formation is therefore required for both membrane-induced structural transitions and for functional lipid-destabilizing activity of the p10 ectodomain.

It was unclear from the above results whether the cystine loop is required for membrane binding, which then induces structural transitions required for ectodomain lipid mixing activity. To address this issue, the ectodomain peptide was incubated with liposomes at room temperature in the absence or presence of DTT, and liposomes were isolated by sucrose-density gradient ultracentrifugation. The resulting liposome fraction was isolated and analyzed for the presence of p10 ectodomain peptide by tricine gel electrophoresis and silver staining. Results indicated the p10 ectodomain partitioned into liposomes, but only under non-reducing conditions (Figure 3.10C). Thus, the p10 cystine loop is required for p10 association with liposomes and structural transitions of the p10 ectodomain, both of which correlate with p10-induced lipid mixing.

3.1.9. Lipid Mixing Activity, but Not Lipid Binding or Lipid-Induced Structural Transitions, is Dependent on Membrane Cholesterol

Lipid composition can have profound effects on membrane fusion (Haque et al., 2001). To examine the effects of lipid composition on p10 lipid mixing activity, lipid mixing assays were performed using liposomes composed of DOPC:DOPE:CH:SM in various molar ratios. For all experiments, the mol % of DOPE was kept constant at 30%, while that of DOPC was varied with CH or SM as indicated. When varying CH, the mol % of SM was kept at 10%. Similarly, when varying the amount of SM, the mol % of CH was kept at 20%. The level of p10-induced lipid mixing increased from 0% CH to 10% CH ($P<0.0001$) and 10% CH to 20% CH ($P=0.0005$), however there was no significant change between 20% CH and 30% CH ($P=0.2227$) (Figure 3.11A). An increase in lipid mixing activity due to increased CH mol % was not observed for the low level of lipid mixing induced by reduced p10 ectodomain peptides ($P=0.3890$) (Figure 3.11C), suggesting the presence of CH does not simply alter the overall fusogenicity of the membrane, but rather the p10 ectodomain specifically disrupts CH-containing membranes. Lipid mixing activity was also sensitive to SM, although not to the same extent as CH; lipid mixing activity increased slightly from 0% SM to 10% SM (the same lipid formulation as 20% CH in Figure 3.11A, $P=0.0182$), but there was no significant change between 10% SM and 20% SM ($P=0.2352$) while 30% SM induced a slight decrease in lipid mixing activity ($P=0.0007$) (Figure 3.11B). These variances suggest that some SM is required, possibly to form complexes with CH and stabilize these membranes (Haque et al., 2001); however, too much SM, and the concomitant decrease in PC, are detrimental to the fusion activity of p10.

CH levels directly influence the structure and lipid mixing activity of the HIV gp41 FP (Lai et al., 2012) and CH also affects the conformation of SNARE transmembrane domains, which modulates the kinetics of membrane fusion (Chang et al., 2009). To further define the role of CH in p10-mediated lipid mixing, the global secondary structure characteristics of the p10 ectodomain peptide were examined in the presence of liposomes containing various mol % of CH (Figure 3.11D). Interestingly, despite the pronounced effect of CH concentration on p10-induced lipid mixing (Figure

3.11A), no there were no discernible differences in the structural conformation of p10 ectodomain peptides interacting with liposomes containing 0%, 10%, 20% or 30% CH. Additionally, the ability of disulfide-bonded p10 peptides to partition into liposomes was not influenced by the CH content (Figure 3.11E). These results identify an important and specific role for CH in p10 FP-induced lipid mixing that is independent of ectodomain structural transitions and partitioning into membranes.

3.1.10. Lipid Mixing Occurs in the Absence of Liposome Tubulation

Overcoming the thermodynamic barriers to membrane fusion in the absence of mechanical energy from protein conformational changes poses a challenge for small membrane fusion proteins, such as the FAST proteins. It has been suggested that such barriers may be overcome via the induction of high positive curvature in the target membrane. In the case of the C2-domains of synaptotagmin-1 and DOC2 components of the SNARE vesicle fusion complexes, membrane insertion of hydrophobic domains is proposed to induce membrane curvature that converts spherical liposomes into narrow tubules, creating highly curved lipidic termini that fuse to the termini of adjacent tubules (Martens et al., 2007; McMahon et al., 2010). To determine whether p10-induced lipid mixing arises via a similar process, 10 μM ARV and NBV p10 ectodomain peptides were mixed at 37^{o} C with 100 μM liposomes composed of 40:30:20:10 DOPC:DOPE:CH:SM, the same conditions under which lipid mixing was observed (Fig 3.11). Samples were then examined by electron microscopy following negative staining. As shown in representative images (Figure 3.12B), there was no evidence of tubulated liposomes. There was, however, a noticeable increase in the heterogeneity of liposome sizes. To quantify this effect, the diameters of approximately 100 liposomes from random fields were measured and binned into size classes. There was a clear increase in the size distribution and mean diameter of liposomes incubated with p10 peptide versus those incubated with buffer when liposome sizes were plotted against the percent of liposomes in each size class (Figure 3.12A, top row). The increase in liposome size was better represented when the liposome numbers were plotted against the percent liposome volume (Figure 3.12A, bottom row). These results provided direct evidence that p10-induced lipid mixing involves liposome merger, and that these fusion events occurred in

the absence of observable liposome tubulation. Hence, large-scale curvature induction does not appear to be an energy contributor to p10-induced membrane fusion.

3.2. The p10 Membrane-Proximal Ectodomain Regions

3.2.1. The p10 Ectodomains Direct Homotypic Clustering on the Plasma Membrane

Results indicated that the ARV and NBV p10 proteins are expressed similarly with respect to total cellular and surface protein levels (Figure 3.2A and B). The previously performed FACS analysis only detected overall surface levels of each protein, not possible differences in plasma membrane distribution of the ARV and NBV p10 proteins. To address this issue, QM5 cells were co-transfected with N-terminally FLAG-tagged ARV p10 and N-terminally myc-tagged NBV p10, and then fixed using paraformaldehyde in order to prevent permeablization. Simultaneous visualization of both proteins on the surface was then performed using immunofluorescence microscopy. Both p10 proteins displayed a punctate staining pattern randomly distributed over the cell surface, with little to no colocalization between ARV and NBV puncta (Figure 3.13A). In contrast, FLAG- and myc-tagged versions of the same parental protein perfectly colocalized in puncta (Figure 3.13B), indicating each punctum comprises a homotypic clustering of more than one p10 protein.

To identify the p10 domain(s) responsible for the distinct ARV and NBV p10 surface clustering, the previously created chimeric p10 domain exchange constructs were N-terminally myc-tagged and co-expressed with N-terminally FLAG-tagged parental constructs. ARV p10 constructs containing an NBV TMD or endodomain perfectly colocalized with parental ARV p10, while the ARV construct containing the NBV ectodomain displayed almost no colocalization with ARV p10 (Figure 3.14A). The same situation occurred with the NBV constructs; an ARV ectodomain prevented colocalization with parental NBV p10 while constructs with an ARV TMD or endodomain colocalized with NBV p10 (Figure 3.14B). Colocalization was also observed

in cells co-expressing FLAG-tagged ARV p10 and myc-tagged NectoA (NBV p10 containing and ARV ectodomain), as well as in cells co-expressing FLAG-tagged NBV p10 and myc-tagged AectoN (ARV p10 with an NBV ectodomain) (Figure 3.14C). The p10 ectodomains are therefore both necessary and sufficient to determine homotypic p10 clustering in the plasma membrane.

3.2.2. Homotypic p10 clustering in the plasma membrane is directed by two MPER motifs

Fortuitously, while investigating factors governing rates of syncytiogenesis for the ARV and NBV p10 proteins, several p10 chimeras with small ectodomain segment exchanges or various point substitutions were created (Figure 3.7A). These constructs, once N-terminally myc-tagged or FLAG-tagged, provided an excellent tool to probe the protein motifs governing p10 homotypic clustering. By transfecting cells with an N-terminally FLAG-tagged version of the ARV C9S construct, which is physically incapable of forming a disulfide bond, I determined that there is no association between disulfide-bond formation and p10 surface localization or distribution patterns; ARV C9S perfectly colocalized with parental ARV p10 (Figure 3.15**)**.

The series of ARV and NBV constructs containing small segment substitutions in the ectodomain were used for fine domain mapping of sequences governing p10 clustering in membrane microdomains. QM5 monolayers were co-transfected with N-terminally FLAG-tagged versions of parental p10 proteins and N-terminally myc-tagged versions of each ectodomain exchange construct (A1-A5 and N1-N5 from Figure 3.7A), and fixed, non-permeablized cells were examined by immunofluorescence microscopy. Remarkably, exchange of the four diverged ectodomain juxtamembrane residues, hereinafter referred to as the p10 neck regions, converted homotypic p10 clustering to heterotypic clustering; ARV p10 with the NBV neck region perfectly colocalized with NBV p10 and visa versa (Figure 3.16).The p10 neck regions are therefore responsible for homotypic p10 clustering in the plasma membrane. Interestingly, these four neck residues, which connect the TMD to the CM, can be exchanged between the ARV and NBV p10 proteins with no effects on syncytiogenesis (Figure 3.7B**)**, indicating the distinct

clustering pattern of ARV and NBV p10 does not influence their respective syncytiogenic activities.

3.2.3. The p10 MPER Motifs Regulate Overall Surface Clustering

The MPERs of various enveloped viral fusion proteins, including gp41 protein of human immunodeficiency virus-1 (HIV-1)(Ivankin et al., 2012), glycoprotein G of VSV (Jeetendra et al., 2003) and the F protein from human parainfluenza virus-2 (HPIV-2) (Tong et al., 2001), have all been shown to play active roles in the membrane fusion reaction. The importance of MPERs in membrane fusion has been attributed to various processes, such as lipid bilayer destabilization (Apellaniz et al., 2011; Shang et al., 2008; Vishwanathan and Hunter, 2008), modulation of viral membrane curvature (Ivankin et al., 2012), and CH recognition/interaction (Apellaniz et al., 2011; Epand et al., 2010). The MPERs of these enveloped virus fusion proteins are 12-41 residues long, they are sometimes enriched in tryptophan, and they frequently contain stretches of highly conserved amino acids (Apellaniz et al., 2011; Jeetendra et al., 2003; Li and Blissard, 2009; Tong et al., 2001). It is possible that the four neck residues exchanged in the p10 A5 and N5 constructs (Figure 3.7A) function as part of larger motifs, which may include the adjacent nine residues of the conserved motif (CM) (Figure 1.5). Earlier work demonstrated that amino acids within the CM are essential for syncytiogenic activity, and that point substitutions in this motif might qualitatively lower cell surface expression levels (Shmulevitz et al., 2004b). To further elucidate the role of the CM in p10-mediated syncytiogenesis, each non-alanine/glycine amino acid of the ARV p10 CM was individually substituted to either a relatively conserved amino acid or alanine (Figure 3.17A**)**. Each alanine/glycine residue was also individually substituted to the obverse. Additionally, the neck residues exchanged in the A5 and N5 constructs, which are responsible for p10 clustering specificity, were collectively mutated to alanine in both the ARV and NBV p10 proteins (Figure 3.17A). Interestingly, although these substitutions had no effect on cell surface expression levels, as measured by FACS analysis of N-terminally FLAG-tagged versions of these constructs, all of the above-mentioned substitutions resulted in syncytiogenically inactive p10 proteins (Figure 3.17A). Surface immunofluorescence also revealed these 14 CM point substitutions, as well as the two

neck region alanine substitutions, had a diffuse, rather than a puncate, surface-staining pattern (Figure 3.17B), indicating the p10 MPER, encompassing both the CM and neck residues, governs the essential clustering of p10 proteins on the cell surface.

3.2.4. Co-clustering of Fusion Incompetent p10 Constructs with Parental p10 Exerts a Dominant-Negative Effect on Syncytiogenesis

Exchange of the neck regions redirected p10 to a heterotypic clustering pattern (Figure 3.16) but had no effect on disulfide loop formation (Figure 3.7C) or syncytiogenic activity (Figure 3.7B), indicating localization of ARV and NBV p10 to discrete clusters does not contribute to differing fusion efficiencies of these FAST proteins. To further explore the relationship between homotypic clustering and fusion activity, syncytium formation was assessed in QM5 cells co-transfected with a parental p10 protein and an equivalent amount of plasmid DNA expressing one of several chimeric or substituted constructs that had various effects on p10 clustering and syncytiogenesis. Co-transfecting cells with the same parental p10 (i.e. twice the dose of p10-expressing plasmid DNA) increased syncytiogenesis ~50-100% relative to cells co-transfected with empty vector (e.g., ARV + ARV relative to ARV + vector, and NBV + NBV relative to NBV + vector; Figure 3.18A). Co-expressing authentic p10 with constructs defective in both syncytium formation and clustering (e.g. CM constructs or alanine substitutions of the neck regions) had the same effect as co-transfecting empty vector; these constructs had no effect on parental p10-induced syncytiogenesis (Figure 3.18A). Alternatively, co-expressing the ARV p10 C9S construct, which is fusion-incompetent but retains the MPER homotypic clustering motif, eliminated ARV p10-induced syncytium formation but had no effect on NBV p10 syncytiogenesis (Figure 3.18B). Conversely, a C9S substitution in an ARV p10 A5 background (i.e., ARV p10 containing the NBV p10 neck region) suppressed NBV p10-induced syncytium formation by ~99% (Figure 3.18B). Fusion-deficient constructs therefore exert a potent dominant-negative effect, but only when co-localized in the same cluster as a parental p10 protein. The low level of residual fusion activity observed in cells co-expressing NBV p10 and

A5-C9S was likely mediated by a limited number of clusters containing only NBV p10. Titrating the amount of NBV p10 plasmid DNA transfected into QM5 cell monolayers confirmed that very low levels of NBV p10 are sufficient to induce syncytiogenesis (Figure 3.18C**).**

Lastly, co-expressing ARV or NBV p10 with heterotypic neck region substitution constructs that co-localize with each other (i.e., ARV p10 with NBV N5, or NBV p10 with ARV A5; see Figure 3.16) resulted in approximately equivalent, intermediate fusion phenotypes; syncytium formation was more extensive than that induced by ARV p10 alone but reduced relative to NBV p10 alone (Figure 3.18A). Taken together, these results indicate each p10 cluster represents a "fusion unit", and the population of p10 proteins present in individual clusters dictates the overall syncytiogenic efficiency.

3.2.5. ARV and NBV p10 Clustering is Dependent on Membrane Cholesterol

CH has been implicated as a major factor in both the multimerization and localization of membrane proteins (Christopherson et al., 2003; Engel et al., 2012; Lindwasser and Resh, 2001; Ono et al., 2007; Scheiffele et al., 1997). It has also been demonstrated that membrane fusion induced by several enveloped viral fusion proteins (Kielian and Helenius, 1984; Rawat et al., 2003; Takeda et al., 2003), by SNARE proteins (Chang et al., 2009; Lang et al., 2001), and by the RRV p14 FAST protein (Corcoran et al., 2006) is dependent on CH-rich microdomains on the cell surface. Acute extraction of CH from QM5 cells expressing N-terminally FLAG-tagged ARV p10 using methyl-β-cyclodextrin (MβCD) for 20 min (Yancey et al., 1996) resulted in a dose-dependent alteration in p10 plasma membrane staining from punctate to diffuse (Figure 3.19A). Live-cell fluorescence imaging with C-terminally EGFP-tagged p10 indicated the punctate plasma membrane localization of p10 was rapidly converted to a diffuse staining pattern following addition of MβCD to cells (Figure 3.19B). Most interestingly, the diffuse, overlapping staining pattern of ARV and NBV p10 in the absence of CH rapidly reverted to segregated, homotypic, punctate staining when membrane CH was restored using CH-loaded MβCD (Figure 3.19C). The differential distribution of ARV and NBV

p10 is therefore not due to differences in protein trafficking, but rather specific protein-protein or protein-lipid interactions occurring in the plasma membrane. Together, this data indicates the p10 ectodomain directs the reversible and preferential homotypic clustering of plasma membrane-localized ARV and NBV p10 into species-specific, CH-dependent microdomains.

Proteins that interact with cholesterol often do so using a cholesterol recognition-interaction amino acid consensus (CRAC) motif. The CRAC motif is defined by the sequence L/VX_{1-5}YX_{1-5}-R/K-, where X_{1-5} represents one to five residues of any amino acid (Epand, 2006). An eight-residue sequence on the C-terminal side of the p10 TMD contains several alternate combinations of a CRAC sequence (L_{60}LYCCKAK_{67}), and previous results indicated alanine substitution of K67 eliminates ARV p10-induced syncytium formation (Shmulevitz et al., 2003). However, as predicted from the chimeric studies indicating that the ectodomain directs p10 clustering, alanine substitutions of either or both lysine residues in this membrane-proximal endodomain motif had no effect on p10 microdomain association (Figure 3.20).

3.2.6. The MPER Directs ARV and NBV p10 Cholesterol-dependent Homomultimerization

Although the p14 FAST protein was recently shown to form multimers using a co-immunoprecipitation assay (Corcoran et al., 2011), previous use of the same assay to detect p10 multimers was unsuccessful (Shmulevitz et al., 2003). We reasoned that ARV and NBV p10 might only form stable multimers when present in CH-rich membrane microdomains, which would be disrupted by detergent conditions employed for co-immunoprecipitation. To determine if p10 puncta stabilize p10 multimers, we employed fluorescence resonance energy transfer (FRET) *in cellulo*. Since the efficiency of energy transfer between fluorophores varies inversely to the 6^{th} power of the distance between donor and acceptor fluorophores, FRET only occurs if the average spatial separation of the fluorophores is <5-10nm, a distance only stably observed during direct protein-protein interactions (Sekar and Periasamy, 2003). The efficiency of this process can be characterized by the Förster radius, R_0, which is the donor-acceptor distance at which the

probability of FRET-mediated donor de-excitation is 50%, given by equation (4).

$$R_0 = ck^2 n^{-4} \phi_D \epsilon_A \frac{\int_0^\infty F_D(\lambda)\epsilon_A(\lambda)\lambda^4 d\lambda}{\int_0^\infty F_D(\lambda) d\lambda} \quad (4)$$

where c is 8.786x10^{-11} mol L^{-1} cm nm^2, k^2 is the orientation factor of the donor and acceptor molecules (2/3 for randomly oriented molecules), n is the refractive index of the medium, Φ_D is the quantum yield of the donor, ϵ_A is the extinction coefficient of the acceptor at the absorption peak, $\epsilon_A(\lambda)$ is the absorption line-shape, and F_D is the fluorescence line-shape.

ARV and NBV p10 proteins were C-terminally tagged with either enhanced green fluorescent protein (EGFP) or a monomeric derivative of red fluorescent protein (mCherry), a FRET pair with good spectral overlap but low donor-acceptor cross-talk levels (Albertazzi et al., 2009). For simplicity, EGFP and mCherry tags will be referred to as GFP and mCh, respectively. These two molecules have an R_0 of 5.1 nm (Patterson et al., 2000). The PixFRET Image-J plug-in (Feige et al., 2005) was used to calculate donor and acceptor spectral bleed-through (SBT) values and normalized FRET (NFRET) intensities using pixel-by-pixel analysis of sensitized emission FRET. Images were acquired from 10 cells for each condition in two separate experiments (a total of twenty images/condition), and mean NFRET (mNFRET) values determined for each image from the best-fit Gaussian distribution as described in Materials and Methods. Positive controls included a uni-molecular FRET pair (i.e., GFP directly attached to mCh via a flexible linker) and a bi-molecular FRET pair, the multimeric p14 FAST protein, both of which gave positive FRET signals (Figure 3.21). The negative controls, free GFP co-expressed with free mCh (Figure 3.21C), ARV-GFP or NBV-GFP co-expressed with free mCh (Figure 3.21) and ARV-mCh or NBV-mCh co-expressed with free GFP (data not shown), yielded no detectible FRET signals.

As shown in the fluorescence images (Figure 3.21A) and NFRET quantification (Figure 3.21C), ARV and NBV p10 both formed homomultimers in cells but failed to heteromultimerize. CH extraction with MβCD eliminated the detectible FRET signal (Figure 3.22), indicating p10 multimerization and p10 clustering in the plasma membrane are both CH-dependent. However, restoring CH in the cell membrane, using CH-loaded

MβCD, allowed multimers to re-form (Figure 3.22), indicating that p10 multimerization, like surface clustering, is reversible. Additionally, two representatives of the CM substitutions that abrogate ARV p10 plasma clustering (D31E and T35A) also eliminated multimerization as shown by loss of FRET signal (Figure 3.23). Similarly, co-expressing ARV p10-GFP with ARV-mCh containing either alanine substitutions of the four neck residues (A-neck construct) or the heterologous neck residues from NBV p10 (ARV A5 construct) eliminated the FRET signal, as did similar co-transfections with NBV p10 constructs (Figure 3.23); all of these neck constructs also abrogated fusion activity and p10 clustering in the plasma membrane (Figures 3.16 and 3.17). Conversely, co-expression of ARV p10 with the NBV N5 construct (NBV p10 with the four neck residues of ARV p10), or co-expression of NBV p10 with the corresponding ARV A5 construct, both generated positive FRET signals (Figure 3.23) and co-clustered in the plasma membrane (Figure 3.16). The MPER therefore controls CH-dependent, reversible homomultimerization and clustering of p10 in plasma membrane fusion platforms, while the tetra-peptide neck residues are solely responsible for determining multimer specificity.

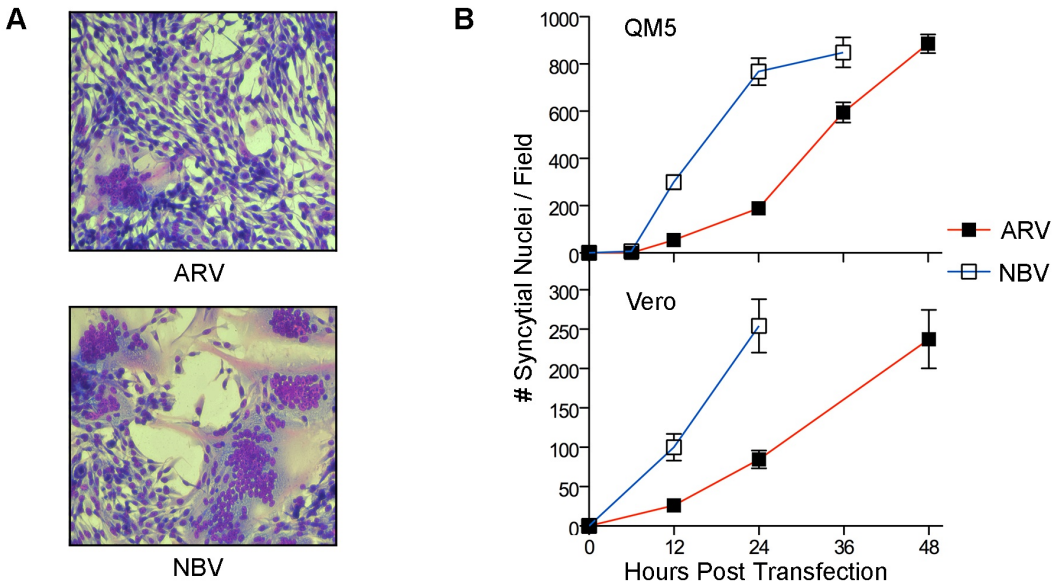

Figure 3.1- NBV p10 induced syncytiogenesis at a faster rate than ARV p10. (A) Representative images of Geimsa stained QM5 monolayers expressing ARV and NBV p10 at 24 hpt. (B) The syncytiogenic progression of ARV (red) and NBV (blue) in transfected QM5 (top) and Vero (bottom) cell monolayers. Syncytial nuclei present in five random fields of Giemsa stained monolayers were counted at indicated times post-transfection and presented as mean ± SEM (n=3).

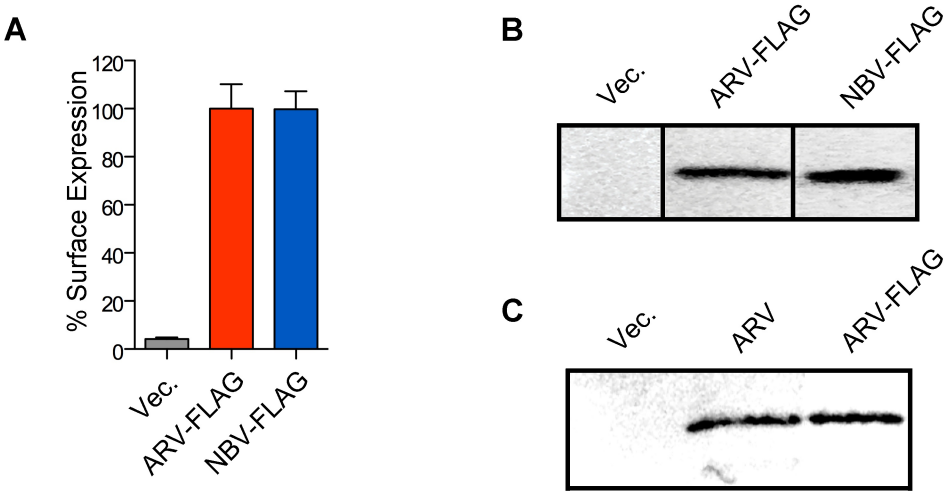

Figure 3.2- ARV and NBV p10 are expressed in the cell at similar levels. (A) Percent surface expression relative to ARV p10 measured by flow cytometry of N-terminally FLAG-tagged ARV and NBV p10 constructs. B) Steady-state expression levels of N-terminally FLAG-tagged ARV and NBV p10 constructs detected by western blotting. Lanes in the western blot were spliced together from a single blot. Surface expression levels are presented as mean ± SEM (n=3). (C) Western blot comparison of steady-state expression levels of authentic ARV p10 and N-terminally FLAG-tagged ARV p10 using α-p10 antiserum.

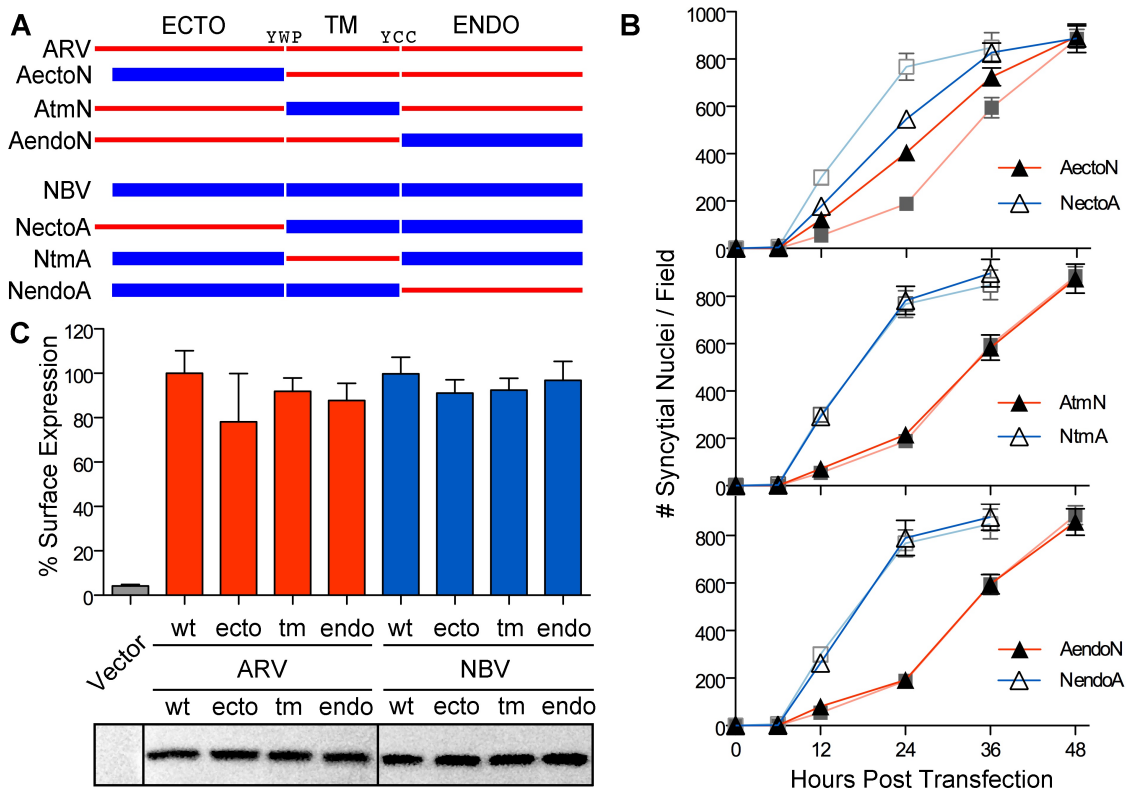

Figure 3.3- The p10 ectodomains are major determinants of syncytiogenic efficiency. (A) The ecto-, TM and endodomains of ARV (red) and NBV (blue) p10 were permutationally exchanged, using sequential PCR reactions, to create six chimeric p10 constructs named as indicated. (B) Syncytiogenic progression of chimeric ecto (top), TM (middle) and endodomain (bottom) p10 constructs in transfected QM5 cell monolayers, determined as in Figure 2B. Parental syncytiogenic rates are shown as watermarks for reference. Numbers of syncytial nuclei at the indicated timepoints are presented as mean ± SEM (n=3). The syncytiogenic progressions induced by parental ARV and NBV p10 are shown in watermark on each graph. (C) Surface expression levels (top) measured by flow cytometry, and steady-state expression levels (bottom) detected by western blotting, of N-terminally FLAG-tagged versions of the parental p10 and chimeric p10 constructs. Lanes in the western blot were spliced together from a single blot. Percent surface expression presented as mean ± SEM (n=3) relative to parental (wt) ARV or NBV p10.

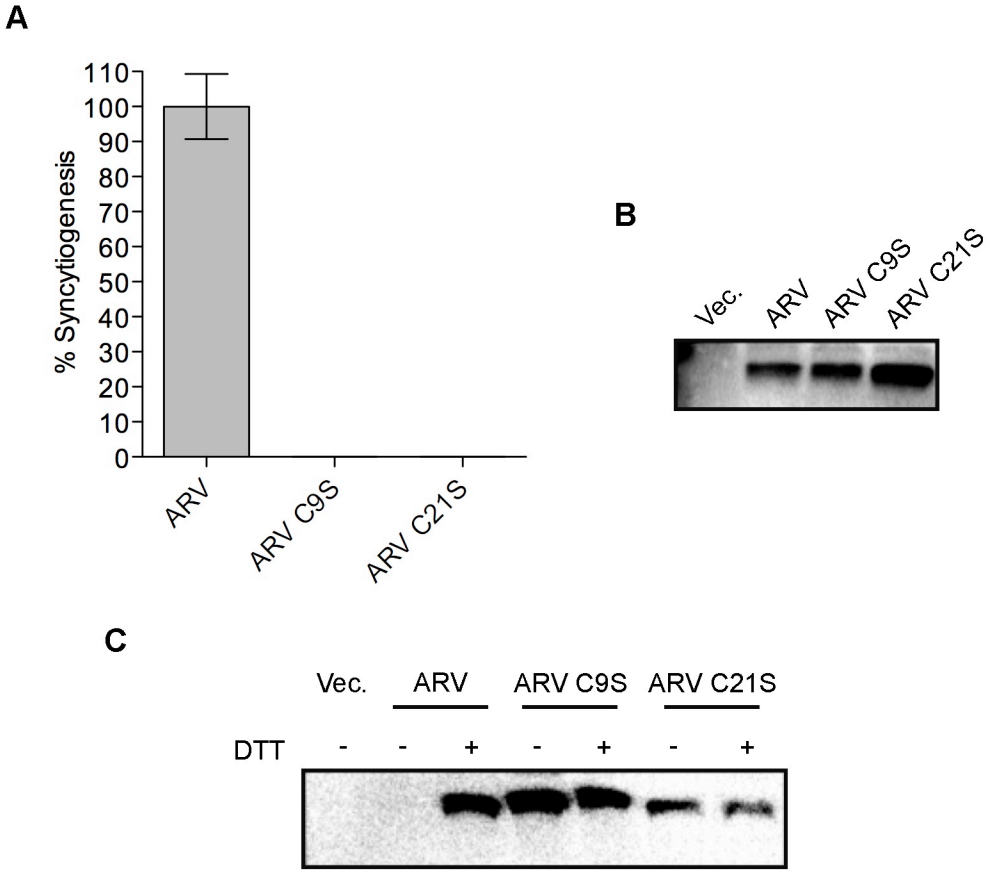

Figure 3.4- The p10 ectodomain cysteine residues form an essential intramolecular disulfide bond. (A) Indicated p10 constructs were transfected into QM5 cell monolayers and the syncytiogenic levelsquantified at 24 hpt. All values are normalized to parental ARV p10 and are presented as the mean ± SEM (n=3) (B) Steady-state levels of ARV p10 and ARV p10 cysteine constructs detected via Western blotting with α-p10 endodomain antiserum. (C) QM5 cell monolayers were transfected with authentic and cysteine knockout p10 constructs, and at 24 h post-transfection, cells were incubated in HBSS with or without 0.1mM DTT prior to treatment with membrane-impermeable maleimide-PEG2-biotin to detect free thiol groups in the p10 ectodomain. Biotinylated proteinswere isolated using neutravidin beads and p10 detected via Western blotting with α-p10 endodomain antiserum.

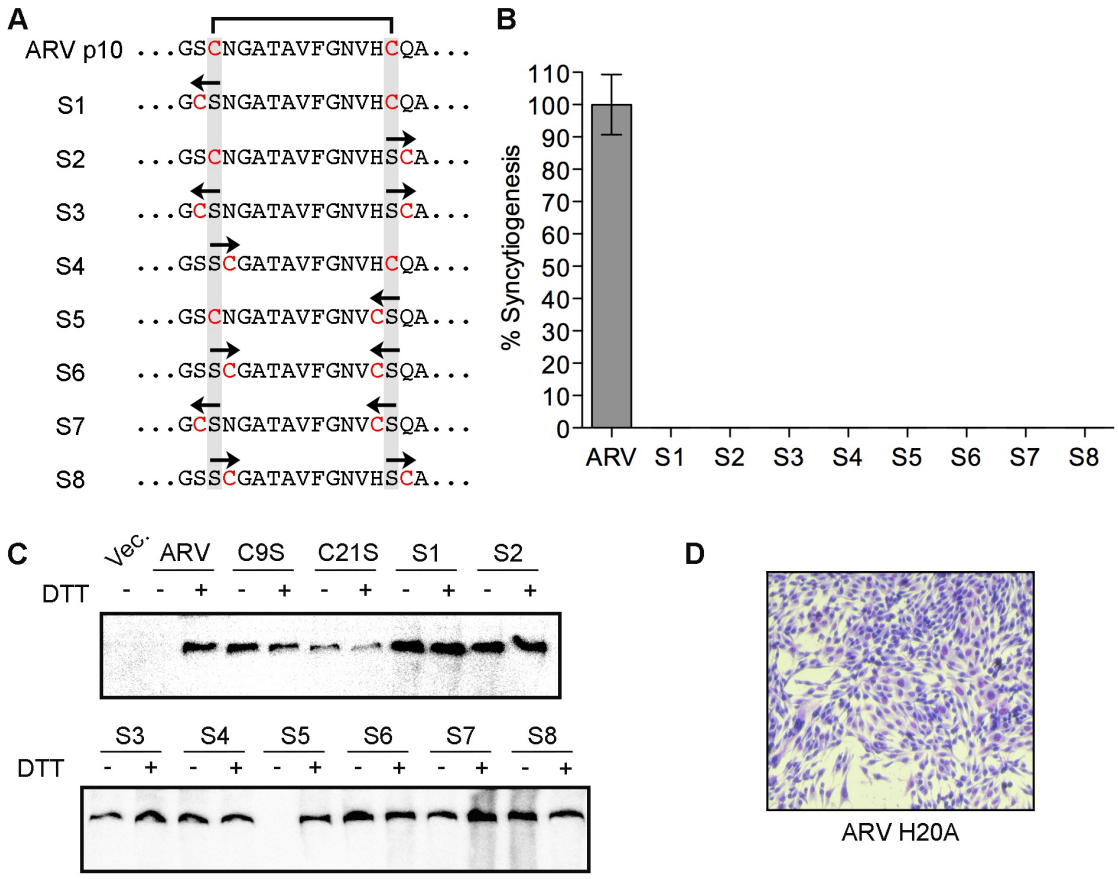

Figure 3.5- Syncytiogenic activity and disulfide bond formation are highly sensitive to the location and context of the cysteine residues. (A) Amino acid substitutions were used to shift the location of the conserved p10 cysteine residues (red). Arrows indicate the relative positional shift of cysteine residues in each construct. (B) Indicated p10 constructs were transfected into QM5 cell monolayers and the syncytiogenic levels were measured at 24 hpt. All values are normalized to parental ARV p10 and are presented as the mean ± SEM (n=3) (C) QM5 cell monolayers transfected with authentic and p10 cysteine shift constructs were transfected into QM5 monolayers and at 24 h post-transfection, cells were incubated in HBSS with or without 0.1mM DTT prior to treatment with membrane-impermeable maleimide-PEG2-biotin to detect free thiol groups in the p10 ectodomain. Biotinylated proteins were isolated using neutravidin beads and detected by western blotting using FLAG-specific antiserum (D) Geimsa stained a QM5 monolayer transfected with ARV p10 H20A constructs.

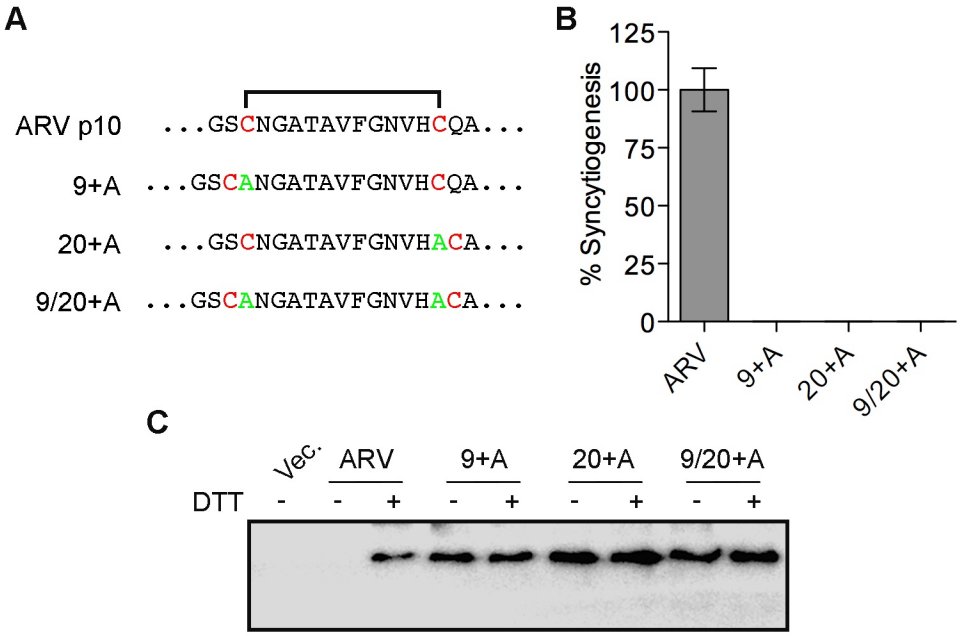

Figure 3.6- Fusion activity and disulfide bond formation are sensitive to the relative spacing of cysteine residues. (A) Alanine residues were inserted at positions 9 and 20 separately and in combination to manipulate the size of the loop and orientation of key residues within the loop. (B) Indicated p10 constructs were transfected into QM5 cell monolayers and the syncytiogenic levels measured at 24 hpt. All values are normalized to parental ARV p10 and are presented as the mean ± SEM (n=3) (C) QM5 cell monolayers transfected with authentic and alanine insertion p10 constructs were transfected into QM5 monolayers and at 24 h post-transfection, cells were incubated in HBSS with or without 0.1mM DTT prior to treatment with membrane-impermeable maleimide-PEG2-biotin to detect free thiol groups in the p10 ectodomain. Biotinylated proteins were isolated using neutravidin beads and detected by western blotting using FLAG-specific antiserum.

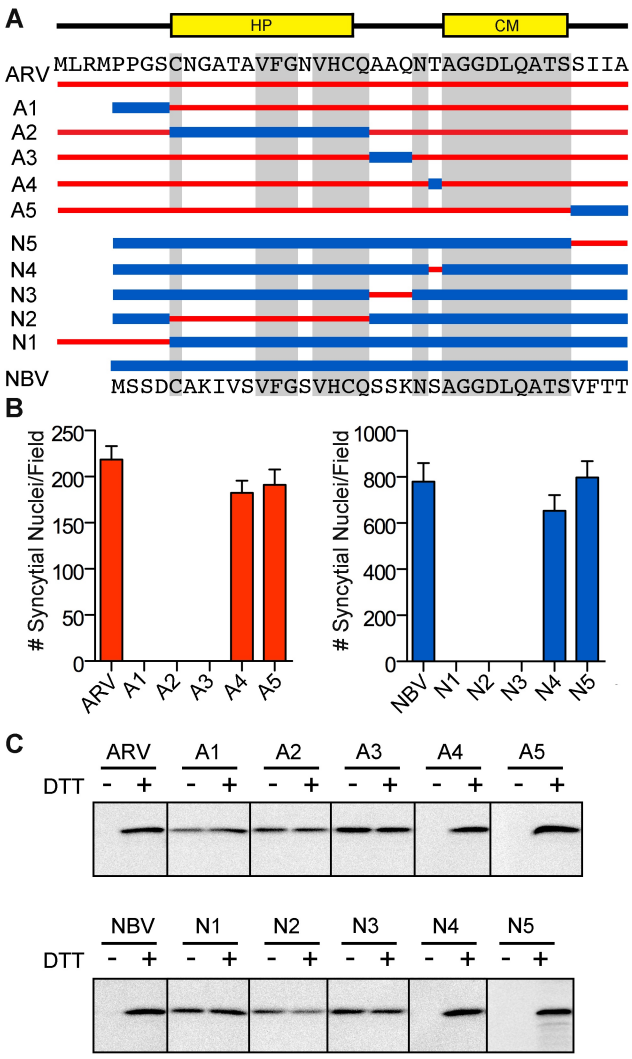

Figure 3.7- A distinct N-terminal ectodomain motif governs species-specific formation of an essential intramolecular disulfide-bond formation. (A) Ectodomain segments were exchanged between ARV and NBV p10 to create ten chimeric constructs (A/N 1-5). ARV sequences are represented as thinner red lines, while those of NBV are thicker blue lines. The amino acid sequences of ARV and NBV are included at the top and bottom, respectively. Background grey boxes denote conserved amino acids. Locations of the HP and CM are indicated above. (B) Syncytiogenic levels induced by each construct in transfected QM5 cells, as determined in Figure 2B, and presented as mean ± SEM (n=3). (C) N-terminally FLAG-tagged versions of the indicated chimeric ectodomain constructs were transfected into QM5 monolayers and at 24 hpt cells were incubated in HBSS with or without 0.1mM DTT prior to treatment with membrane-impermeable maleimide-PEG2-biotin to detect free thiol groups in the p10 ectodomain. Biotinylated proteins were isolated using neutravidin beads and detected by western blotting using FLAG-specific antiserum.

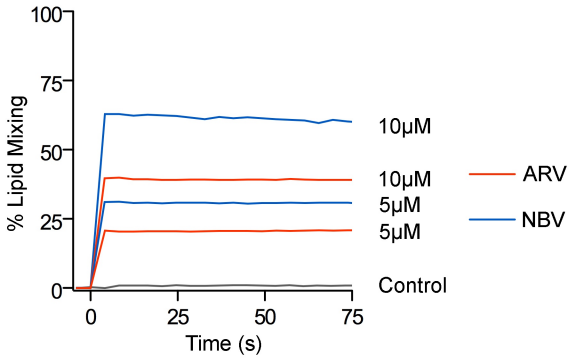

Figure 3.8- The NBV p10 ectodomain is more lipid destabilizing than that of ARV p10. Fluorescence resonance energy transfer was used to monitor the extent of lipid mixing induced by 5μM and 10μM ARV (red) and NBV (blue) ectodomain synthetic peptides incubated with 100 μM LUVs composed of DOPC-DOPE-cholesterol-sphingomyelin (40:20:20:20). The same assay was performed using buffer phosphate buffer instead of peptide (control, black).

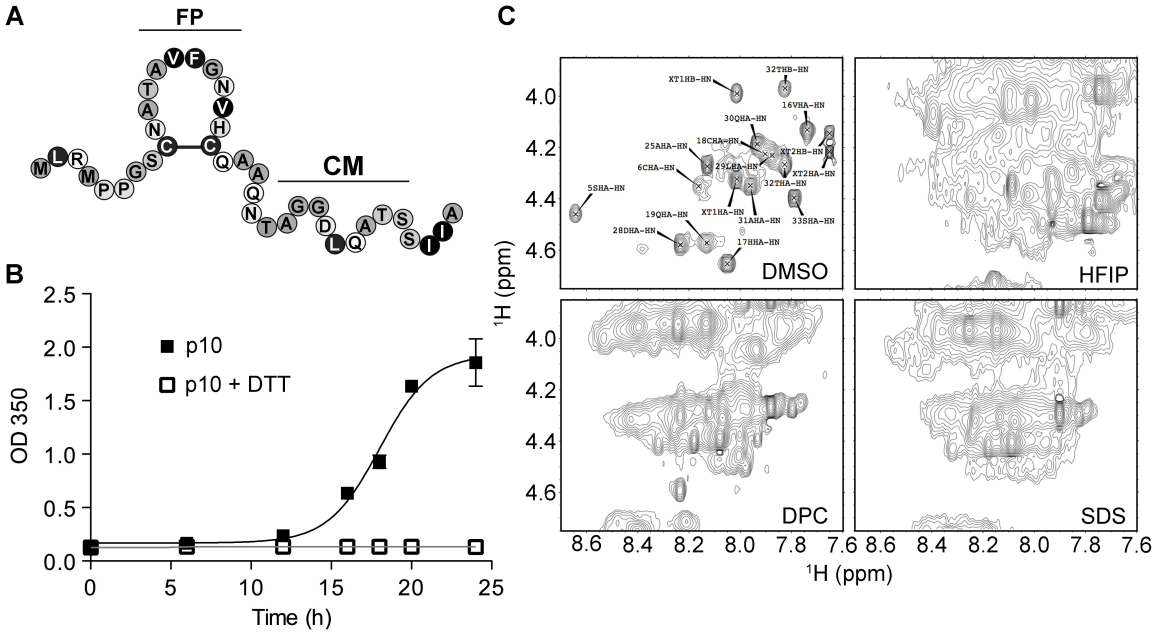

Figure 3.9- The p10 disulfide bond caused hydrophobic aggregation of synthetic peptides. (A) Pictorial representation of the ARV p10 ectodomain. Relative amino acid hydrophobicity (based on the Kyte and Doolittle hydrophobicity scale) is indicated by shading, with darker shades corresponding to higher hydrophobicity. Locations of the cystine loop fusion peptide (FP) and conserved motif (CM) are indicated. (B) OD350 measurements of p10ecto peptide (1 mM) aggregation in phosphate buffer (10 mM with 100 mM NaF, pH 7) over time with and without DTT (5mM). (C) H^{α}-H^{N} region of the 2D ^{1}H-^{1}H TOCSY of the truncated p10 ectodomain in two organic solvent and two micellar environments at 37 ºC. Spin systems from only a small proportion of the constituent amino acids, out of the 33 total, are observable. Sequential assignments were performed only in the DMSO condition, where the Ala28-Ser36 region was unambiguously assignable. NMR data kindly provided by Muzaddid Sarker.

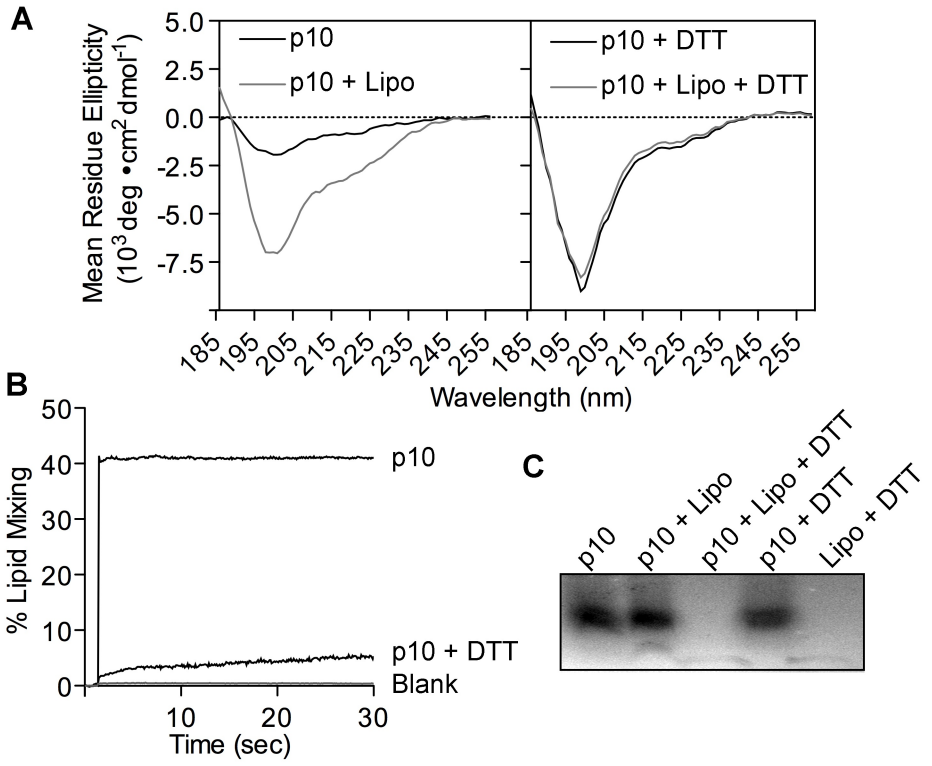

Figure 3.10- The p10 disulfide bond is required for structural transitions, membrane binding and lipid mixing activity. (A) CD measurements of the p10ecto synthetic peptide (50 μM) in aqueous (buffer) conditions or in the presence of liposomes (5 mM), with and without DTT (5 mM). (B) The liposome lipid mixing activity of the p10ecto synthetic peptide with and without DTT was determined as in Figure 3.8. (C) p10ecto synthetic peptide (10 μM) was mixed with liposomes (100 uM) in the absence (p10 + Lipo) or presence (p10 + Lipo + DTT) of 5 mM DTT, liposomes were isolated by sucrose gradient centrifugation, and liposome-associated p10ecto peptide assessed by electrophoresis on a tricine gel and silver staining. Input peptide levels in the absence (p10) or presence (p10+DTT) of DTT, and liposomes treated with DTT (Lipo + DTT) were included as controls

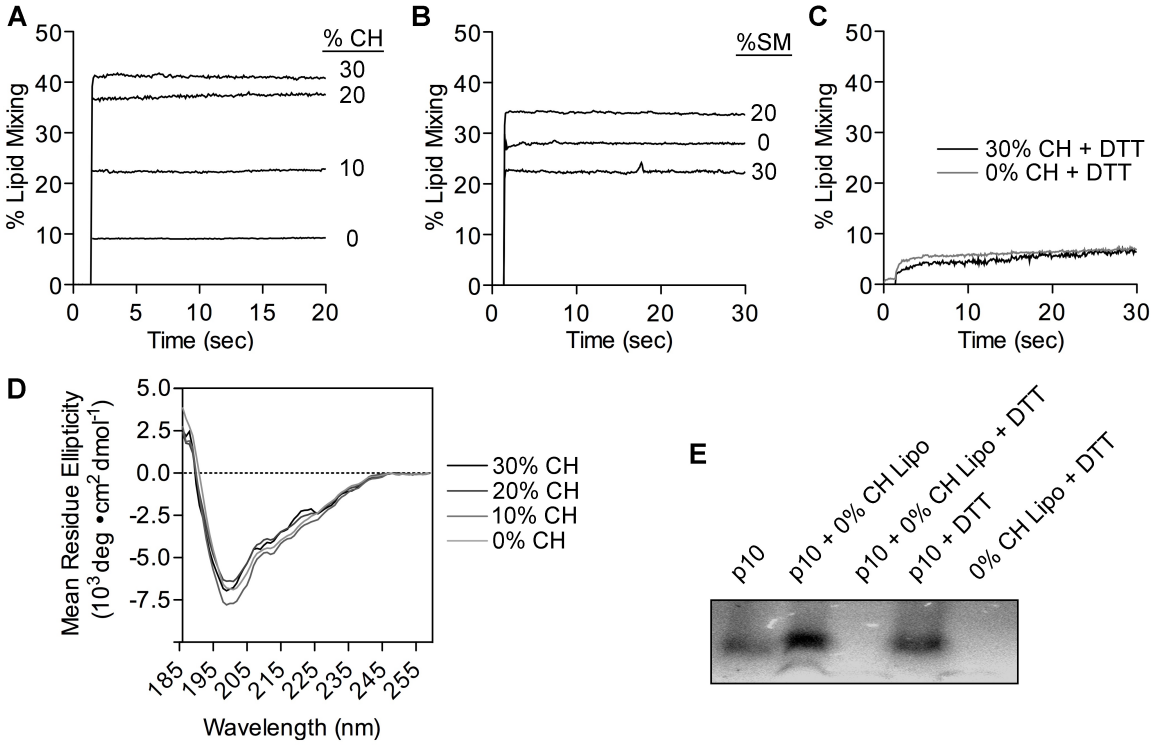

Figure 3.11- Cholesterol influences the lipid mixing stage of p10-mediated membrane fusion. The liposome lipid mixing activity of p10ecto synthetic peptides (10 μM) with liposomes (100 μM) of varying cholesterol (CH) content in the absence (A) or presence (C) of DTT (5 mM) (C), or with liposomes (100 μM) of varying sphingomelin (SM) content (B) were determined as in Figure 3.8. (D) CD measurements of the p10ecto synthetic peptide (50 μM) incubated with liposomes (5mM) of varying cholesterol content. (E) Silver-stained tricine gel showing the liposome binding abilities of p10ecto synthetic peptide to liposomes containing no CH were assessed as described in Figure 3.10C. Input peptide levels in the absence (p10) or presence of DTT (p10+DTT) and liposomes treated with DTT (Lipo + DTT) were included as controls.

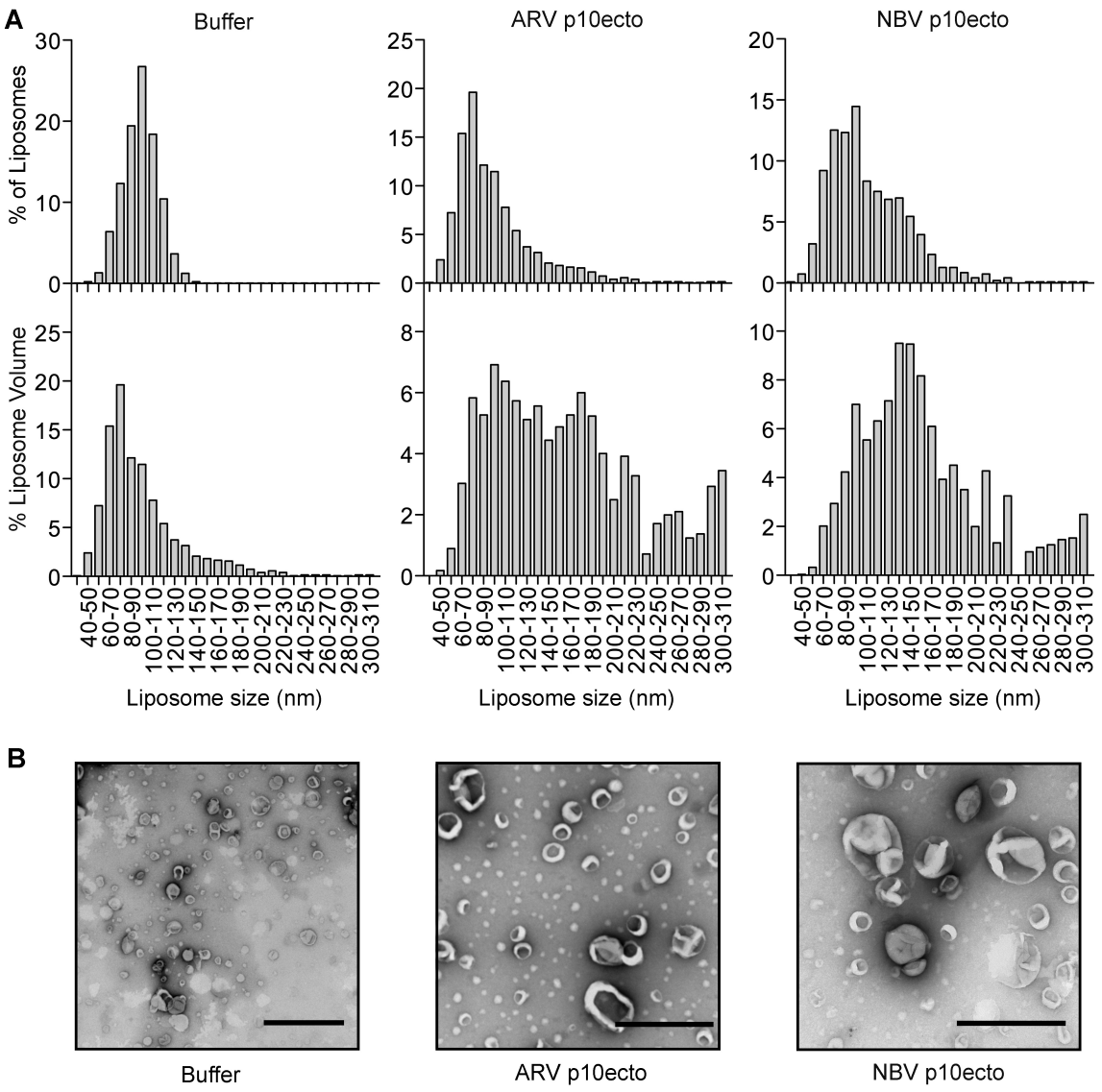

Figure 3.12- The p10 proteins induce liposome lipid mixing in the absence of tubulation. (A) Liposomes were incubated with buffer, ARV p10ecto peptide or NBV p10ecto peptide under lipid mixing conditions for 5 min, and electron microscopy of negative-stained samples was used to measure liposome diameters. Liposomes were binned into the indicated diameter ranges, and size distributions based on percent of total liposome counts (top) and percent of total liposome volume (bottom) are shown. Results are from duplicate experiments (B) Representative EM images of control liposomes (buffer), and liposomes incubated with ARV p10ecto and NBV p10ecto. Scale bars represent 500 nm.

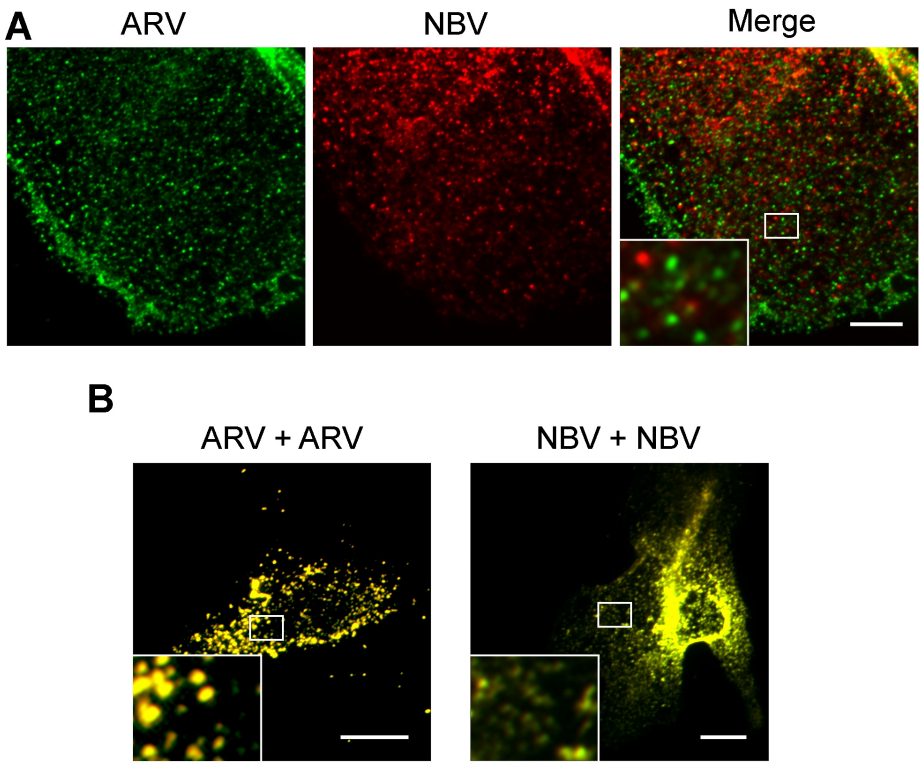

Figure 3.13- The p10 proteins homotypically cluster in the plasma membrane. (A) QM5 cell monolayers were co-transfected with N-terminally FLAG-tagged ARV p10 and N-terminally myc-tagged NBV p10. Cells were fixed without permeabilization and surface-localized ARV and NBV p10 detected with mouse-α-FLAG and rabbit-α-myc antisera, respectively. Bound antibodies were detected with Alexa Fluor 488 goat-α-mouse (green) and Alexa Fluor 647 goat-α-rabbit (red), and superposed in the merged image. (B) QM5 cell monolayers were co-transfected with N-terminally FLAG-tagged and N-terminally myc-tagged ARV or NBV p10. Cells were fixed with paraformaldehyde and surface-localized p10 was detected using mouse-α-FLAG and rabbit-α-myc antisera. Bound antibodies were then detected with Alexa Fluor 488 goat-α-mouse (green) and Alexa Fluor 647 goat-α-rabbit (red). Images are merged to show colocalization (yellow). Scale bars = 10 μm.

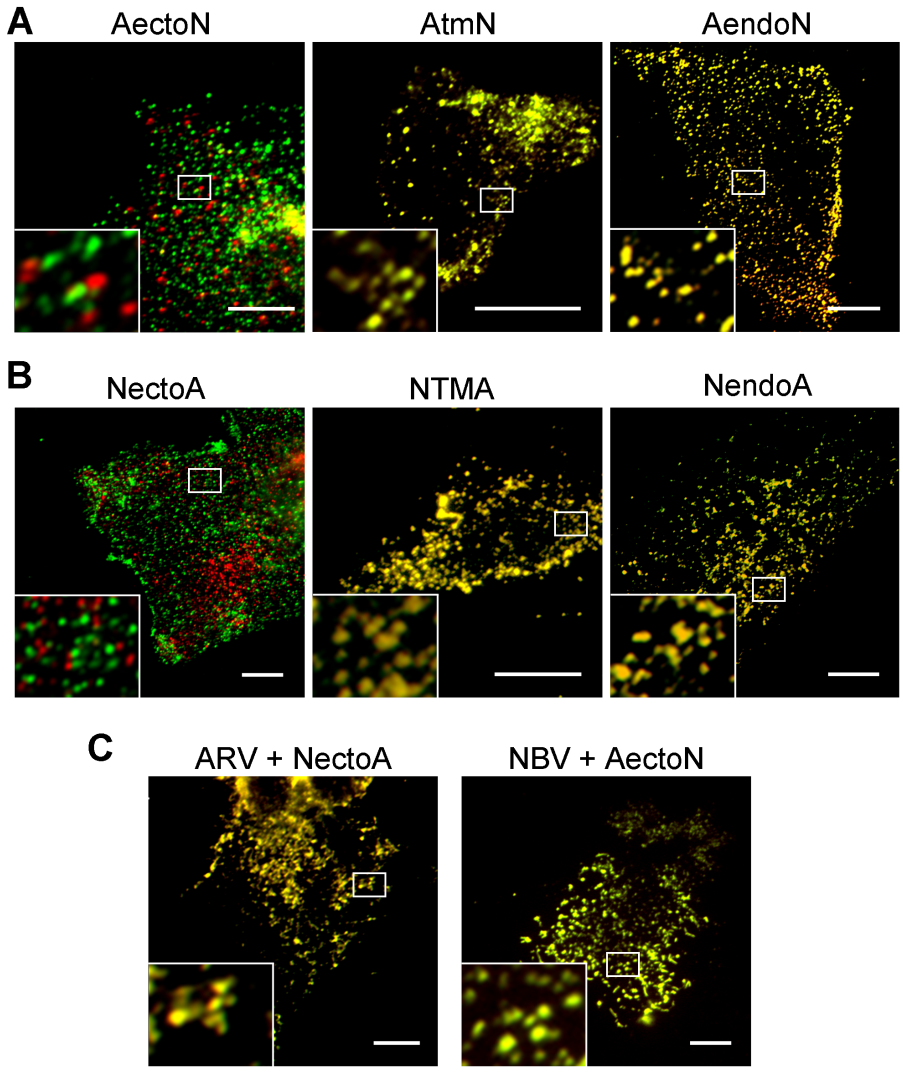

Figure 3.14- The p10 ectodomains determine homotypic clustering in the plasma membrane. (A) As in Figure 3.13, except cells were co-transfected with N-terminally FLAG-tagged ARV p10 (top row) or N-terminally FLAG-tagged NBV p10 (bottom row) and the indicated N-terminally myc-tagged chimeric constructs. (B) QM5 cell monolayers were co-transfected with N-terminally FLAG-tagged versions of the indicated parental p10 proteins and N-terminally myc-tagged versions of the indicated ectodomain chimeras. Cells were fixed and stained as in panel A. Scale bars = 10 µm. Insets are 400% enlargements of the indicated areas.

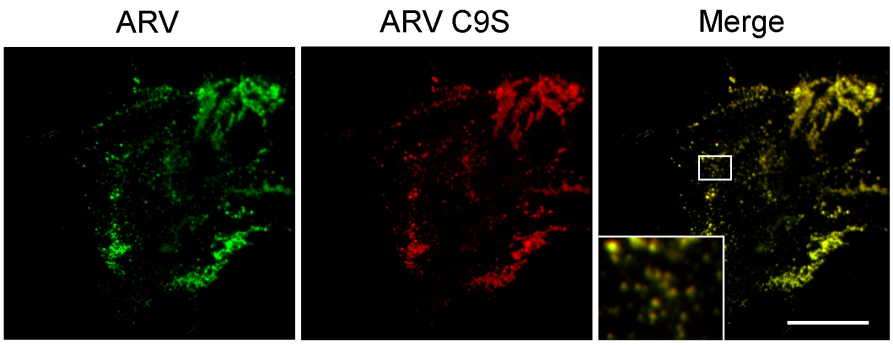

Figure 3.15- The p10 cystine loop is not required for cell-surface clustering. QM5 cell monolayers were transfected with N-terminally FLAG-tagged ARV p10 or myc-tagged ARV C9S. Cells were fixed with paraformaldehyde and surface-localized p10 was detected as in Figure 3.13. Scale bars = 10 μm. Insets are 400% enlargements of the indicated areas.

A

Parental	Mutant	Colocalize
ARV	A1	+
	A2	+
	A3	+
	A4	+
	A5	-
	N1	-
	N2	-
	N3	-
	N4	-
	N5	+
NBV	N1	+
	N2	+
	N3	+
	N4	+
	N5	-
	A1	-
	A2	-
	A3	-
	A4	-
	A5	+

B

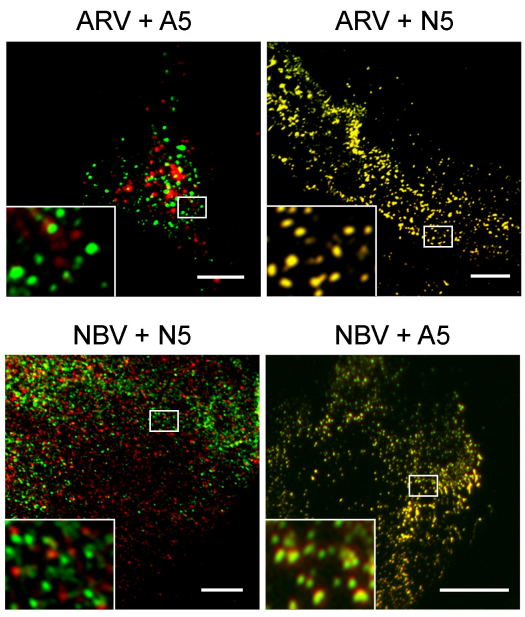

Figure 3.16- Ectodomain neck region determines species-specific p10 homotypic clustering in plasma membranes. (A) Summary table of colocalization results obtained from co-transfections of QM5 cell monolayers with N-terminally FLAG-tagged versions of ARV or NBV p10 and the indicated N-terminally myc-tagged p10 ectodomain chimeras, listed in Figure 3.7. (B) Representative images of QM5 cell monolayers co-transfected with N-terminally FLAG-tagged ARV or NBV p10 and N-terminally myc-tagged chimeric neck constructs (A5 and N5 from Figure 3.7). Cell surface-localized p10 was detected by immunofluorescence microscopy as in Figure 3.13, and merged images are shown. Scale bars = 10 μm.

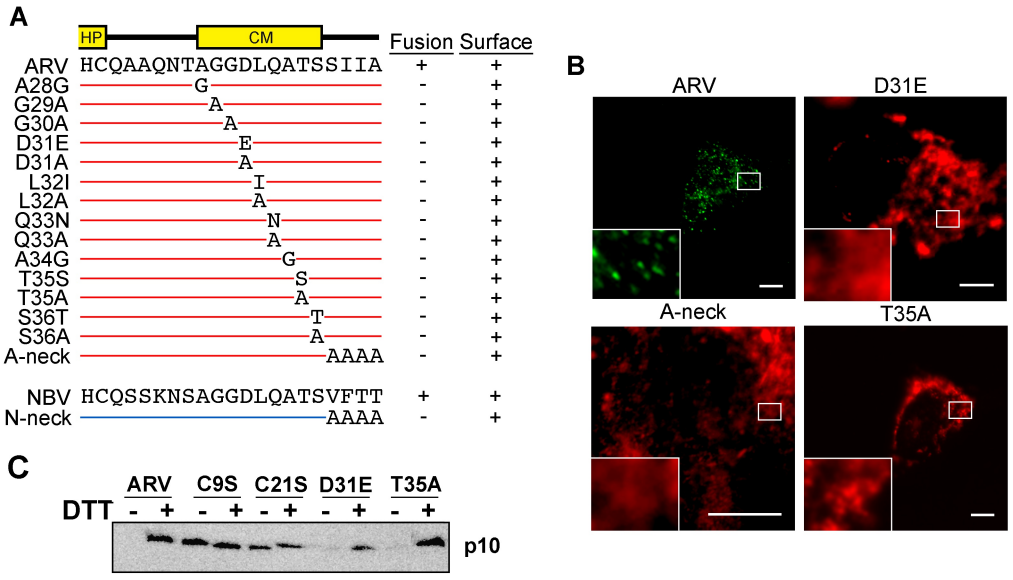

Figure 3.17- CM and neck region residues are essential for p10 clustering in plasma membranes. (A) In the context of ARV p10, each non-Ala/Gly CM residue was substituted to either Ala or a conserved amino acid, while each Ala/Gly residue was substituted to the obverse. Constructs are named at left according to the substitution. The tetra-peptide neck residues were substituted to Ala in the context of both ARV (A-neck) and NBV (N-neck) p10. All substituted constructs were assessed for syncytiogenic activity ("– "indicates no cell-cell fusion) and for cell surface expression levels by flow cytometry ("+" indicates no significant difference relative to the parental p10 construct). (B) Representative immunofluorescence images of QM5 cell monolayers transfected with N-terminally FLAG-tagged ARV p10 or N-terminally myc-tagged ARV p10 containing substitutions in the CM (D31E and T35A), or the A-neck construct, stained as in Figure 3.13. Scale bars = 10 µm. Insets are 400% enlargements of the indicated areas. (C) N-terminally FLAG-tagged versions of the indicated point substitution constructs were subjected to the surface biotinylation assay to detect formation of the intramolecular disulfide bond as in Figure 3.4C.

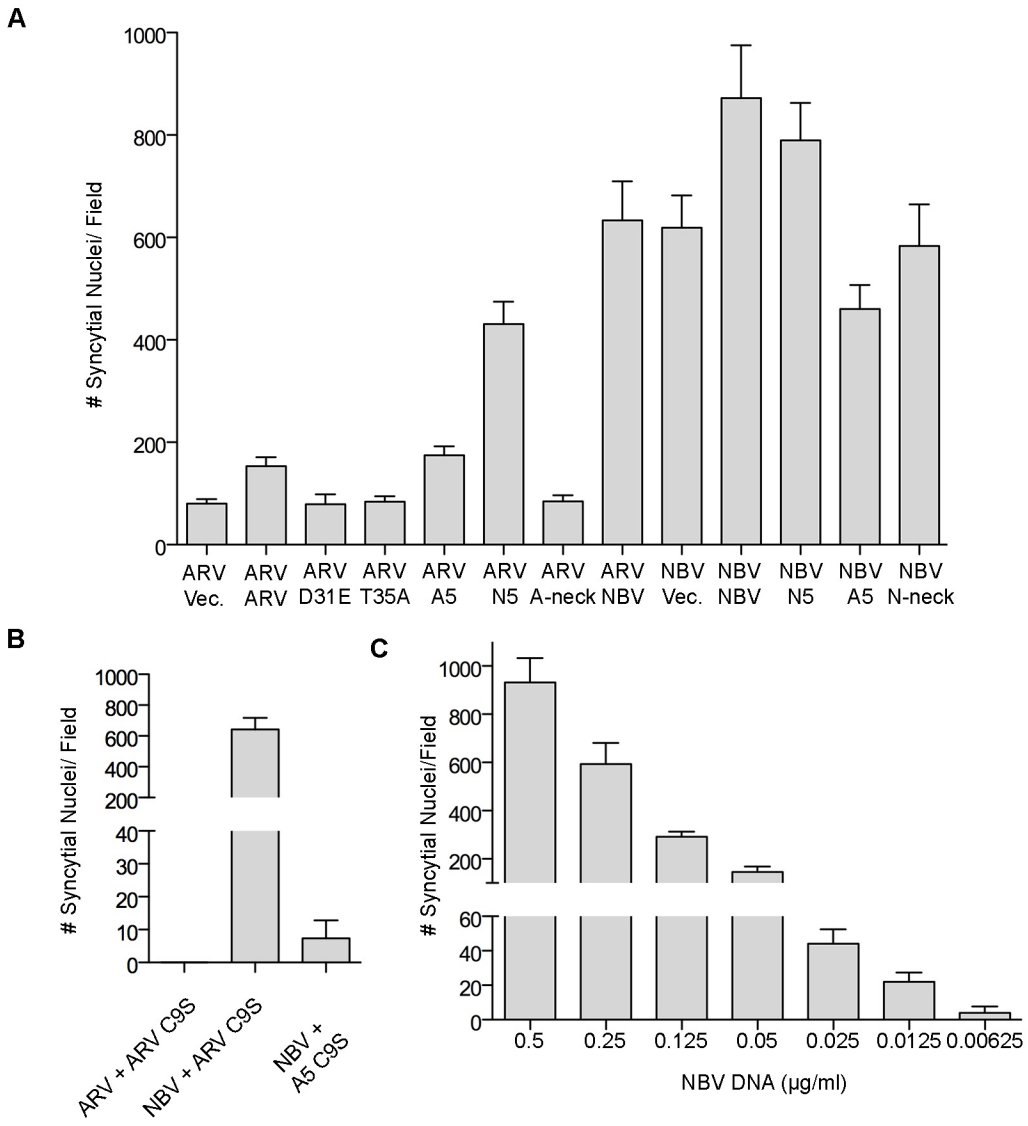

Figure 3.18- The p10 proteins function in concert to determine syncytiogenic efficiency. (A) The numbers of syncytiogenic nuclei induced by co-transfections of the indicated constructs, including CM and neck Ala constructs, as well as neck region exchange constructs from Figure 3.17. Syncytial nuclei present in five random fields of Geimsa-stained monolayers were counted at 24 hpt and averaged over three experiments. (B) The numbers of syncytiogenic nuclei induced by parental p10 proteins co-transfected with co-clustering, but syncytiogenically inactive, constructs in QM5 cell monolayers were quantified as in panel A and averaged over three experiments. (C) The numbers of syncytiogenic nuclei induced by transfections of the indicated amounts of NBV p10 DNA in QM5 cell monolayers at 24 hpt. Error bars in all panels represent standard error propagated within and across experiments.

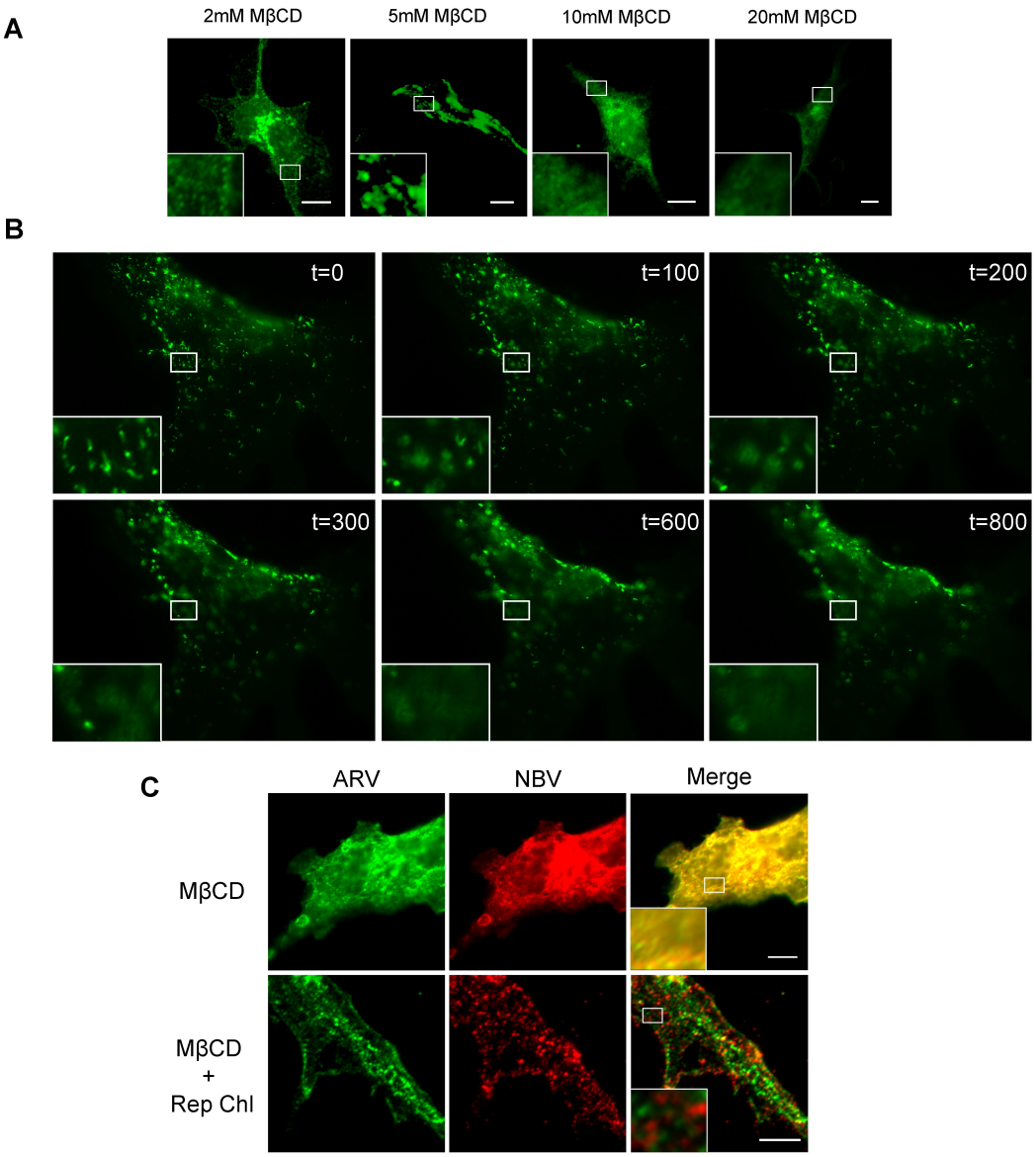

Figure 3.19- Clustering of p10 proteins is cholesterol-dependent. (A) QM5 cell monolayers co-transfected with N-terminally FLAG-tagged ARV p10 were incubated with the indicated amounts of MβCD to deplete membrane cholesterol. Cells were then fixed using paraformaldehyde and cell surface-localized proteins were detected as described in Figure 3.13. (B) QM5 cells transfected with EGFP-tagged p10 were imaged using a spinning-disc confocal microscope at 100x magnification. At t=100 s, 20 mM MβCD was percolated into the sample chamber to chelate cholesterol. Images are stills from a video at the indicated times (in seconds). (C) QM5 cell monolayers co-transfected with N-terminally FLAG-tagged ARV p10 and N-terminally myc-tagged NBV p10 were incubated with 20 mM MβCD to deplete membrane cholesterol. Cells were then either fixed or cholesterol was repleted, using MβCD-cholesterol complexes, prior to fixation. Cell surface-localized proteins were detected as in Figure 3.13. Scale bars = 10 µm. Insets are 400% enlargement of indicated area.

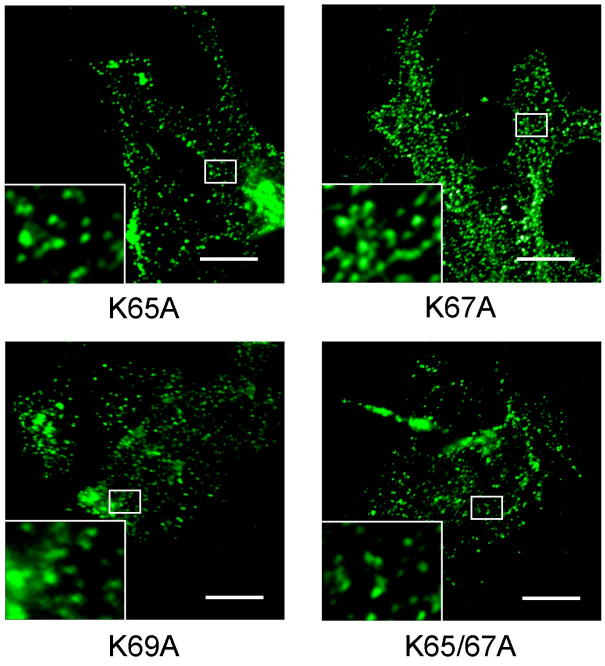

Figure 3.20- The putative p10 CRAC motifs do not affect surface clustering. Representative immunofluorescence images of QM5 cell monolayers transfected with ARV p10 containing the indicated substitutions. Cells were stained as in Figure 3.13. Scale bars = 10 μm. Insets are 400% enlargements of the indicated areas.

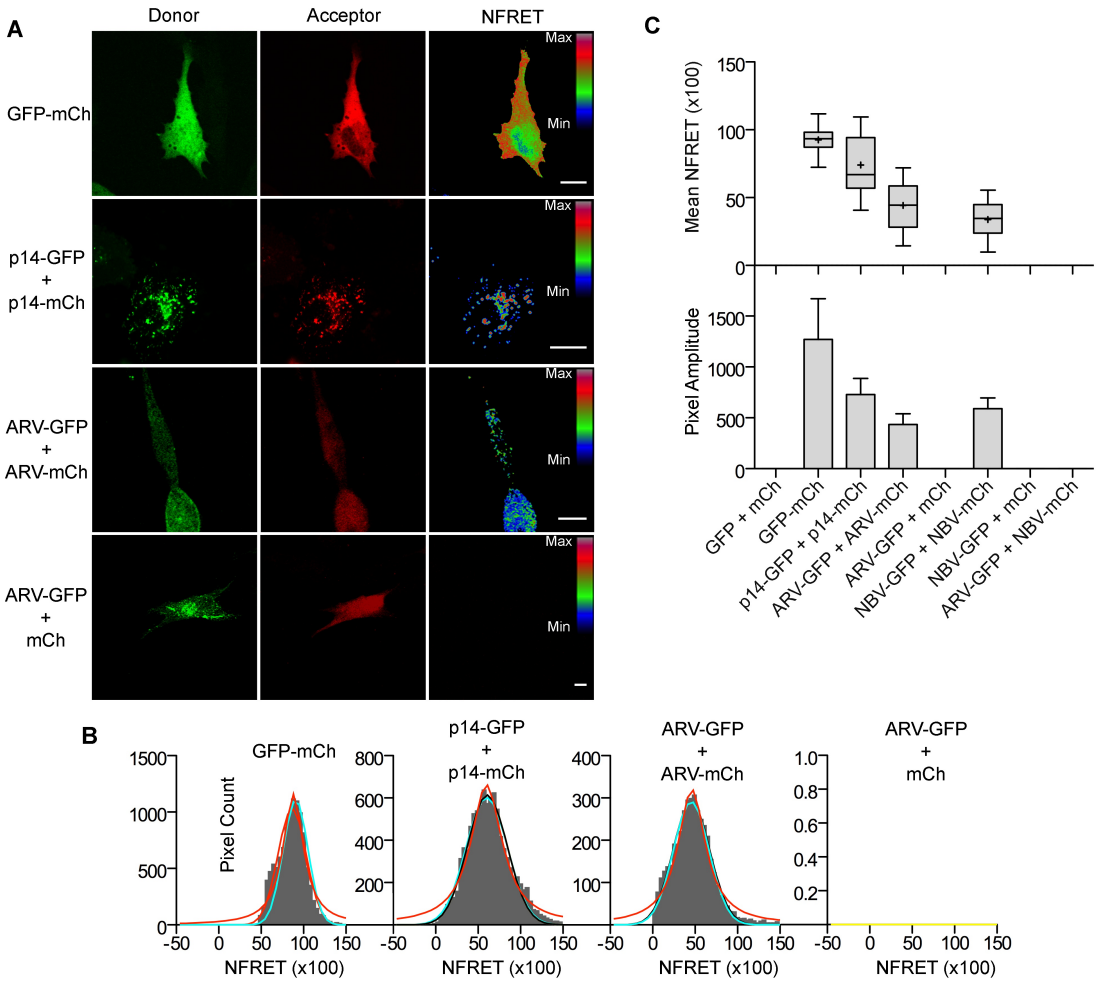

Figure 3.21- The ARV and NBV p10 proteins form homo- but not heteromultimers. (A) Representative images of sensitized emission FRET, showing the donor channel, acceptor channel and the calculated normalized FRET (NFRET) image. Calculated NFRET from positive (EGFP directly linked to mCherry), and negative (ARV p10-EGFP cotransfected with free mCherry) controls are shown above and below the NFRET from ARV-p10 homomultimerization, respectively. NFRET range is denoted by color gradations. Scale bars = 10 µm. (B) Example histograms displaying the distribution and amplitude of the calculated NFRET images from A (bin width=0.03906). Distributions were fit with four Gaussians (red, yellow and blue curves) and the best fits (R2 closest to 0.99) were used to calculate the pixel amplitude and mean NFRET (mNFRET) for each condition. (C) Fitted Gaussian distributions of twenty calculated NFRET images from two separate experiments were used to calculate the mNFRET of each indicated condition (top). The box highlights the standard deviation of mNFRETs, + is the mean mNFRET, the line is the median mNFRET and the whiskers ends indicate the min and max mNFRETs. The fitted NFRET distributions were also used to calculate the mean pixel amplitude (top) from each image. Error bars represent standard error propagated within and across experiments.

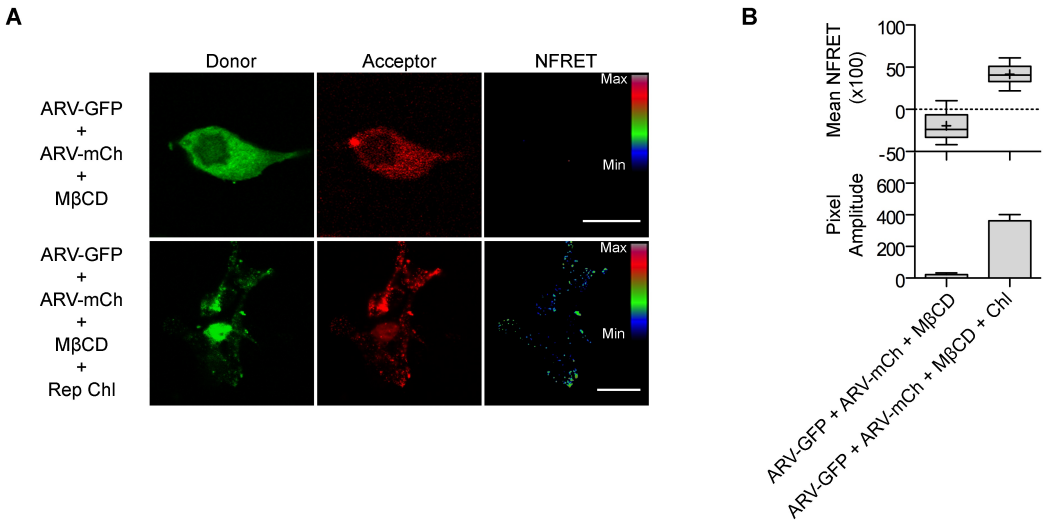

Figure 3.22- Cholesterol is required for p10 multimerization. (A) Representative images of sensitized emission FRET, showing the donor channel, acceptor channel and the calculated normalized FRET (NFRET) image for cells expressing indicated EGFP and mCherry-tagged constructs treated with MβCD then either fixed (top) or with cholesterol repleted, then fixed (bottom). NFRET range is denoted by color graduations. Scale bars = 10μm. (B) Fitted Gaussian distributions of twenty calculated NFRET images from two separate experiments were used to calculate the mNFRET of each indicated condition (top). The box highlights the standard deviation of mNFRETs, + is the mean mNFRET, the line is the median mNFRET and the whiskers ends indicate the min and max mNFRETs. The fitted NFRET distributions were also used to calculate the mean pixel amplitude (top) from each image. Error bars represent standard error propagated within and across experiments.

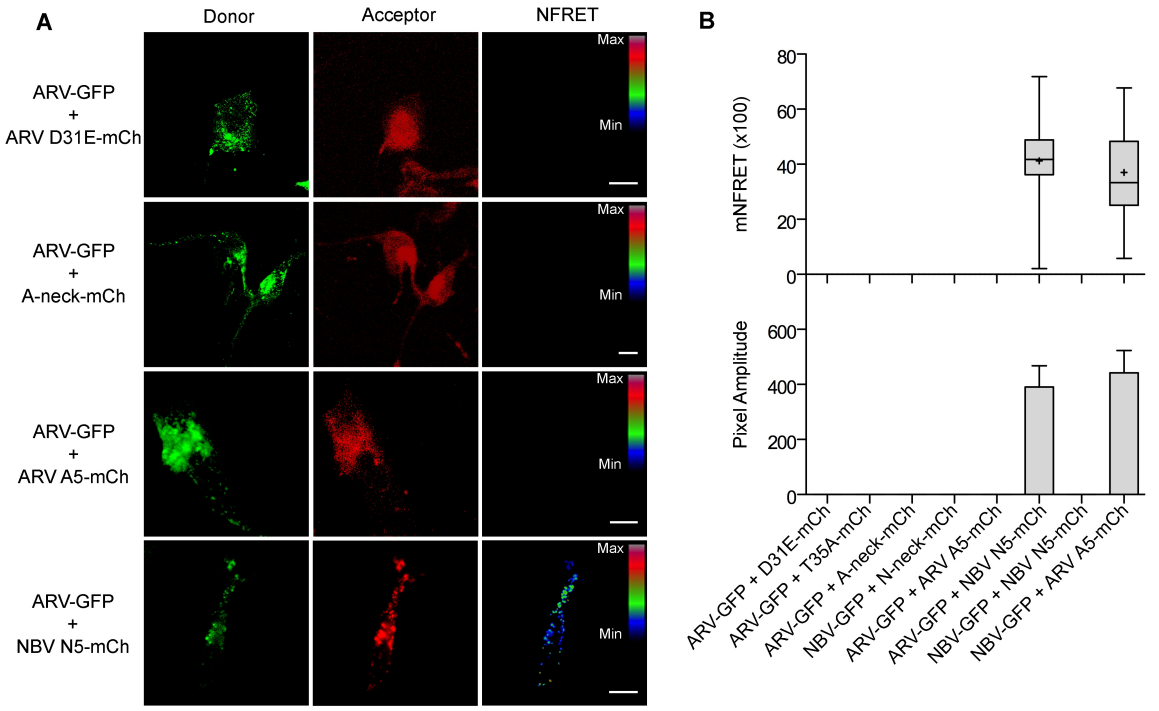

Figure 3.23- The CM and neck region are required for p10 multimerization. (A) Representative images of sensitized emission FRET, showing the donor channel, acceptor channel and the calculated normalized FRET (NFRET) image for the indicated EGFP and mCherry-tagged constructs. NFRET range is denoted by color graduations. Scale bars = 10µm. (B) Fitted Gaussian distributions of twenty calculated NFRET images from two separate experiments were used to calculate the mNFRET of each indicated condition (top). The box highlights the standard deviation of mNFRETs, + is the mean mNFRET, the line is the median mNFRET and the whiskers ends indicate the min and max mNFRETs. The fitted NFRET distributions were also used to calculate the mean pixel amplitude (top) from each image. Error bars represent standard error propagated within and across experiments.

CHAPTER 4

Discussion

4.1. Overview

The syncytiogenic capabilities of the fusogenic orthoreoviruses have various implications for viral pathogenesis (Brown et al., 2009; Duncan et al., 1996; Salsman et al., 2005; Schriff et al., 2007). A comprehensive understanding of how the FAST proteins mediate syncytiogenesis, including descriptions of functional motifs, would provide valuable insight into the pathogenic effects of these proteins. This thesis describes a comparative analysis of the homologous avian and pteropine orthoreovirus p10 FAST proteins. Results indicate the 36-40-residue ectodomains of these diminutive fusogens operate as remarkably compact, multifunctional fusion modules that function as the predominant determinant of species-specific p10 fusion efficiency. Mechanistically, the ectodomain comprises two separate components, one of which directs formation of a cystine loop FP and the other co-dependent clustering and multimerization of p10 in plasma membrane microdomains. Plasma membrane clustering and multimerization are CH-dependent, required for syncytiogenesis, reversible, and governed by the MPER, which includes a juxtamembrane tetra-peptide segment responsible for species-specific p10 clustering in microdomains and homomultimerization. Most notably, co-transfections revealed that overall syncytiogenic efficiency is dictated by the p10 composition of individual microdomains, identifying these p10 plasma membrane clusters as multimeric FAST protein fusion platforms.

4.2. The p10 Ectodomains are the Predominant Determinants of Syncytiogenic Efficiency

The ability of the NBV p10 protein to induce syncytiogenesis at a faster rate than ARV p10 has been known for some time, however the basis of this disparity had not been examined. It has been suggested that the difference may reflect variability in protein expression levels or stability between ARV and NBV (Salsman et al., 2005). In this study,

I established that surface expression and total protein levels are equivalent for the p10 homologues (Figure 3.2). Furthermore, cell-type was shown to be inconsequential to the overall difference in syncytiogenic rate (Figure 3.1). Taken together, these results indicate that the NBV p10 protein is a more robust fusogen than ARV p10. This knowledge, when used in combination with the known sequence conservation and divergence of the avian and pteropine p10 isolates (Figure 1.5), provides a powerful tool to dissect the protein constituents governing p10 FAST protein-mediated syncytiogenesis.

The homologous nature of the ARV and NBV p10 proteins facilitated functional recombination of the ecto-, TMD and endodomains (Figure 3.3A), which revealed the relative contribution of each domain to the overall rate of syncytiogenesis (Figure 3.3C). One might expect that any differences in syncytiogenic rate would arise from protein regions with high sequence divergence, which could facilitate disparate structures, conformational changes or binding partners that influence syncytiogenesis. Surprisingly, while the ectodomains of ARV and NBV p10 share a considerably higher amino acid identity than the endodomains (44% versus 19%), the only chimeras in which the syncytiogenic rates were affected by a single domain substitution were the ectodomain exchange constructs (AectoN and NectoA). The NBV ectodomain on an ARV backbone (AectoN) conferred an increase in the overall syncytiogenic rate compared to parental ARV, and likewise the ARV ectodomain on an NBV backbone (NectoA) decreased the relative syncytiogenic rate compared to NBV. However, there was not a complete exchange of syncytiogenic rate (i.e. ARVectoNBV does not induce syncytiogenesis at the same rate as NBV), suggesting that the TMDs and endodomains somehow influence the rate of syncytiogenesis. Interestingly, while exchanging either the TMD or endodomains alone had no effect on the observed syncytiogenic rate, when either domain was present in conjunction with the ectodomain from the same parental protein (i.e. ARV TMD or endodomain with ARV ectodomain, or NBV TMD or endodomain with NBV ectodomain) the observed rate of syncytiogenesis was equivalent to that of the parental p10 from which these two domains originated.

The p10 ectodomain HPs have been suggested to function similarly to the FPs of enveloped viral fusion proteins (Barry et al., 2010; Shmulevitz et al., 2004b). Common features of these motifs include moderate hydrophobicity, enrichment in alanine and

glycine residues, and high conservation across fusion proteins from different isolates of the same virus. The FPs are critical for fusion activity, highly sensitive to mutation, and synthetic versions of these peptides insert into lipid bilayers to promote lipid mixing (Cross et al., 2009; Earp et al., 2004; Martin et al., 1999; Martin and Ruysschaert, 2000; Pecheur et al., 1999 ; Skehel et al., 2001; Tamm et al., 2002). To test if the syncytiogenic efficiency of the ARV and NBV p10 ectodomains was related to the lipid-destabilizing properties of the HPs, I measured the lipid mixing activities of synthetic versions of the ectodomains. Indeed, NBV p10 ectodomain synthetic peptides induced higher levels of lipid mixing relative to the ARV p10 ectodomain in a dose-dependent manner (Figure 3.8). In the paradigmatic membrane fusion reaction, peptide insertion into the lipid bilayer and the consequent lipid destabilization/mixing is a relatively early stage of syncytiogenesis (Chernomordik and Kozlov, 2008; Earp et al., 2004; Jahn et al., 2003a). The correlation between relative lipid mixing activity of their ectodomains and overall syncytiogenic efficiency of the ARV and NBV p10 proteins suggests lipid mixing may be a rate-limiting step in the p10 fusion reaction and responsible for the differences in syncytium formation induced by these p10 homologues.

While the p10 ectodomains predominantly determine syncytiogenic rate, the overall syncytiogenic efficiency is dictated by complex interactions with the TMD and endodomains. A similar situation occurs with influenza virus HA, although in this instance it reflects the preference for a homotypic combination of TMD and endodomain (Nowak and Wengler, 1987). These two domains have been shown to play active, potentially overlapping roles in the later stages of the membrane fusion reaction (Armstrong et al., 2000; Dennison et al., 2002; Kemble et al., 1994; Owens et al., 1994; Sakai et al., 2002; West et al., 2001). Similarly, the TMD and endodomains of the FAST proteins have been implicated in the later stages of syncytiogenesis, including fusion pore formation and pore expansion (Barry and Duncan, 2009; Clancy and Duncan, 2009), while their ectodomains mediate the early lipid mixing stage of membrane fusion (Barry et al., 2010; Rey et al., 1995a; Shmulevitz et al., 2004b; Top et al., 2012), as is shown above for the p10 proteins. However, how these individual domains function in concert during the fusion process has not been determined, either for the FAST proteins or for enveloped virus fusogens. It is clear that, in the context of the p10 FAST proteins, the

TMD and endodomains collaboratively function during late stages of syncytiogenesis, and thus do not individually affect the syncytiogenic rate. However, it is possible ectodomain-mediated lipid mixing and pore formation may be more efficient when a homotypic TMD and/or endodomain links this process to pore stabilization and expansion, allowing for energetically favorable progression through the fusion reaction.

4.3. Structural and Functional Implications of the p10 Disulfide Bond

The results presented in this thesis indicate the p10 HP exists as an 11-residue disulfide-stabilized FP loop (Figure 3.4). Formation of the essential disulfide bond is highly sensitive to the location and context of the cysteine residues. Additionally, the relative location or spatial arrangement of essential hydrophobic amino acids within the loop has direct effects on fusion activity. Similar to the p10 HP, disulfide-stabilized FP loops have been predicted or detected in class I, II and III enveloped viral fusion proteins (Abell and Brown, 1993; Bressanelli et al., 2004; Einer-Jensen et al., 1998; Gibbons et al., 2003; Gibbons et al., 2004; Gros et al., 1997; Hannah et al., 2009; Heldwein et al., 2006; Nowak and Wengler, 1987; Rey et al., 1995a; Roche et al., 2006). However, unlike the p10 FP loop, these structures are usually between 41 and 45 residues and form large, extended loop structures consisting of β-sheet secondary structures flanking relatively short FP sequences. The overall structures of these FP loops are mainly determined by the presence of β-sheets rather than by disulfide bonding (Gibbons et al., 2004) . This suggests that the structural and biochemical characteristics of the p10 FP loop are likely quite different than the extended FP loops of enveloped viral fusion proteins.

4.3.1. Disulfide Bond Formation Forces Exposure of Residues Within the p10 Cystine Loop Fusion Peptide

It is possible, if not likely, that the p10 cystine loop FP exists as a cystine noose. A cystine noose is a fairly recently described structural motif consisting of 4-10 residues flanked by disulfide-bonded cysteine residues (Lapthorn et al., 1995). The tight structural constraints imposed by such tight loop structures results in Φ and Ψ bond angles that fall

outside of the favorable region on the Ramachandran plot, and thus disruption of α-helical and β-sheet secondary structures. Additionally, the side chains of amino acids contained within these small loops are significantly exposed and show high surface accessibility. There are few identified examples of these structures, with the best-characterized being found in the receptor binding proteins human endothelin (hET), respiratory syncytial virus (RSV) G protein and measles virus H protein (Gorman et al., 1997; Hu and Norrby, 1994; Janes et al., 1994; Langedijk et al., 1996). However, in none of these examples are the cystine nooses involved in membrane fusion.

The small size of the p10 cystine loop likely forces exposure of residues contained within this region. Synthetic versions of the p10 ectodomain slowly aggregate under aqueous conditions, but stay in solution under reducing conditions (Figure 3.9B). This is suggestive of a role for the disulfide bond in the forced exposure of hydrophobic residues and hydrophobic-induce peptide aggregation. Additionally, previous studies on the p10 protein revealed that syncytiogenesis is limited by rapid degradation of newly synthesized p10. The ectodomain of p10 appears to target the protein for degradation after insertion into an early membrane compartment, which results in only small amounts of p10 reaching the cell surface. However, once at the cell surface, p10 accumulates in a relatively stable form, where it mediates cell-cell fusion (Shmulevitz et al., 2004a). Interestingly, mutation of either cysteine residue, and thus elimination of p10 disulfide bonding, prevents rapid degradation. Similarly, mutations that lower overall hydrophobicity of the HP reduce the rate of p10 degradation, while those that increase overall hydrophobicity accelerate degradation (Shmulevitz et al., 2004a). Since cellular quality control machinery functions through recognition of exposed hydrophobic sequences on misfolded proteins, the p10 proteins seem to have evolved to possess a certain level of hydrophobicity that is essential for membrane fusion activity, but results in the targeting of the majority of newly synthesized p10 proteins by cellular degradation machinery.

Interestingly, the NBV p10 HP is predicted to be more hydrophobic than the ARV p10 HP. However, surface expression and whole cell levels are equivalent for both proteins (Figure 3.2), suggesting that the degradation rates of these proteins are

comparable. While the sequences of the ARV and NBV p10 HPs are relatively similar, it is possible that these two regions have evolved to be structurally divergent. The NBV p10 cystine noose may adopt a tertiary structure that allows for additional concealing of hydrophobic residue side chains. This hypothesis is supported by the intolerance of alanine insertions, cysteine shifts and ARV/NBV segment exchanges within and around the HPs. All constructs with mutations within and around the HP region did not form a disulfide bond (with the exception of the S5 construct) and were syncytiogenically inactive (Figures 3.5, 3.6 and 3.7). It is possible that the fusogenic structures of ARV and NBV p10 are high-energy, metastable structural intermediates. All of these mutations would theoretically change the protein folding energy landscapes, and with it any metastable structural states, making disulfide bonding no longer favorable. Unfortunately, our attempts to solve the three-dimensional structures of the ARV p10 ectodomain with the putative cystine noose using solution NMR spectroscopy were unsuccessful. However, we can conclude from this data that the cystine loop region exists as a highly dynamic structure, which may or may not indicate a metastable state. Taken together, this data suggests that intramolecular disulfide bonding within the p10 ectodomains exposes hydrophobic residues, creating a highly dynamic, metastable structure that is targeted for degradation, but is absolutely essential for membrane fusion activity.

Perhaps the most surprising result was that of the S5 construct. This construct shifted the cysteine at position 21 towards the N-terminus, which shortened the loop by one residue, altered the geometry of the loop and location of hydrophobic residues at the apex of the loop, and deleted a conserved histidine residue (Figure 3.5A). This was the only cysteine shift construct that retained the ability to form a disulfide bond (Figure 3.5C), however it was still syncytiogenically inactive (Figure 3.5B). It was previously observed that the positioning of key residues within FPs of enveloped viral fusion proteins is of functional importance (Delos and White, 2000; Fredericksen and Whitt, 1995; Ito et al., 1999). Specifically, the FPs from the fusion proteins of ASLV, Ebola virus, HSV, tick-borne encephalitis (TBE) virus and VSV have specific functional requirements for either a hydrophobic residue or proline residue at the apex of the loop (Allison et al., 2001; Delos et al., 2000; Fredericksen and Whitt, 1995; Hannah et al., 2009; Ito et al., 1999; Roche et al., 2006). Alternatively, the elimination of the conserved

histidine residue that accompanied shifting the cysteine residue may have direct functional implications. Substitution of this histidine residue with an alanine completely eliminated p10-induced syncytiogenesis (Figure 3.5D). This may indicate a novel role for the histidine residue in p10-mediated membrane fusion, possibly as a pH sensor. The pKa of the imidazole ring on histidine is approximately 6.0, and the overall amino acid pKa is 6.5 (Voet and Voet, 2004a). Thus, a relatively small shift from physiological pH would cause protonation of the imidazole ring, imparting a positive charge on the amino acid. This positive charge could have important implications for p10 cystine loop membrane interactions. However, the disulfide-bonding status of this construct needs to be determined before any firm conclusions can be drawn on the functional implications of this residue.

4.3.2. The p10 Cystine Loop is Required for Membrane Interactions and Lipid Destabilization

Disulfide bond formation within the p10 ectodomain, along with the corresponding exposure of hydrophobic residues within this region, is required for membrane partitioning of the p10 ectodomain as well as p10-induced membrane destabilization and lipid mixing (Figure 3.10). The exposure and insertion of hydrophobic domains into bilayers is a unifying theme of protein-mediated membrane fusion. As illustrated by influenza HA, triggered exposure of a hydrophobic FP is closely coupled to membrane insertion (Skehel et al., 1982b; White et al., 1982). The fusogenic ability of FPs is proposed to be dependent on their ability to obliquely insert into bilayers, which has been suggested to induce local bending of the membrane, creating a highly fusogenic "bulge" (Kozlov et al., 2010). Generation of such highly curved membranes has been directly shown to be induced by synaptotagmin-1 and DOC2 (Martens et al., 2007; McMahon et al., 2010), which are components of the SNARE vesicle fusion proteins. In this instance, incubation of liposomes with either of these proteins induced highly curved, tubulated liposomes, which were required for fusion activity. The lipid mixing induced by synthetic peptides of homologous p10 proteins from two host ranges did not result in the stable formation of tubulated liposomes (Figure 3.12). In the presence of tubulation induced by the SNARE vesicle complex components, there is a slow, gradual relief of

FRET in a similar lipid mixing assay (Martens et al., 2007). In contrast, the extremely rapid kinetics of p10 induced lipid mixing is more analogous to that of the HIV gp41 FP (Lai et al., 2012; Sackett et al., 2010), for which liposome tubulation has not been shown. One explanation for this discrepancy is that an initial, shallow FP insertion produces localized, high membrane curvature and promotes rapid fusion. Afterwards, the peptide is more deeply embedded in the membrane, where the curvature effects are significantly less pronounced, rendering the peptide non-reusable. The insertion of hydrophobic C2-domains from SNARE proteins may initially be slow to interact and insert into the bilayer, however after insertion they may maintain a shallow insertion depth, thus stably inducing high positive curvature, resulting in liposome tubulation. We can conclusively state that the p10 ectodomains do not induce stable, large-scale liposome tubulation. However, from the present data, we cannot exclude that other p10 domains (i.e. TM or endodomain) may play an active role in the membrane fusion reaction by effecting membrane curvature. Further studies on the roles of these domains in the fusion reaction are required to comprehensively understand the mechanism of p10-induced membrane fusion.

4.4. Cholesterol-Dependent Multimerization and the p10 Membrane Proximal Ectodomain Regions

4.4.1. The p10 Proteins Function as Higher-Order Multimers

Indirect evidence suggests that p10-containing plasma membrane microdomains contain higher-order p10 complexes and function as fusion platforms. The ARV p10 construct containing the neck region of NBV (A5 construct) co-clusters with NBV p10 (Figure 3.16) and influences syncytiogenic efficiency. Additionally, an ARV p10 C9S substitution prevents formation of the cystine loop and eliminates cell-cell fusion (Figure 3.4) but has no effect on p10 homotypic clustering (Figure 3.15). Co-transfection of NBV p10 with an equivalent amount of the A5 construct containing the C9S substitution resulted in a 99.15% decrease in NBV p10 syncytiogenesis (Figure 3.18B). A rudimentary estimation of the number of p10 proteins per fusion platform can be obtained

from these results. A comparison of this level of syncytiogenesis to that induced by parental NBV p10 reveals that only 0.85±0.53% of the parental syncytiogenic level was induced by co-transfection of these constructs. If it is assumed that a single ARV A5 C9S present in an NBV p10 punctum results in a non-functional fusion platform, then all observed syncytiogenesis could only arise from puncta containing solely NBV p10. Based on a Poisson distribution, the probability of having NBV p10-only complexes is 0.78% and 0.39% if these puncta contained seven or eight p10 polypeptides respectively, which approximates the 0.85±0.53% of residual syncytiogenesis observed in cells co-transfected with NBV p10 and ARV A5 C9S. Titration of the levels of NBV p10 transfected into monolayers revealed that these levels are adequate to induce detectable syncytiogenesis (Figure 3.18C). We interpret this estimate simply as an indicator of the likelihood that fusion platforms comprise higher-order assemblies of p10 monomers, and this estimate places the number in the range of hepatmers or octomers. Estimates of the number of enveloped viral fusion proteins involved in an effective fusion reaction have varied from 1-3 influenza virus HA trimers (3-9 proteins) based on free-energy calculations (Kuzmin et al., 2001a), to upwards of 5 SFV E1 trimers (15 proteins) from observed lateral contacts (Gibbons et al., 2004). We have identified a theoretical minimum number of p10 proteins required for an effective fusion reaction, however it is impossible to infer whether this number reflects stable, lateral p10 interactions, or dynamic and variable clustering.

4.4.2. The p10 MPER Motifs Direct Homotypic Clustering and Multimerization

Homomultimerization of ARV and NBV p10 affects cell surface localization patterns, resulting in similarly distributed, but distinctly separate puncta (Figure 3.13). Novel protein motifs located in the ectodomain neck region confer multimerization specificity between ARV and NBV (Figure 3.16) and function in conjunction with the CM as part of the extended MPER motif. Although noted as an invariant sequence in all p10 isolates from avian and pteropine hosts, no functions have previously been ascribed to the CM. FRET analysis and a panel of CM point substitutions suggested a striking requirement for sequence-specific, spatial self-complementarity in the CM to generate a

binding interface suitable for p10 multimerization (Figure 3.20). While homotypic CM interactions are necessary for multimerization, they are not sufficient; stable multimerization only occurred in conjunction with CH-dependent clustering of p10 in plasma membrane microdomains (Figure 3.21**)**. The MPERs of enveloped viral fusogens tend to be short (~12-41 residues), hydrophobic or amphiphilic sequences frequently enriched in aromatic residues (Lorizate et al., 2008). Their ability to adopt amphipathic helical structures, self-aggregate, and partition into membrane interfacial regions suggests the role of MPERs in membrane fusion reflects their ability to perturb bilayer structure (Allison et al., 2001; Gibbons et al., 2003; Ivankin et al., 2012). In contrast, the 13-residue MPERs of ARV and NBV p10 are mostly polar and almost devoid of aromatic residues, and their essential role in membrane fusion is to direct reversible, CH-dependent p10 multimerization. However, some similarities may exist between these motifs. The MPERs of several enveloped viral fusion proteins, including those from VSV, rabies virus, and HIV, have been proposed to self-aggregate within the low-polarity membrane interface environment (Sal-Man et al., 2007). Also, these motifs have been either proposed or confirmed to form α-helical structures (Schibli et al., 2001; White et al., 2001). NMR structural analysis of the ARV p10 ectodomain suggested residues 28-36, which correspond to the CM, were homogeneously structured in DMSO. We calculated the secondary chemical shifts (Δδ) for H^{α} resonances by subtracting the random coil chemical shifts for peptides of sequence GGXAGG measured in DMSO (Tremblay et al., 2010) from those measured in this region of the p10 ectodomain. Interestingly, all residues returned negative Δδ (H^{α}) values, implying that this region of the p10 FAST protein adopts an α-helical conformation (Tremblay et al., 2010; Wishart et al., 1992). Confirming the alpha-helical structure of the CM and the spatial self-complementarity might be quite challenging in view of the role of CH-dependent clustering in generating or stabilizing p10 multimers.

4.5. Cholesterol is a Major Regulator of p10-Induced Membrane Fusion

4.5.1. Donor Membrane Cholesterol is Required for p10 Multimerization

Cell-surface clustering, similar to that of ARV and NBV p10, is common amongst membrane fusion proteins. This behavior is critical for SNARE vesicle fusion proteins to localize to sites of membrane fusion (Lang et al., 2001). While the multimeric status of SNARE proteins within these clusters was not investigated, the authors did identify an essential role for CH in clustering. CH-dependent lateral segregation of proteins and lipids creates submicroscopic membrane domains with unique biophysical properties, such as increased membrane thickness and altered lipid order (Lingwood and Simons, 2010). The role of CH-rich membrane microdomains in the lateral distribution, sorting and function of several membrane-associated proteins has been extensively investigated (Epand et al., 2010; Germain et al., 2012; Melkonian et al., 1999). It has also been demonstrated that membrane fusion induced by several enveloped viral fusion proteins, such as those from SFV, HIV, Influenza, murine leukemia virus, human T-cell leukemia virus, Ebola virus and Marburg virus (Bavari et al., 2002; Gorman et al., 1997; Kielian and Helenius, 1984; Lu and Silver, 2000; Lu et al., 2002; Niyogi and Hildreth, 2001; Rawat et al., 2003; Takeda et al., 2003), as well as the RRV p14 FAST protein, are influenced by CH-rich microdomains (Corcoran et al., 2006). The p10 proteins also require CH for membrane fusion activity, and some features of lipid microdomains appear to be needed to stabilize low-affinity p10 multimer interactions. Similar co-dependent raft assembly and multimerization have been reported in other systems (Latif et al., 2007; Panchal et al., 2003; Wong et al., 2009) (Christopherson et al., 2003; Lindwasser and Resh, 2001; Ono et al., 2007). While CH microdomains have been implicated in the function of numerous enveloped virus fusogens, we are unaware of any instance where they are needed for enveloped virus fusogen multimerization. The one exception is Semliki Forest virus (SFV) E1, where FP binding to sterol- and sphingolipid-rich microdomains in the target membrane appears to be required for low-pH-dependent conversion of E1 pre-fusion heterodimers to fusion active homotrimers (Chatterjee et al., 2000; Klimjack et al., 1994). In contrast, the CH dependence of p10 multimerization

reflects an undefined functional interaction between the MPER and donor membrane CH needed to convert p10 monomers to stable multimers.

The separate ARV and NBV puncta are laterally dispersed upon CH depletion, then separately re-cluster and multimerize upon CH repletion (Figure 3.19 and 3.22). Several feasible explanations exist for how the p10 neck regions may function to mediate this specificity: I) Transition of p10 proteins to the thicker membrane environment of a liquid-ordered membrane phase may be accompanied by structural transitions in the neck region, which augment p10-p10 interactions. In this instance, the neck residues would function as an extension of the TM domain, and would serve as a nucleation point for p10-p10 interactions; II) The neck region residues may function together with the palmitoylated cysteine residues as raft-targeting signals, similar to that of influenza HA. The hydrophobic residues within the neck regions may contact the exoplasmic leaflets of the membrane to mediate raft-interaction. This would suggest that multimerization specificity arises from the differential association of ARV and NBV p10 with heterologous CH rich microdomains; III) Putative disparate raft-associated cellular interacting partners may specifically recognize neck region residues of ARV and NBV p10 and mediate transition into rafts to favor multimerization. Such a process may resemble that of plasma membrane H^+-ATPase (Pma1p), which is influenced to cluster in lipid rafts through interactions with the heterologous protein, Ast1p (Bagnat et al., 2001). Whether specificity of p10 multimerization is governed by homo protein-protein, protein-lipid, or hetero protein-protein interactions, it is clear that CH microdomain intercalation and multimerization are closely related processes that are essential for syncytiogenic competency of the p10 proteins.

4.5.2. Cholesterol is Required for Lipid Mixing Activity of the p10 Fusion Peptide

The strict requirement of membrane CH has important functional implications for p10-mediated syncytiogenesis; however, the actual role of CH remains undefined. CH has been shown to influence membrane fusion through modulation of overall membrane fusogenicity (Haque et al., 2001) and direct effects on membrane fusion proteins (Lai et

al., 2012; Lang et al., 2001; Panchal et al., 2003; Scheiffele et al., 1997; Takeda et al., 2003). For example, CH has been shown to be essential in the early stages of SFV E1-induced membrane fusion, where there is a strict requirement for CH during the low-pH-triggered conformational changes, as well as FP insertion into the target membrane (Ahn et al., 2002). CH has also been shown to be required during the hemifusion and pore widening stages of influenza virus HA-induced membrane fusion (Biswas et al., 2008). It has also been suggested that CH influences the conformations of SNARE TMDs, which modulates fusion kinetics by strongly stimulating fusion stalk formation (Chang et al., 2009). It is clear that CH promotes the multimerization and higher-order functional interactions of the p10 proteins in what we have termed fusion platforms. However, it is also possible that CH contributes to the efficiency of p10-mediated fusion by modifying local membrane environments. Fusion platforms may also mediate co-clustering of p10-multimers with adhesion-complex proteins, such as β-catenin and cadherin (Salsman et al., 2008b), which could create areas of close membrane apposition between cells, where the p10 FP could effect membrane fusion.

To determine the effects of CH on p10-mediated membrane fusion, we measured the global structural changes, membrane binding and lipid mixing activity of the p10 ectodomains with liposomes containing varying concentrations of CH. Our results indicate that the concentration of CH in a membrane does not influence the membrane binding or secondary structure transitions of the p10 ectodomain (Figures 3.10 and 3.11), but does have a direct influence on the post-binding lipid destabilization and mixing activities (Figure 3.11C). CH may influence p10-mediated membrane fusion in several ways. As a prerequisite to lipid mixing and fusion-stalk formation, two bilayers must be closely apposed. However, at these short separation distances, repulsive "hydration forces" dominate (Leikin et al., 1993). The strength of these forces is directly related to the lipid composition of the bilayers at the point of apposition. Specifically, the head group of CH is more weakly hydrated than those of PC and SM (Sen and Hui, 1988). Thus, the presence of CH facilitates membrane dehydration and promotes membrane contact (Aeffner et al., 2012). Additionally, the molecular shape of CH has been suggested to promote negative curvature in the outer bilayer leaflet by influencing lamellar-to-H_{II} phase transitions and membrane bending elasticity (Chen and Rand,

1997), which can increase the formation of fusion intermediates by lowering free energy barriers. While membrane fusion is an essential cellular process, it is critical that this process be controlled. The location of fusion is tightly regulated for the enveloped viral fusion proteins through a strict requirement for activation, either through receptor binding or a drop in pH (Earp et al., 2004). The location of fusion mediated by the SNARE vesicle fusion proteins is controlled via complex assembly and trans-SNARE interactions (Chen and Scheller, 2001). As of yet, there has been no identified control mechanism of FAST protein-mediated membrane fusion. They are promiscuous fusogens that function in the absence of a known trigger or control mechanism; however, they do not seem to induce fusion of intracellular membranes. Membrane CH levels increase from about 0.5-1% in the endoplasmic reticulum to 25-40% in the plasma membrane (Meer et al., 2008). The relatively low CH content of intracellular membranes would curb the ability of p10 to initiate membrane fusion by obstructing the initial lipid mixing stage. Thus, membrane CH content may regulate the location of p10-mediated membrane fusion, restricting its activity prior reaching the plasma membrane.

4.5.3 Dynamic Clustering and Dispersion of Cholesterol Microdomains may be an Essential Element of p10-Mediated Membrane Fusion

It has been demonstrated that, in the absence of a known fusogen, dynamic clustering and dispersion of CH microdomains contributes to the fusion competency of myogenic cells (Mukai et al., 2009). These processes have been shown to specifically contribute to both the cell adhesion and membrane fusion stages of myogenic cell fusion. It is possible that CH microdomain association and multimerization of p10 in a fusion platform generates fusion competent sites on the cell surface. The presence of CH at these sites would induce negative curvature and promote the early stages of membrane fusion (Chen and Rand, 1997). However, the increased membrane rigidity would theoretically impede downstream fusion events. Thus, redistribution of the p10-containing fusion competent sites would allow for completion of the fusion process. We suggest that the novel reversibility of p10 homomultimers in response to CH depletion and repletion illustrates that such dynamics are indeed possible, and may play a role in controlling p10-mediated membrane fusion. This is mechanistically in contrast to the

enveloped fusogens, which are locked in metastable dimeric or trimeric conformations (Backovic and Jardetzky, 2009; Harrison, 2008; Wahlberg and Garoff, 1992); an external trigger induces irreversible conformational conversion to a post-fusion trimeric conformation, which releases energy to drive fusion (Harrison, 2008; Jahn et al., 2003b). However, after FP exposure and target membrane interaction, the conformational changes required to form the post-fusion structure are impossible unless the ternary structure is dissociated (Weissenhorn et al., 2007). It has been argued that monomeric intermediates exist for both TBE virus E fusion protein (Stiasny et al., 1996) and the VSV G fusion protein (Albertini et al., 2012) during transition from pre- to post-fusion conformations. Monomeric intermediates and dynamic clustering and dispersion at sites of fusion, either raft-mediated or otherwise, may be a general requirement for membrane fusion.

4.6. Summary

The results described above provide important insights into the mechanistic contributions of the p10 ectodomains to membrane fusion and syncytiogenesis. We have identified two ectodomain motifs that are highly conserved, species specific, and are essential for syncytiogenic activity: A 25-residue N-terminal FP motif consisting of an 11 residue disulfide bonded loop that is essential for membrane destabilization and syncytiogenic activity, and a C-terminal 13 residue MPER motif consisting of a stretch of nine absolutely conserved amino acids and four species-specific juxtamembrane residues, which together govern CH-dependent homotypic multimerization. However, this work mainly focused on the protein clustering and lipid mixing stages of membrane fusion. It remains unclear if or how the p10 ectodomains are involved in other stages of the membrane fusion reaction. Additionally, through permutational recombination of the ecto-, TMD and endodomains of ARV and NBV p10 we identified clear contributions of the TMD and endodomains to the overall syncytiogenic rate, although specific roles were not defined. It is clear that different regions of the p10 proteins mediate different stages of the fusion reaction, and previous studies have implicated the TMD and endodomains in the pore-formation and expansion stages of the fusion reaction, however these studies fell short of describing a mechanism.

CHAPTER 5

Conclusions and Future Directions

5.1. Breaking the Paradigm of Mechanically Driven Membrane Fusion

The current model of protein-mediated membrane fusion suggests that energy stored in complex, metastable fusion protein ectodomains is released during triggered conformational rearrangements to drive the membrane fusion reaction. This model is well suited for the enveloped viral fusogens, and aspects of it may even translate to the mechanism employed by the vesicular SNARE fusion proteins. However, because the diminutive size of the p10 FAST protein excludes it from driving membrane merger by mechanical pushing and pulling, a new model must be developed to explain how they may mediate this reaction. The following sections will describe how the data presented in this thesis contribute to our knowledge and understanding of FAST-mediated membrane fusion, as well as how these findings may influence current models of protein mediated membrane fusion.

5.2. Spatial and Temporal Regulation of FAST Protein-Mediated Membrane Fusion

The enveloped viral and SNARE fusion proteins closely couple membrane binding and fusion (Bagnat et al., 2001; Bentz, 2000; Carr et al., 1997; Charloteaux et al., 2009; Chernomordik and Kozlov, 2008; Cohen and Melikyan, 2004; Earp et al., 2004; Epand, 2003; Gerst, 2003; Harrison, 2008; Martens and McMahon, 2008; Tamm and Han, 2000). We have previously reported that the p14 FAST protein localizes to adherens junctions (Salsman et al., 2008b), where it may exploit pre-existing areas of short intermembrane spacing produced by several different adhesion molecules, effectively outsourcing the binding stage of the fusion reaction. Unlike the enveloped viral and SNARE fusion proteins, the sequence variability across the FAST proteins, the diversity of adherent cell types susceptible to FAST protein-mediated fusion and the variety of adhesion molecules capable of enhancing FAST-mediated fusion make it unlikely that

the FAST proteins associate with a receptor to trigger fusion. However, the FAST proteins are detectable on the cell surface well before any syncytiogenesis is observed, suggesting there exists some mechanism of temporal coordination. Additionally, degradation studies on the p10 FAST proteins suggest the HP exists in a solvent-exposed, fusion active state during trafficking, but does not induce fusion of intracellular membrane compartments. This suggests that FAST protein-mediated membrane fusion is untriggered, but temporally and spatially regulated by the cell.

The results presented in this thesis indicate potential roles for CH in regulating FAST protein-mediated membrane fusion. As mentioned earlier, CH is a major component in the membranes of eukaryotic cells, and the concentrations of CH in membranes increase from the ER, to the Golgi, to the plasma membrane. While the p10 FAST proteins do not appear to contain functional CRAC motifs, CH in the plasma membrane still promotes p10 clustering and multimerization, which are essential for membrane fusion activity. This requirement allows p10 to be synthesized with the HP in a solvent-exposed, fusion active state without causing intracellular membrane fusion, thus spatially and temporally coordinating p10-mediated membrane fusion. Additionally, CH-mediated p10 clustering may promote colocalization with adhesion molecules, which have also been identified in cholesterol-rich membrane microdomains (Causeret et al., 2005; Nusrat et al., 2000). However, it is unknown if the FAST proteins actively recruit cellular adhesions, or preferentially partition into plasma membrane domains in which these proteins reside and consequently increase the probability of colocalization. Putative protein-protein interactions between the FAST proteins and cellular adhesions could be probed using a similar FRET assay employed to measure p10-p10 homomultimerization. Adaptation of this assay to a FACS-based system is achievable (Banning et al., 2010), and would provide a fast, high-throughput option to identify and analyze cellular interacting partners of the FAST proteins.

5.3. Membrane Apposition During FAST Protein-Mediated Membrane Fusion

The large ectodomains of the enveloped viral fusion proteins extend approximately 10 nm away from the cell surface and can interact with target membranes outside of the repulsive hydration layer (Harrison, 2008; Leikin et al., 1993; Rand and Parsegian, 1989). Mechanical energy provided by hairpin formation is then considered to pull membranes into close apposition and induce fusion. While adherens junctions typically bring cells within 28 to 38 nm of each other (Irie et al., 2004; Koch et al., 2004; Leckband and Sivasankar, 2000; Zhu et al., 2003), the FAST proteins must still contend with the hydration layer, and thus must supply energy into the system. The CH mediated clustering of p10 proteins may influence the energies associated with fusion. The intercalation of CH between PC head groups decreases the overall hydration of the area, and likewise the repulsive hydration forces (Kucerka et al., 2008; McIntosh et al., 1989). The presence of CH also favours membrane dehydration, which lowers the energy barrier to lipid mixing (Simon and McIntosh, 1989). The moderate hydrophobicity of a single p10 HP is likely not sufficient to dehydrate lipid head groups and reduce the hydration force enough to drive apposition. However, CH-dependent higher-order multimerization of p10 proteins would increase local hydrophobicity levels, which could reduce lipid head group hydration to the point that membrane apposition and merger are energetically favorable. Peptide induced membrane aggregation could be qualitatively demonstrated using X-ray scattering, as has been done for PEG-induced membrane fusion (Boni et al., 1984). It may even be possible to quantify p10-induced membrane dehydration by using a combination of solid-state ^{1}H magic-angle spinning (MAS) NMR, two-dimensional NOESY and ^{13}C MAS NMR techniques (Gawrisch et al., 2007; Volke and Pampel, 1995). Recent measurements of energies associated with membrane dehydration have found that the free energy required for this process is sufficient to stabilize stalk formation (Aeffner et al., 2012). It has also been suggested that the inhibition of both SNARE-mediated and enveloped viral protein-mediated fusion after cholesterol depletion is likely a result of effects on the hydration barrier (Chang et al., 2009; Ivankin et al., 2012; Lai et al., 2012).

5.4. Lipid Mixing and Non-Bilayer Transition States

Some small molecules, such as PEG, can induce membrane aggregation through volume exclusion, which results in an osmotic force driving membranes into close contact in the dehydrated region (Kuhl et al., 1996; Malinin and Lentz, 2004). At higher concentrations these molecules are capable of creating extended areas of dehydration to induce membrane fusion (Lentz, 2007). Studies on the hydration layers of membranes have found that each DOPC head group can coordinate between 5.4 and 22 water molecules, with an average of ~12 waters/lipid (Hristova and White, 1998; Mashl et al., 2001; Volke et al., 1994). The presence of CH lowers the hydration potential of DOPC membranes by spreading the DOPC head groups apart and decreasing the dipole density (Aeffner et al., 2012; Klymchenko et al., 2004). Based on cross-sectional head group sizes of 22.3 and 70 $Å^2$ for CH and DOPC, respectively (Chang et al., 1995; Chiu et al., 2002), a 10 nm microdomain composed of 2:1 DOPC:CH could still coordinate approximately 1720 water molecules, based on the relative hydration ratios calculated by Klymchenko and coworkers (Klymchenko et al., 2004). By comparison, the number of water molecules in a layer one molecule thick (approximately 0.2 nm) in the bulk phase water of the same diameter as the theoretical 10 nm CH microdomain is 525. Assuming that the p10 proteins function as heptamers or octomers, as was roughly estimated earlier, the moderate hydrophobicities of the p10 HPs make it unlikely that extended areas of the membrane are sufficiently dehydrated to drive membrane fusion. There are likely energy inputs from disruption of hydrophobic boundaries or phospholipid packing that promotes lipid mixing and hemifusion after dehydration-driven close apposition.

The enhancement of p10 lipid mixing activity by CH, indicates an essential role for this molecule in membrane fusion. Interestingly, CH effects were independent of p10 binding and conformational changes. It is possible that the unfavorable exposure of hydrophobic residues creates a metastable structure that is conformationally dynamic. Our attempts to solve the three-dimensional structure were unsuccessful, but the results did support the hypothesis of a structurally dynamic p10 ectodomain. Upon lipid binding, there was an observed structural transition that may reflect a stabilization of the cystine

loop. It is possible that energy from the metastable structure could be transmitted into the membrane by inducing local perturbations of the hydrophilic-hydrophobic boundary or of phospholipid packing in a CH-dependent manner. The CH-dependent multimerization and higher-order clustering of the p10 proteins is essential for fusion, so it is logical that CH could play a role throughout the membrane fusion reaction as well. Superficially, it would seem as though the increased lipid ordering and membrane rigidity imparted by CH would inhibit membrane deformations and thermal undulations required for membrane fusion. However, the high lateral mobility and ability to migrate between the inner and outer leaflets (Muller and Herrmann, 2002; Steck et al., 2002), as well as its ability to promote H_{II} phase transitions (Kinnunen, 1996) could make CH an essential element in promoting favorable energy transitions throughout the fusion reaction. It may be possible to visualize the interactions and dynamics of CH during p10-mediated membrane fusion by using time-lapse confocal microscopy of fluorescently tagged p10 in cells loaded with fluorescent cholesterol analogs (Mukherjee et al., 1998).

The mechanism of FAST protein-mediated membrane fusion is likely to progress through a disordered intermediate stage, as membrane curvature agents that inhibit hemifusion or promote pore formation during the membrane fusion reactions mediated by other fusogens have no effect on FAST protein-mediated membrane fusion (Clancy et al., 2010). This disordered state may be a more accurate description of the intermediates observed during many, if not all, membrane fusion reactions (Jahn and Grubmuller, 2002). The energy calculations of membrane fusion employed by Kozlov and coworkers (Kozlov et al., 2010) models membranes as continuous, elastic entities. While this model is very useful for describing the energies associated with membrane bending, it uses a simplified assumption that lipid and water molecules partition into well-defined layers and maintain these structures throughout the fusion process. This assumption inherently excludes the effects of possible incorporation of water molecules into the lipid bilayer, as well as any lipid undulations, thermal movements or discontinuities at the molecular level. The hypothesis that intermediate stages of the membrane fusion reaction may be much more disordered than assumed by the elastic model is supported by several studies describing membrane fusion using atomistic simulations and X-ray diffraction studies (Aeffner et al., 2012; Jahn and Grubmuller, 2002).

Thus, rather than contributing energy by mechanically bending membranes and inducing sustained curvature, the FAST proteins may transmit energy into the system through dehydration-induced aggregation coupled with alterations in the molecular order of the bilayer at the point of contact between CH-rich regions of cell membranes. Several motifs contained within the FAST proteins actively contribute to the fusion reaction and are presumably contributors to these chaotropic effects; these motifs include the HPs, TMDs, polyproline helices, fatty acid modifications, and membrane-proximal β-branched and polar residues (Barry et al., 2010; Clancy and Duncan, 2009, 2011; Corcoran and Duncan, 2004; Corcoran et al., 2004; Shmulevitz et al., 2004b; Shmulevitz et al., 2003; Top et al., 2012). Several membrane destabilizing and deforming features of these motifs may also collaborate to stabilize the post-mixing non-bilayer transition states during membrane fusion.

5.5. Implications for Enveloped Viral Fusogens

The p10 FAST proteins are the smallest known viral or cellular membrane fusion proteins. Their mechanism of membrane fusion clearly cannot follow the paradigmatic fusion reaction driven by conformational dynamics and mechanical pulling of membranes. However, the knowledge garnered through the study of the p10 FAST proteins may have important implications for enveloped viral protein-mediated membrane fusion. The enveloped viral fusion proteins have evolved to mediate virus-cell fusion, and thus contain all elements required for each stage of the fusion reaction, such as membrane binding, close apposition, lipid mixing, pore formation and pore expansion. The FAST proteins, in contrast, have evolved to specifically mediate cell-cell fusion, and thus have access to cellular machinery that can be commissioned to either aid in the fusion reaction, or completely take over certain aspects. This allows us to uncouple the various stages of the fusion reaction and focus on the minimal requirements for each step. It is possible that the membrane fusion mediated by the enveloped viral fusion proteins is less coupled than the current paradigm suggests. The large, complex structures may be

required to bridge membranes during the initial receptor binding stages of membrane fusion, similar to the adhesion molecules during FAST-mediated fusion, but the conformational changes are required to allow for fusion rather than to drive fusion. This theory is supported by the observation that the proposed conformational folding of the enveloped viral fusion proteins after target membrane interaction is impossible without dissociation of the ternary structure (Albertini et al., 2012; Stiasny et al., 1996; Weissenhorn et al., 2007). This dissociation would significantly dissipate the potential energy of the complex and reduce the available mechanical energy for pulling membranes together. It is possible that the enveloped viral fusion proteins and the FAST proteins share a common mechanism of membrane fusion, the discovery of which has been obscured by the complex structures required to mediate several stages of the fusion reaction. The FPs of the enveloped viral fusion proteins, then, may act in a similar fashion to the HPs of the p10 proteins by inducing local dehydration-induced aggregation and bilayer perturbations to drive fusion (Tamm and Han, 2000).

5.6. Final Thoughts

To fully understand p10 FAST protein-mediated membrane fusion, a complete understanding of the stoichiometry, temporal and spatial recruitment and interacting partners of these proteins is required. It is likely that the FAST proteins have outsourced many of the pre- and post-fusion stages to cellular components, however these stages remain poorly understood. Through additional biochemical and biophysical characterizations, it may be possible to observe the complex molecular motions, as well as cellular interactions, of the FAST proteins during syncytiogenesis. Although considerable progress has been made towards understanding the functional motifs of the FAST proteins, a comprehensive mechanism remains elusive. The studies presented here were aimed at exploiting the sequence conservation and divergence, as well as functional disparities between homologous FAST proteins to identify different regions that contribute to membrane fusion activity. This has led to the discovery of a remarkably compact, multifunctional ectodomain fusion module comprising two independent functional motifs: an N-terminal disulfide bonded FP motif that governs CH-facilitated

membrane destabilization, and a C-terminal MPER motif that governs reversible, CH-dependent clustering and multimerization in distinct, species-specific fusion platforms. Perhaps not surprisingly, these motifs function differently than any other currently identified fusion protein functional motif. However, knowledge of their function may be informative in the search for the undiscovered cellular fusion proteins. It is unlikely that such proteins will share any amino acid identity with the FAST proteins, as there is very little sequence similarity between the FAST proteins themselves, but it is possible that these proteins share similar functional characteristics to the FAST proteins. Alternatively, through the identification of additional cellular interacting partners and the elucidation of cellular pathways exploited by the FAST proteins during syncytiogenesis it may be possible to identify a "fusion pathway". This information could provide a novel method for identifying cellular fusogens. In this respect, the FAST proteins may become the paradigm for membrane fusion during physiological syncytium formation.

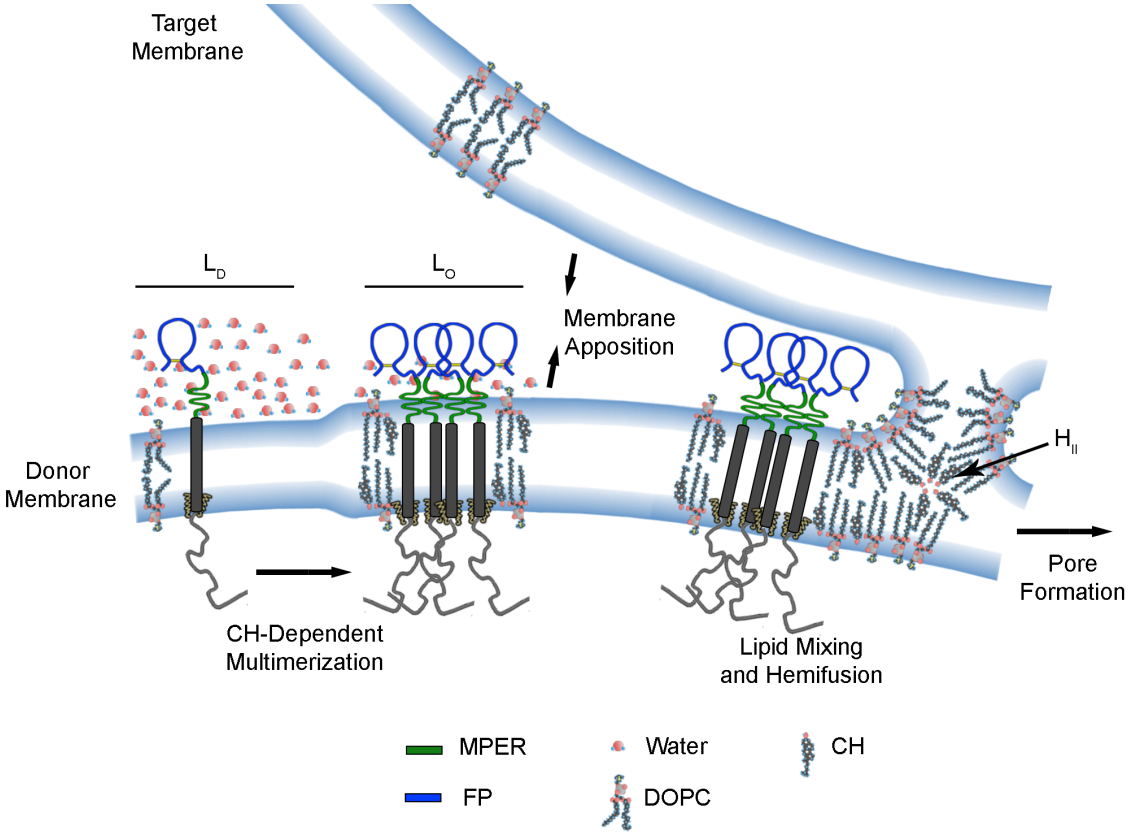

Figure 5.1- An early-stage model for p10 membrane fusion. In the L_D phase, the p10 proteins exist as monomers, which are incapable of inducing membrane fusion. Upon transitioning into CH-rich, L_O membrane microdomains, the p10 proteins are able to form multimers, which are mediated by the MPER motifs. This multimerization results in clustering of p10 FPs, which can then affect lipid destabilization/mixing and induce fusion of donor and target membranes.

APPENDIX

Letters of Copyright Permission

Letter of Permission for Figure 1.1

NATURE PUBLISHING GROUP LICENSE TERMS AND CONDITIONS

Oct 15, 2013

This is a License Agreement between Timothy Key ("You") and Nature Publishing Group ("Nature Publishing Group") provided by Copyright Clearance Center ("CCC"). The license consists of your order details, the terms and conditions provided by Nature Publishing Group, and the payment terms and conditions.

All payments must be made in full to CCC. For payment instructions, please see information listed at the bottom of this form.

License Number	3250400438101
License date	Oct 15, 2013
Licensed content publisher	Nature Publishing Group
Licensed content publication	Nature Structural and Molecular Biology
Licensed content title	Mechanics of membrane fusion
Licensed content author	Leonid V Chernomordik and Michael M Kozlov
Licensed content date	Jul 1, 2008
Volume number	15
Issue number	7
Type of Use	reuse in a thesis/dissertation
Requestor type	academic/educational
Format	print and electronic
Portion	figures/tables/illustrations
Number of figures/tables/illustrations	1
High-res required	no
Figures	Figure 1.1
Author of this NPG article	no
Your reference number	
Title of your thesis / dissertation	Mechanistic Contributions of the p10 FAST Protein Ectodomains to Membrane Fusion and Syncytiogenesis
Expected completion date	Dec 2013
Estimated size (number of pages)	300
Total	0.00 USD
Terms and Conditions	

Nature Publishing Group hereby grants you a non-exclusive license to reproduce this material for this purpose, and for no other use, subject to the conditions below:

1. NPG warrants that it has, to the best of its knowledge, the rights to license reuse of this material. However, you should ensure that the material you are requesting is original to Nature Publishing Group and does not carry the copyright of another entity (as credited in the published version). If the credit line on any part of the material you have requested indicates that it was reprinted or adapted by NPG with permission from another source, then you should also seek permission from that source to reuse the material.

2. Permission granted free of charge for material in print is also usually granted for any electronic version of that work, provided that the material is incidental to the work as a whole and that the electronic version is essentially equivalent to, or substitutes for, the print version. Where print permission has been granted for a fee, separate permission must be obtained for any additional, electronic re-use (unless, as in the case of a full paper, this has already been accounted for during your initial request in the calculation of a print run).NB: In all cases, web-based use of full-text articles must be authorized separately through the 'Use on a Web Site' option when requesting permission.

3. Permission granted for a first edition does not apply to second and subsequent editions and for editions in other languages (except for signatories to the STM Permissions Guidelines, or where the first edition permission was granted for free).

4. Nature Publishing Group's permission must be acknowledged next to the figure, table or abstract in print. In electronic form, this acknowledgement must be visible at the same time as the figure/table/abstract, and must be hyperlinked to the journal's homepage.

5. The credit line should read: Reprinted by permission from Macmillan Publishers Ltd: [JOURNAL NAME] (reference citation), copyright (year of publication) For AOP papers, the credit line should read: Reprinted by permission from Macmillan Publishers Ltd: [JOURNAL NAME], advance online publication, day month year (doi: 10.1038/sj.[JOURNAL ACRONYM].XXXXX) **Note: For republication from the *British Journal of Cancer*, the following credit lines apply.** Reprinted by permission from Macmillan Publishers Ltd on behalf of Cancer Research UK: [JOURNAL NAME] (reference citation), copyright (year of publication)For AOP papers, the credit line should read: Reprinted by permission from Macmillan Publishers Ltd on behalf of Cancer Research UK: [JOURNAL NAME], advance online publication, day month year (doi:10.1038/sj.[JOURNAL ACRONYM].XXXXX)

6. Adaptations of single figures do not require NPG approval. However, the adaptation should be credited as follows: Adapted by permission from Macmillan Publishers Ltd: [JOURNAL NAME] (reference citation), copyright (year of publication) **Note: For adaptation from the *British Journal of Cancer*, the following credit line applies.** Adapted by permission from Macmillan Publishers Ltd on behalf of Cancer Research UK: [JOURNAL NAME] (reference citation), copyright (year of publication)

7. Translations of 401 words up to a whole article require NPG approval. Please visit http://www.macmillanmedicalcommunications.com for more information.Translations of up to a 400 words do not require NPG approval. The translation should be credited as follows: Translated by permission from Macmillan Publishers Ltd: [JOURNAL NAME] (reference citation), copyright (year of publication). **Note: For translation from the *British Journal of Cancer*, the following credit line applies.** Translated by permission from Macmillan Publishers Ltd on behalf of Cancer Research UK: [JOURNAL NAME] (reference citation), copyright (year of publication)

We are certain that all parties will benefit from this agreement and wish you the best in the use of this

material. Thank you.

Special Terms: v1.1

If you would like to pay for this license now, please remit this license along with your payment made payable to "COPYRIGHT CLEARANCE CENTER" otherwise you will be invoiced within 48 hours of the license date. Payment should be in the form of a check or money order referencing your account number and this invoice number RLNK501136243.

Once you receive your invoice for this order, you may pay your invoice by credit card. Please follow instructions provided at that time.

Make Payment To: Copyright Clearance Center Dept 001 P.O. Box 843006 Boston, MA 02284-3006

For suggestions or comments regarding this order, contact RightsLink Customer

Support: customercare@copyright.com or +1-877-622-5543 (toll free in the US) or +1-978-646-2777.

Gratis licenses (referencing $0 in the Total field) are free. Please retain this printable license for your reference. No payment is required.

Letter of Permission for Figures 1.2 and 1.3.

NATURE PUBLISHING GROUP LICENSE TERMS AND CONDITIONS

Oct 15, 2013

This is a License Agreement between Timothy Key ("You") and Nature Publishing Group ("Nature Publishing Group") provided by Copyright Clearance Center ("CCC"). The license consists of your order details, the terms and conditions provided by Nature Publishing Group, and the payment terms and conditions.

All payments must be made in full to CCC. For payment instructions, please see information listed at the bottom of this form.

License Number	3250421047873
License date	Oct 15, 2013
Licensed content publisher	Nature Publishing Group
Licensed content publication	Nature Structural and Molecular Biology
Licensed content title	Viral membrane fusion
Licensed content author	Stephen C Harrison
Licensed content date	Jul 1, 2008
Volume number	15
Issue number	7
Type of Use	reuse in a thesis/dissertation
Requestor type	academic/educational
Format	print and electronic
Portion	figures/tables/illustrations
Number of figures/tables/illustrations	3
High-res required	no
Figures	Figures 1.2 and 1.3
Author of this NPG article	no
Your reference number	
Title of your thesis / dissertation	Mechanistic Contributions of the p10 FAST Protein Ectodomains to Membrane Fusion and Syncytiogenesis
Expected completion date	Dec 2013
Estimated size (number of pages)	300
Total	0.00 USD
Terms and Conditions	

Terms and Conditions for Permissions

Nature Publishing Group hereby grants you a non-exclusive license to reproduce this material for this purpose, and for no other use,subject to the conditions below:

1. NPG warrants that it has, to the best of its knowledge, the rights to license reuse of this material. However, you should ensure that the material you are requesting is original to Nature Publishing Group and does not carry the copyright of another entity (as credited in the published version). If the credit line on any part of the material you have requested indicates that it was reprinted or adapted by NPG with permission from another source, then you should also seek permission from that source to reuse the material.

2. Permission granted free of charge for material in print is also usually granted for any electronic version of that work, provided that the material is incidental to the work as a whole and that the electronic version is essentially equivalent to, or substitutes for, the print version. Where print permission has been granted for a fee, separate permission must be obtained for any additional, electronic re-use (unless, as in the case of a full paper, this has already been accounted for during your initial request in the calculation of a print run).NB: In all cases, web-based use of full-text articles must be authorized separately through the 'Use on a Web Site' option when requesting permission.

3. Permission granted for a first edition does not apply to second and subsequent editions and for editions in other languages (except for signatories to the STM Permissions Guidelines, or where the first edition permission was granted for free).

4. Nature Publishing Group's permission must be acknowledged next to the figure, table or abstract in print. In electronic form, this acknowledgement must be visible at the same time as the figure/table/abstract, and must be hyperlinked to the journal's homepage.

5. The credit line should read:
   Reprinted by permission from Macmillan Publishers Ltd: [JOURNAL NAME] (reference citation), copyright (year of publication)
   For AOP papers, the credit line should read:
   Reprinted by permission from Macmillan Publishers Ltd: [JOURNAL NAME], advance online publication, day month year (doi: 10.1038/sj.[JOURNAL ACRONYM].XXXXX)

   Note: For republication from the *British Journal of Cancer,* the following credit lines apply.
   Reprinted by permission from Macmillan Publishers Ltd on behalf of Cancer

Research UK: [JOURNAL NAME] (reference citation), copyright (year of publication)For AOP papers, the credit line should read:
Reprinted by permission from Macmillan Publishers Ltd on behalf of Cancer Research UK: [JOURNAL NAME], advance online publication, day month year (doi: 10.1038/sj.[JOURNAL ACRONYM].XXXXX)

6. Adaptations of single figures do not require NPG approval. However, the adaptation should be credited as follows:

   Adapted by permission from Macmillan Publishers Ltd: [JOURNAL NAME] (reference citation), copyright (year of publication)

   Note: For adaptation from the *British Journal of Cancer*, the following credit line applies.
   Adapted by permission from Macmillan Publishers Ltd on behalf of Cancer Research UK: [JOURNAL NAME] (reference citation), copyright (year of publication)

7. Translations of 401 words up to a whole article require NPG approval. Please visit http://www.macmillanmedicalcommunications.com for more information.Translations of up to a 400 words do not require NPG approval. The translation should be credited as follows:

   Translated by permission from Macmillan Publishers Ltd: [JOURNAL NAME] (reference citation), copyright (year of publication).

   Note: For translation from the *British Journal of Cancer*, the following credit line applies.
   Translated by permission from Macmillan Publishers Ltd on behalf of Cancer Research UK: [JOURNAL NAME] (reference citation), copyright (year of publication)

We are certain that all parties will benefit from this agreement and wish you the best in the use of this material. Thank you.

Special Terms:

v1.1

If you would like to pay for this license now, please remit this license along with your payment made payable to "COPYRIGHT CLEARANCE CENTER" otherwise you will be invoiced within 48 hours of the license date. Payment should be in the form of a check or money order referencing your account number and this invoice number RLNK501136266.
Once you receive your invoice for this order, you may pay your invoice by credit card. Please follow instructions provided at that time.

Make Payment To:

REFERENCES

Abell, B.A., Brown, D.T., 1993. Sindbis virus membrane fusion is mediated by reduction of glycoprotein disulfide bridges at the cell surface. J Virol 67, 5496-5501.

Aeffner, S., Reusch, T., Weinhausen, B., Salditt, T., 2012. Energetics of stalk intermediates in membrane fusion are controlled by lipid composition. Proc Natl Acad Sci USA 109, E1609-E1618.

Ahn, A., Gibbons, D., Kielian, M., 2002. The fusion peptide of Semliki Forest virus associates with sterol-rich membrane domains. J Virol 76, 3267-3275.

Albertazzi, L., Arosio, D., Marchetti, L., Ricci, F., Beltram, F., 2009. Quantitative FRET analysis with the E0GFP-mCherry fluorescent protein pair. Photochem Photobiol 85, 287-297.

Albertini, A.A., Merigoux, C., Libersou, S., Madiona, K., Bressanelli, S., Roche, S., Lepault, J., Melki, R., Vachette, P., Gaudin, Y., 2012. Characterization of monomeric intermediates during VSV glycoprotein structural transition. PLoS Pathog 8, e1002556.

Allen, J.A., Halverson-Tamboli, R.A., Rasenick, M.M., 2006. Lipid raft microdomains and neurotransmitter signalling. Nat Rev Neurosci 8, 128-140.

Allison, S.L., Schalich, J., Stiasny, K., Mandl, C.W., Heinz, F.X., 2001. Mutational evidence for an internal fusion peptide in flavivirus envelope protein E. J Virol 75, 4268-4275.

Almeida, P.F., Pokorny, A., Hinderliter, A., 2005. Thermodynamics of membrane domains. Biochim Biophys Acta 1720, 1-13.

Apellaniz, B., Ivankin, A., Nir, S., Gidalevitz, D., Nieva, J.L., 2011. Membrane-proximal external HIV-1 gp41 motif adapted for destabilizing the highly rigid viral envelope. Biophys J 101, 2426-2435.

Armstrong, R.T., Kushnir, A.S., White, J.M., 2000. The transmembrane domain of influenza hemagglutinin exhibits a stringent length requirement to support the hemifusion to fusion transition. J Cell Biol 151, 425-437.

Arnold, K., Herrmann, A., Gawrisch, K., Pratsch, L., 1985. Mechanisms of poly(ethylene oxide)-induced fusion. Stud Biophys 110, 135-141.

Arnold, K., Zschoernig, O., Barthel, D., Herold, W., 1990. Exclusion of poly(ethylene glycol) from liposome surfaces. Biochim Biophys Acta 1022, 303-310.

Backovic, M., Jardetzky, T.S., 2009. Class III viral membrane fusion proteins. Curr Opin Struct Biol 19, 189-196.

Bagnat, M., Chang, A., Simons, K., 2001. Plasma membrane proton ATPase Pma1p requires raft association for surface delivery in yeast. Mol Biol Cell 12, 4129-4138.

Baker, K.A., Dutch, R.E., Lamb, R.A., Jardetzky, T.S., 1999. Structural basis for paramyxovirus-mediated membrane fusion. Mol Cell 3, 309-319.

Banning, C., Votteler, J., Hoffmann, D., Koppensteiner, H., Warmer, M., Reimer, R., Kirchhoff, F., Schubert, U., Hauber, J., Schindler, M., 2010. A flow cytometry-based FRET assay to identify and analyse protein-protein interactions in living cells. PLoS One 5, e9344. .

Barry, C., Duncan, R., 2009. Multifaceted sequence-dependent and -independent roles for reovirus FAST protein cytoplasmic tails in fusion pore formation and syncytiogenesis. J Virol 83, 12185-12195.

Barry, C., Key, T., Haddad, R., Duncan, R., 2010. Features of a spatially constrained cystine loop in the p10 FAST protein ectodomain define a new class of viral fusion peptide. J Biol Chem 285, 16424-16433.

Basanez, G., 2002. Membrane fusion: the process and its energy suppliers. Cell Mol Life Sci 59, 1478-1490.

Baumert, M., Maycox, P.R., Navone, F., De Camilli, P., Jahn, R., 1989. Synaptobrevin: an integral membrane protein of 18,000 daltons present in small synaptic vesicles of rat brain. EMBO J 8, 379-384.

Bavari, S., Bosio, C.M., Wiegand, E., Ruthel, G., Will, A.B., Geisbert, T.W., Hevey, M., Schmaljohn, C., Schmaljohn, A., Aman, M.J., 2002. Lipid raft microdomains: a gateway for compartmentalized trafficking of ebola and marburg viruses. J Exp Med 195, 593–602.

Benirschke, K., 2003. Remarkable placenta. Clin Anat 11, 194–205.

Bentz, J., 2000. Membrane fusion mediated by coiled coils: a hypothesis. Biophys J 78, 886-900.

Berne, B.J., Weeks, J.D., Zhou, R., 2009. Dewetting and hydrophobic interaction in physical and biological systems. Annu Rev Phys Chem 60, 85-103.

Biswas, S., Yin, S.-R., Blank, P.S., Zimmerberg, J., 2008. Cholesterol promotes hemifusion and pore widening in membrane fusion induced by influenza hemagglutinin. J Gen Physiol 131, 503-513.

Bleil, J.D., Wassarman, P.M., 1983. Sperm-egg interactions in the mouse: sequence of events and induction of the acrosome reaction by a zona pellucida glycoprotein. Dev Biol 95, 317-324.

Bock, J.B., Matern, H.T., Peden, A.A., Scheller, R.H., 2001. A genomic perspective on membrane compartment organization. Nature 409, 839-841.

Boni, L.T., Stewart, T.P., Hui, S.W., 1984. Alterations in phospholipid polymorphism by polyethylene glycol. J Membr Biol 80, 91-104.

Bonifacino, J.S., Glick, B.S., 2004. The mechanisms of vesicle budding and fusion. Cell 116, 153-166.

Boyle, W.J., Simonet , W.S., Lacey, D.L., 2003. Osteoclast differentiation and activation. Nature 423, 337-342.

Bressanelli, S., Stiasny, K., Allison, S.L., Stura, E.A., Duquerroy, S., Lescar, J., Heinz, F.X., Rey, F.A., 2004. Structure of a flavivirus envelope glycoprotein in its low-pH-induced membrane fusion conformation. EMBO J 23, 728-738.

Bretscher, M.S., 1972. Asymmetrical lipid bilayer structure for biological membranes. Nat New Biol 236, 11-12.

Brown, C.W., Stephenson, K.B., Hanson, S., Kucharczyk, M., Duncan, R., Bell, J.C., Lichty, B.D., 2009. The p14 FAST protein of reptilian reovirus increases vesicular stomatitis virus neuropathogenesis. J Virol 83, 552-561.

Brown, D.A., Rose, J.K., 1992. Sorting of GPI-anchored proteins to glycolipid-enriched membrane subdomains during transport to the apical cell surface. Cell 68, 533-544.

Bullough, P.A., Hughson, F.M., Skehel, J.J., Wiley, D.C., 1994. Structure of influenza haemagglutinin at the pH of membrane fusion. Nature 37, 37-43.

Burgess, S.W., McIntosh, T.J., Lentz, B.R., 1992. Modulation of poly(ethylene glycol)-induced fusion by membrane hydration: importance of interbilayer separation. Biochem 31, 2653-2661.

Buzon, V., Natrajan, G., Schibli, D., Campelo, F., Kozlov, M.M., Weissenhorn, W., 2010. Crystal structure of HIV-1 gp41 including both fusion peptide and membrane proximal external regions. PLoS Pathog 6, e1000880.

Campelo, F., McMahon, H.T., Kozlov, M.M., 2008. The hydrophobic insertion mechanism of membrane curvature generation by proteins. Biophys J 95, 2325-2339.

Carr, C.M., Chaudhry, C., Kim, P.S., 1997. Influenza hemagglutinin is spring-loaded by a metastable native conformation. Proc Natl Acad Sci USA 94.

Causeret, M., Taulet, N., Comunale, F., Favard, C., Gauthier-Rouviere, C., 2005. N-cadherin association with lipid rafts regulates its dynamic assembly at cell-cell junctions in C2C12 myoblasts. Mol Biol Cell 16, 2168-2180.

Cavanagh, J., Fairbrother, W.J., Palmer, A.G., Rance, M., Skelton, N.J., 2007. Protein NMR spectroscopy: principles and practice, 2nd ed. Elsevier Academic Press, San Diego, USA.

Cevc, G., Richardsen, H., 1999. Lipid vesicles and membrane fusion. Adv Drug Deliv Rev 38, 207-232.

Chandler, D., 2005. Interfaces and the driving force of hydrophobic assembly. Nature 437, 640-647.

Chang, C., Chen, P.T., Chang, G.D., Huang, C.J., Chen, H., 2004. Functional characterization of the placental fusogenic membrane protein syncytin. Biol Reprod 71, 1956-1962.

Chang, H.M., Reitstetter, R., Gruener, R., 1995. Lipid-ion channel interactions: increasing phospholipid headgroup size but not ordering acyl chains alters reconstituted channel behavior. J Membr Biol 145, 13-19.

Chang, J., Kim, S.-A., Lu, X., Su, Z., Kim, S.K., Shin, Y.-K., 2009. Fusion step-specific influence of cholesterol on SNARE-mediated membrane fusion. Biophys J 96, 1839-1846.

Chanturiya, A., Chernomordik, L.V., Zimmerberg, J., 1997. Flickering fusion pores comparable with initial exocytotic pores occur in protein-free phospholipid bilayers. Proc Natl Acad Sci USA 94, 14423-14428.

Charloteaux, B., Lorin, A., Brasseur, R., Lins, L., 2009. The "Tilted Peptide Theory" links membrane insertion properties and fusogenicity of viral fusion peptides. Protein Pept lett 16, 718-725.

Chatterjee, P.K., Vashishtha, M., Kielian, M., 2000. Biochemical consequences of a mutation that controls the cholesterol dependence of Semliki Forest virus fusion. J Virol 74, 1623-1631.

Chen, E.H., Olson, E.N., 2004. Towards a molecular pathway for myoblast fusion in Drosophila. Trends Cell Biol 14, 452-460.

Chen, J., Lee, K.H., Steinhauer, D.A., Stevens, D.J., Skehel, J.J., Wiley, D.C., 1998. Structure of the hemagglutinin precursor cleavage site, a determinant of influenza pathogenicity and the origin of the labile conformation. Cell 95, 409-417.

Chen, Y.A., Scheller, R.H., 2001. SNARE-mediated membrane fusion. Nat Rev Mol Cell Biol 2, 98-106.

Chen, Z., Rand, R.P., 1997. The Influence of cholesterol on phospholipid membrane curvature and bending elasticity. Biophys J 73, 267-276.

Chen, Z., Zhu, Y., Li, C., Liu, G., 2012. Outbreak-associated novel duck reovirus, China, 2011. Emerg. Infect. Dis. 18, 1209-1211.

Cheng, J.-X., Pautot, S., Weitz, D.A., Xie, X.S., 2003. Ordering of water molecules between phospholipid bilayers visualized by coherent anti-Stokes Raman scattering microscopy. Proc Natl Acad Sci USA 100, 9826-9830.

Cheng, L.T., Plemper, R.K., Compans, R.W., 2005. Atypical fusion peptide of nelson bay virus fusion-associated small transmembrane protein. J Virol 79, 1853-1860.

Cheng, P., Lau, C.S., Lai, A., Ho, E., Leung, P., Chan, F., Wong, A., Lim, W., 2009. A novel reovirus isolated from a patient with acute respiratory disease. J Clin Virol 45, 79-80.

Chernomordik, L., 1996. Non-bilayer lipids and biological fusion intermediates. Chem Phys Lipids 81, 203-213.

Chernomordik, L.V., Frolov, V.A., Leikina, E., Bronk, P., Zimmerberg, J., 1998. The pathway of membrane fusion catalyzed by influenza hemagglutinin: restriction of lipids, hemifusion, and lipidic fusion pore formation. J Cell Biol 140, 1369-1382.

Chernomordik, L.V., Kozlov, M.M., 2003. Protein-lipid interplay in fusion and fission of biological membranes. Annu Rev Biochem 72, 175-207.

Chernomordik, L.V., Kozlov, M.M., 2008. Mechanics of Membrane Fusion. Nat Struct Mol Biol 15, 675-683.

Chiu, S.W., Jakobsson, E., Mashl, R.J., Scott, H.L., 2002. Cholesterol-induced modifications in lipid bilayers: A simulation study. Biophys J 83, 1842-1853.

Chizmadzhev, Y.A., Cohen, F.S., Shcherbakov, A., Zimmerberg, J., 1995. Membrane mechanics can account for fusion pore dilation in stages. Biophys J 69, 2489-2500.

Christopherson, K.S., Sweeney, N.T., Craven, S.E., Kang, R., El-Husseini, A.E.-D., Bredt, D.S., 2003. Lipid- and protein-mediated multimerization of PSD- 95: implications for receptor clustering and assembly of synaptic protein networks. J Cell Sci 116, 3213-3219.

Chua, K.B., Bellini, W.J., Rota, P.A., Harcourt, B.H., Tamin, A., Lam, S.K., Ksiazek, T.G., Rollin, P.E., Zaki, S.R., Shieh, W.-J., Goldsmith, C.S., Gubler, D.J., Roehrig, J.T., Eaton, B., Gould, A.R., Olson, J., Field, H., Daniels, P., Ling, A.E., Peters, C.J., Anderson, L.J., Mahy, B.W.J., 2000. Nipah virus: A recently emergent deadly paramyxovirus. Science 288, 1432-1435.

Chua, K.B., Crameri, G., Hyatt, A., Yu, M., Tompang, M.R., Rosli, J., McEachern, J., Crameri, S., Kumarasamy, V., Eaton, B.T., Wang, L.-F., 2007. A previously unknown reovirus of bat origin is associated with an acute respiratory disease in humans. Proc Natl Acad Sci USA 104, 11424-11429.

Chua, K.B., Voon, K., Crameri, G., Tan, H.S., Rosli, J., Mceachern, J.A., Suluraju, S., Yu, M., Wang, L.-f., 2008. Identification and characterization of a new orthoreovirus from patients with acute respiratory infections. PLOS ONE 3, 1-7.

Chua, K.B., Voon, K., Yu, M., Keniscope, C., Abdul Rasid, K., Wang, L.-F., 2011. Investigation of a potential zoonotic transmission of orthoreovirus associated with acute influenza-like illness in an adult patient. PLOS ONE 6, e25434.

Clancy, E.K., Barry, C., Ciechonska, M., Duncan, R., 2010. Different activities of the reovirus FAST proteins and influenza hemagglutinin in cell-cell fusion assays and in response to membrane curvature agents. Virol 397, 119-129.

Clancy, E.K., Duncan, R., 2009. Reovirus FAST protein transmembrane domains function in a modular, primary sequence-independent manner to mediate cell-cell membrane fusion. J Virol 83, 2941-2950.

Clancy, E.K., Duncan, R., 2011. Helix-destabilizing, β-branched, and polar residues in the baboon reovirus p15 transmembrane domain influence the modularity of FAST proteins. J Virol 85, 4707-4719.

Cohen, F.S., Melikyan, G.B., 2004. The energetics of membrane fusion from binding, through hemifusion, pore formation and pore enlargement. J Membr Biol 199, 1-14.

Corcoran, J.A., Clancy, E.K., Duncan, R., 2011. Homomultimerization of the reovirus p14 fusion-associated small transmembrane protein during transit through the ER–Golgi complex secretory pathway. J Gen Virol 92, 162-166.

Corcoran, J.A., Duncan, R., 2004. Reptilian reovirus utilizes a small type III protein with an external myristylated amino terminus to mediate cell-cell fusion. J Virol 78, 4342–4351.

Corcoran, J.A., Salsman, J., Antueno, R.D., Touhami, A., Jericho, M.H., Clancy, E.K., Duncan, R., 2006. The p14 fusion-associated small transmembrane (FAST) protein effects membrane fusion from a subset of membrane microdomains. J Biol Chem 281, 31778-31789.

Corcoran, J.A., Syvitski, R., Top, D., Epand, R.M., Epand, R.F., Jakeman, D., Duncan, R., 2004. Myristoylation, a protruding loop, and structural plasticity are essential features of a nonenveloped virus fusion peptide motif. J Biol Chem 279, 51386-51394.

Cross, K.J., Langley, W.A., Russell, R.J., Skehel, J.J., Steinhauer, D.A., 2009. Composition and functions of the influenza fusion peptide. Protein Pept Lett 16, 766-778.

Cui, W., Ke, J.Z., Zhang, Q., Ke, H.-Z., Chalouni, C.c., Vignery, A.s., 2006. The intracellular domain of CD44 promotes the fusion of macrophages. Blood 107, 796-805.

Dawe, S., and R. Duncan, 2002. The S4 genome segment of baboon reovirus is bicistronic and encodes a novel fusion-associated small transmembrane protein. J Virol 76, 2131-2140.

de Vries, T.J., Schoenmaker, T., Beertsen, W., van der Neut, R., Everts, V., 2005. Effect of CD44 deficiency on in vitro and in vivo osteoclast formation. J Cell Biochem 94, 954-966.

del Campo, J.J., Opoku-Serebuoh, E., Isaacson, A.B., Scranton, V.L., Tucker, M., Han, M., Mohler, W.A., 2005. Fusogenic activity of EFF-1 is regulated via dynamic localization in fusing somatic cells in C. elegans. Curr Biol 15, 413-423.

Delos, S.E., Gilbert, J.M., White, J.M., 2000. The central proline of an internal viral fusion peptide serves two important roles. J Virol 74, 1686-1693.

Delos, S.E., White, J.M., 2000. Critical role for the cysteines flanking the internal fusion peptide of avian sarcoma/leukosis virus envelope glycoprotein. J Virol 74, 9738-9741.

Dennison, S.M., Greenfield, N., Lenard, J., Lentz, B.R., 2002. VSV transmembrane domain (TMD) peptide promotes PEG-mediated fusion of liposomes in a conformationally sensitive fashion. Biochem 41.

Dickey, A., Faller, R., 2008. Examining the contributions of lipid shape and headgroup charge on bilayer behavior. Biophys J 95, 2636-2646.

Drake, J.W., 1993. Rates of spontaneous mutation among RNA viruses. Proc Natl Acad Sci USA 90, 4171-4175.

Drake, J.W., Holland, J.J., 1999. Mutation rates among RNA viruses. Proc Natl Acad Sci USA 96, 13910-13913.

Duncan, R., 1999. Extensive sequence divergence and phylogenetic relationships between the fusogenic and nonfusogenic orthoreoviruses: a species proposal. Virol 260, 316-328.

Duncan, R., Chen, Z., Walsh, S., Wu, S., 1996. Avian reovirus-induced syncytium formation is independent of infectious progeny virus production and enhances the rate, but is not essential, for virus-induced cytopathology and virus egress. . Virol 224, 453–464.

Duncan, R., Corcoran, J., Shou, J., Stoltz, D., 2004. Reptilian reovirus: a new fusogenic orthoreovirus species. Virol 319, 131-140.

Duncan, R., Murphy, F.A., Mirkovic, R.R., 1995. Characterization of a novel syncytium-inducing baboon reovirus. Virol 212, 752–756.

Duncan, R., Sullivan, K., 1998. Characterization of two avian reoviruses that exhibit strain-specific quantitative differences in their syncytium-inducing and pathogenic capabilities. Virol 250, 263-272.

Duquerroy, S., Vigouroux, A., Rottier, P.J., Rey, F.A., Bosch, B.J., 2005. Central ions and lateral asparagine/glutamine zippers stabilize the post-fusion hairpin conformation of the SARS coronavirus spike glycoprotein. Virol 335, 276-285.

Durell, S., Martin, I., Ruysschaert, J., Shai, Y., Blumenthal, R., 1997. What studies of fusion peptides tell us about viral envelope glycoprotein-mediated membrane fusion. Mol Membr Biol 14, 97-112.

Durrer, P., Galli, C., Hoenke, S., Corti, C., Gluck, R., Vorherr, T., Brunner, J., 1996. H+-induced membrane insertion of influenza virus hemagglutinin involves the HA2 amino- terminal fusion peptide but not the coiled coil region. J Biol Chem 271, 13417-13421.

Dutch, R.E., Jardetzky, T.S., Lamb, R.A., 2000. Virus membrane fusion proteins: biological machines that undergo a metamorphosis. Biosci Rep 20, 597-612.

Dutch, R.E., Leser, G.P., Lamb, R.A., 1999. Paramyxovirus fusion protein: characterization of the core trimer, a rod-shaped complex with helices in anti-parallel orientation. Virol 254, 147-159.

Earp, L.J., Delos, S.E., Park, H.E., White, J.M., 2004. The many mechanisms of viral membrane fusion proteins. Curr Top Microbiol Immunol 285, 25-66.

Eckert, D.M., Kim, P.S., 2001. Mechanisms of viral membrane fusion and its inhibition. Annu Rev Biochem 70, 777-810.

Einer-Jensen, K., Krogh, T.N., Roepstorff, P., Lorenzen, N., 1998. Characterization of intramolecular disulfide bonds and secondary modifications of the glycoprotein

from viral hemorrhagic septicemia virus, a fish rhabdovirus. J Virol 72, 10189-10196.

Ellena, J.F., Liang, B., Wiktor, M., Stein, A., Cafiso, D.S., Jahn, R., Tamm, L.K., 2009. Dynamic structure of lipid-bound synaptobrevin suggests a nucleation-propagation mechanism for trans-SNARE complex formation. Proc Natl Acad Sci USA 106, 20306-20311.

Engel, S., Vries, M.d., Herrmann, A., Veit, M., 2012. Mutation of a raft-targeting signal in the transmembrane region retards transport of influenza virus hemagglutinin through the Golgi. FEBS Letters 586, 277-282.

Epand, R.M., 1998. Lipid polymorphism and protein-lipid interactions. Biochim Biophys Acta 1376, 353-368.

Epand, R.M., 2003. Fusion peptides and the mechanism of viral fusion. Biochim Biophys Acta 1614, 116-121.

Epand, R.M., 2006. Cholesterol and the interaction of proteins with membrane domains. Prog Lipid Res 45, 279-294.

Epand, R.M., Thomas, A., Brasseur, R., Epand, R.F., 2010. Cholesterol interaction with proteins that partition into membrane domains: an overview. Subcell Biochem 51, 253-278.

Fadok, V.A., Voelker, D.R., Campbell, P.A., Cohen, J.J., Bratton, D.L., Henson, P.M., 1992. Exposure of phosphatidylserine on the surface of apoptotic lymphocytes triggers specific recognition and removal by macrophages. J Immunol 148, 2207-2216.

Fasshauer, D., Sutton, R.B., Bru□nger, A.T., Jahn, R., 1998. Conserved structural features of the synaptic fusion complex: SNARE proteins reclassified as Q- and R-SNAREs. Proc Natl Acad Sci USA 95, 15781-15786.

Feige, J.N., Sage, D., Wahli, W., Desvergne, B., Gelman, L., 2005. PixFRET, an ImageJ plug-in for FRET calculation that can accommodate variations in spectral bleed-throughs. Microsc Res Tech 68, 51-58.

Fernandez, J.M., Neher, E., Gomperts, B.D., 1984. Capacitance measurements reveal stepwise fusion events in degranulating mast cells. Nature 312, 453-455.

Fredericksen, B.L., Whitt, M.A., 1995. Vesicular stomatitis virus glycoprotein mutations that affect membrane fusion activity and abolish virus infectivity. J Virol 69, 1435- 1443.

Frolov, V.A., Cho, M.S., Bronk, P., Reese, T.S., Zimmerberg, J., 2000. Multiple local contact sites are induced by GPI-linked influenza hemagglutinin during hemifusion and flickering pore formation. Traffic 1, 622-630.

Fukuma, T., Higgins, M.J., Jarvis, S.P., 2007. Direct imaging of individual intrinsic hydration layers on lipid bilayers at angstrom resolution. Biophys J 92, 3603-3609.

Fuller, N., Rand, R.P., 2001. The influence of lysolipids on the spontaneous curvature and bending elasticity of phospholipid membranes. Biophys J 81, 243-254.

Fumagalli, G., Brigonzi, A., Tachikawa, T., Clementi, F., 1981. Rat myoblast fusion: morphological study of membrane apposition, fusion, and fission during controlled myogenesis in vitro. J Ultrastruct Res 75.

Garry, C.E., Garry, R.F., 2004. Proteomics computational analyses suggest that the carboxyl terminal glycoproteins of Bunyaviruses are class II viral fusion protein (beta-penetrenes). Theor Biol Med Model 1, 10.

Garry, C.E., Garry, R.F., 2009. Proteomics computational analyses suggest that the bornavirus glycoprotein is a class III viral fusion protein (gamma penetrene). Virol J 6, 145.

Gawrisch, K., Gaede, H.C., Mihailescu, M., White, S.H., 2007. Hydration of POPC bilayers studied by 1H-PFG-MAS-NOESY and neutron diffraction. Eur Biophys J 36, 281-291.

Germain, V., Perraki, A., Mongrand, S., 2012. Lipid rafts, eLS. John Wiley & Sons, Ltd, Chichester.

Gerst, J.E., 2003. SNARE regulators: matchmakers and matchbreakers. Biochim Biophys Acta 1641, 99-110.

Gibbons, D.L., Erk, I., Reilly, B., Navaza, J., Kielian, M., Rey, F.A., Lepault, J., 2003. Visualization of the target-membrane-inserted fusion protein of Semliki Forest virus by combined electron microscopy and crystallography. Cell 114, 573-583.

Gibbons, D.L., Vaney, M.C., Roussel, A., Vigouroux, A., Reilly, B., Lepault, J., Kielian, M., Rey, F.A., 2004. Conformational change and protein-protein interactions of the fusion protein of Semliki Forest virus. Nature 427, 320-325.

Giraudo, C.G., Hu, C., You, D.Q., Slovic, A.M., Mosharov, E.V., Sulzer, D., Melia, T.J., Rothman, J.E., 2005. SNAREs can promote complete fusion and hemifusion as alternative outcomes. J Cell Biol 170, 249-260.

Goldenberg, D.P., Bekeart, L.S., Laheru, D.A., Zhou, J.D., 1993. Probing the determinants of disulfide stability in native pancreatic trypsin inhibitor. Biochemistry 32, 2835-2844.

Goldenberg, D.P., Zhang, J.X., 1993. Small effects of amino acid replacements on the reduced and unfolded state of pancreatic trypsin inhibitor. Proteins 15, 322-329.

Gorman, J.J., Ferguson, B.L., Speelman, D., Mills, J., 1997. Determination of the disulfide bond arrangement of human respiratory syncytial virus attachment (G) protein by matrix-assisted laser desorption/ionization time-of-flight mass spectrometry. Protein Sci 6, 1308-1315.

Green, M., Sambrook, J., 2012. Molecular Cloning: A Laboratory Manual, 4 ed. Cold Spring Harbor Laboratory Press.

Groffen, A.J., Martens, S., Arazola, R.D., Cornelisse, L.N., Lozovaya, N., Jong, A.P.H.d., Goriounova, N.A., Habets, R.L.P., Takai, Y., Borst, J.G., Brose, N., McMahon, H.T., Verhage, M., 2010. Doc2b is a high-affinity Ca2+ sensor for spontaneous neurotransmitter release. Science 327, 1614-1618.

Gros, C., Linder, M., Wengler, G., Wengler, G., 1997. Analyses of disulfides present in the rubella virus E1 glycoprotein. Virology 230, 179-186.

Gunther-Ausborn, S., Schoen, P., Bartoldus, I., Wilschut, J., Stegmann, T., 2000. Role of hemagglutinin surface density in the initial stages of influenza virus fusion: lack of evidence for cooperativity. J Virol 74, 2714-2720.

Halpin, K., Young, P.L., Field, H.E., Mackenzie, J.S., 2000. Isolation of Hendra virus from pteropid bats: a natural reservoir of Hendra virus. J Gen Virol 81, 1927-1932.

Hamm, M., Kozlov, M., 1998. Tilt model of inverted amphiphilic mesophases. Eur Phys J B6, 519-528.

Hamm, M., Kozlov, M., 2000. Elastic energy of tilt and bending of fluid membranes. Eur Phys J E 3.

Han, X., Bushweller, J.H., Cafiso, D.S., Tamm, L.K., 2001. Membrane structure and fusion-triggering conformational change of the fusion domain from influenza hemagglutinin. Nat Struct Biol 8, 715-720.

Han, X., Sterling, H., Chen, Y., Saginario, C., Brown, E.J., Frazier, W.A., Lindberg, F.P., Vignery, A., 2000. CD47, a ligand for the macrophage fusion receptor, participates in macrophage multinucleation. J Biol Chem 275, 37984-37992.

Hannah, B.P., Cairns, T.M., Bender, F.C., Whitbeck, J.C., Lou, H., Eisenberg, R.J., Cohen, G.H., 2009. Herpes simplex virus glycoprotein B associates with target membranes via its fusion loops. J Virol 83, 6825-6836.

Hanson, P.I., Roth, R., Morisaki, H., Jahn, R., Heuser, J.E., 1997. Structure and conformational changes in NSF and its membrane receptor complexes visualized by quick-freeze/deep-etch electron microscopy. Cell 90, 523-535.

Haque, E., McIntosh, T.J., Lentz, B.R., 2001. Influence of lipid composition on physical properties and PEG-mediated fusion of curved and uncurved model membrane vesicles: “Nature’s own” fusogenic lipid bilayer. Biochem 40, 4340-4348.

Harrison, S.C., 2008. Viral membrane fusion. Nat Struct Mol Biol 15, 690-698.

Heerklotz, H., 2002. Triton promotes domain formation in lipid raft mixtures. Biophys J 83, 2693-2701.

Heerklotz, H., Szadkowska, H., Anderson, T., Seelig, J., 2003. The sensitivity of lipid domains to small perturbations demonstrated by the effect of Triton. J Mol Biol 329, 793-799.

Heinz, F.X., Allison, S.L., 2001. The machinery for flavivirus fusion with host cell membranes. Curr Opin Microbiol 4, 450-455.

Heinz, F.X., Stiasny, K., Puschner-Auer, G., Holzmann, H., Allison, S.L., Mandl, C.W., Kunz, C., 1994. Structural changes and functional control of the tick-borne encephalitis virus glycoprotein E by the heterodimeric association with protein prM. Virol 198, 109-117.

Heldwein, E.E., Lou, H., Bender, F.C., Cohen, G.H., Eisenberg, R.J., Harrison, S.C., 2006. Crystal structure of glycoprotein B from herpes simplex virus 1. Science 313, 217-220.

Hernandez, L.D., Hoffman, L.R., Wolfsberg, T.G., White, J.M., 1996. Virus-cell and cell-cell fusion. Annu Rev Cell Dev Biol 12, 627-661.

Higgins, M.J., Polcik, M., Fukuma, T., Sader, J.E., Nakayama, Y., Jarvis, S.P., 2006. Structured water layers adjacent to biological membranes. Biophys J 91, 2532-2542.

Howard, M.W., Travanty, E.A., Jeffers, S.A., Smith, M.K., Wennier, S.T., Thackray, L.B., Holmes, K.V., 2008. Aromatic amino acids in the juxtamembrane domain of severe acute respiratory syndrome coronavirus spike glycoprotein are important for receptor-dependent virus entry and cell-cell fusion. J Virol 82, 2883-2894.

Hristova, K., White, S.H., 1998. Determination of the hydrocarbon core structure of fluid DOPC bilayers by x-ray diffraction using specific bromination of the double-bonds: effect of hydration. Biophys J 74, 2419-2433.

Hu, A., Norrby, E., 1994. Role of individual cysteine residues in the processing and antigenicity of the measles virus haemagglutinin protein. J Gen Virol 75, 2173-2181.

Huang, Q., Opitz, R., Knapp, E.W., Herrmann, A., 2002. Protonation and stability of the globular domain of influenza virus hemagglutinin. Biophys J 82, 1050-1058.

Hui, E., Johnson, C.P., Yao, J., Dunning, F.M., Chapman, E.R., 2009. Synaptotagmin-mediated bending of the target membrane is a critical step in Ca(2+)-regulated fusion. Cell 138, 709-721.

Hung, C.H., Srivastava, M., Pollard, H.B., 1996. Membrane fusion protein synexin (annexin VII) as a Ca2+/GTP sensor in exocytotic secretion. Proc Natl Acad Sci USA 93, 10797-10802.

Huppertz, B., Borges, M., 2008. Placenta trophoblast fusion. Methods Mol Biol 475, 135-147.

Inoue, N., Ikawa, M., Isotani, A., Okabe, M., 2005. The immunoglobulin superfamily protein Izumo is required for sperm to fuse with eggs. Nature 434, 234-238.

Irie, K., Shimizu, K., Sakisaka, T., Ikeda, W., Takai, Y., 2004. Roles and modes of action of nectins in cell-cell adhesion. Semin Cell Dev Biol 15, 643-656.

Ito, H., Watanabe, S., Sanchez, A., Whitt, M.A., Kawaoka, Y., 1999. Mutational analysis of the putative fusion domain of Ebola virus glycoprotein. J Virol 73, 8907-8912.

Ivankin, A., Apellaniz, B., Gidalevitz, D., Nieva, J.L., 2012. Mechanism of membrane perturbation by the HIV-1 gp41 membrane-proximal external region and its modulation by cholesterol. Biochim Biophys Acta 1818, 2521-2528.

Jahn, R., Grubmuller, H., 2002. Membrane fusion. Curr Opin Cell Biol 14, 488-495.

Jahn, R., Lang, R., Sudhof, T.C., 2003a. Membrane fusion. Cell 112, 519-533.

Jahn, R., Lang, T., Sudhof, T.C., 2003b. Membrane fusion. Cell 112, 519-533.

Janes, R.W., Peapus, D.H., Wallace, B.A., 1994. The crystal structure of human endothelin. Nat Struct Biol 1, 311-319.

Jansen, I.D.C., Vermeer, J.A.F., Bloemen, V., Stap, J., Everts, V., 2012. Osteoclast fusion and fission. Calcif Tissue Int 90, 515-522.

Jeetendra, E., Ghosh, K., Odell, D., Li, J., Ghosh, H.P., Whitt, M.A., 2003. The membrane-proximal region of vesicular stomatitis virus glycoprotein G ectodomain is critical for fusion and virus infectivity. J Virol 77, 12807-12818.

Kadlec, J., Loureiro, S., Abrescia, N.G., Stuart, D.I., Jones, I.M., 2008. The postfusion structure of baculovirus gp64 supports a unified view of viral fusion machines. Nat Struct Mol Biol 15, 1024-1030.

Kaji, K., Oda, S., Shikano, T., Ohnuki, T., Uematsu, Y., Sakagami, J., Tada, N., Miyazaki, S., Kudo, A., 2000. The gamete fusion process is defective in eggs of Cd9-deficient mice. Nat Genet 24, 279-282.

Kanai, R., Kar, K., Anthony, K., Gould, L.H., Ledizet, M., Fikrig, E., Marasco, W.A., Koski, R.A., Modis, Y., 2006. Crystal structure of West Nile virus envelope glycoprotein reveals viral surface epitopes. J Virol 80, 11000-11008.

Kanaseki, T., Kawasaki, K., Murata, M., Ikeuchi, Y., Ohnishi, S., 1997. Structural features of membrane fusion between influenza virus and liposome as revealed by quick-freezing electron microscopy. J Cell Biol 137, 1041-1056.

Kasson, P.M., Lindahl, E., Pande, V.S., 2011. Water ordering at membrane interfaces controls fusion dynamics. JACS 133, 3812-3815.

Kasson, P.M., Pande, V.S., 2007. Control of membrane fusion mechanism by lipid composition: predictions from ensemble molecular dynamics. PLoS Comp Biol 3, 2228-2238.

Katsov, K., Muller, M., Schick, M., 2004. Field theoretic study of bilayer membrane fusion. I. Hemifusion mechanism. Biophys J 87, 3277-3290.

Kemble, G.W., Danieli, T., White, J.M., 1994. Lipid-anchored influenza hemagglutinin promotes hemifusion, not complete fusion. Cell 76, 383-391.

Kielian, M., 2006. Class II virus membrane fusion proteins. Virol 344, 38-47.

Kielian, M., Rey, F.A., 2006. Virus membrane-fusion proteins: more than one way to make a hairpin. Nat Rev Microbiol 4, 67-76.

Kielian, M.C., Helenius, A., 1984. Role of cholesterol in fusion of Semliki Forest virus with membranes. J Virol 52, 281–283.

Kinnunen, K.J., 1996. On the molecular-level mechanisms of peripheral protein-membrane interactions induced by lipids forming inverted non-lamellar phases. Chem Phys Lipids 81, 151-166.

Klimjack, M.R., Jeffrey, S., Kielian, M., 1994. Membrane and protein interactions of a soluble form of the Semliki Forest virus fusion protein. J Virol 68, 6940-6946.

Klymchenko, A.S., Melya, Y., Demchenko, A.P., Duportail, G., 2004. Simultaneous probing of hydration and polarity of lipid bilayers with 3-hydroxyflavone fluorescent dyes. BBA-Rev Biomembranes 1665, 6-19.

Knudsen, K.A., Smith, L., McElwee, S., 1989. Involvement of cell surface phosphatidylinositol-anchored glycoproteins in cell-cell adhesion of chick embryo myoblasts. J Cell Biol 109, 1779-1786.

Koch, A.W., Manzur, K.L., Shan., W., 2004. Structure-based models of cadherin-mediated cell adhesion: the evolution continues. Cell Mol Life Sci 61, 1884-1895.

Kontani, K., Rothman, J.H., 2005. Cell fusion: EFF is enough. Curr Biol 15, R252-254.

Kozlov, M.M., Chernomordik, L.V., 1998. A mechanism of protein-mediated fusion: coupling between refolding of the influenza hemagglutinin and lipid rearrangements. Biophys J 75, 1384-1396.

Kozlov, M.M., McMahon, H.T., Chernomordik, L.V., 2010. Protein-driven membrane stresses in fusion and fission. Trends Biochem Sci 35, 699-706.

Kozlovsky, Y., Kozlov, M.M., 2002. Stalk model of membrane fusion: solution of energy crisis. Biophys J 82, 882-895.

Krey, T., d'Alayer, J., Kikuti, C.M., Saulnier, A., Damier-Piolle, L., Petitpas, I., Johansson, D.X., Tawar, R.G., Baron, B., Robert, B., England, P., Persson, M.A., Martin, A., Rey, F.A., 2010. The disulfide bonds in glycoprotein E2 of hepatitis C virus reveal the tertiary organization of the molecule. PLoS Pathog 6, e1000762.

Kucerka, N., Perlmutter, J.D., Pan, J., Tristram-Nagle, S., Katsaras, J., Sachs, J.N., 2008. The effect of cholesterol on short-and long-chain monounsaturated lipid bilayers

as determined by molecular dynamics simulations and X-ray scattering. Biophys J 95, 2792-2805.

Kuhl, T., Guo, Y.Q., Alderfer, J.L., Berman, A.D., Leckband, D., Israelachvili, J., Hui, S.W., 1996. Direct measurement of polyethylene glycol induced depletion attraction between lipid bilayers. Langmuir 12, 3003-3014.

Kuzmin, P.I., Zimmerberg, J., Chizmadzhev, Y.A., Cohen, F.S., 2001a. A quantitative model for membrane fusion based on low-energy intermediates. Proc Natl Acad Sci USA 98, 7235-7240.

Kuzmin, P.I., Zimmerberg, J., Chizmadzhev, Y.A., Cohen, F.S., 2001b. A quantitative model for membrane fusion based on low-energy intermediates. Proc Natl Acad Sci USA 98, 7235-7240.

Lai, A.L., Moorthy, A.E., Li, Y., Tamm, L.K., 2012. Fusion activity of HIV gp41 fusion domain is related to its secondary structure and depth of membrane insertion in a cholesterol-dependent fashion. J Mol Biol 418, 3-15.

Lamb, R.A., Jardetzky, T.S., 2007. Structural basis of viral invasion: lessons from paramyxovirus F. Curr Opin Struct Biol 17, 427-436.

Lang, T., Bruns, D., Wenzel, D., Riedel, D., Holroyd, P., Thiele, C., Jahn, R., 2001. SNAREs are concentrated in cholesterol-dependent clusters that defne docking and fusion sites for exocytosis. EMBO J 20, 2202-2213.

Langedijk, J.P., Schaaper, W.M., Meloen, R.H., van Oirschot, J.T., 1996. Proposed three-dimensional model for the attachment protein G of respiratory syncytial virus. J Gen Virol 77, 1249-1257.

Lapthorn, A.J., Janes, R.W., Isaacs, N.W., Wallace, B.A., 1995. Cystine nooses and protein specificity. Nat Struct Biol 2, 266-268.

Latif, R., Ando, T., Davies, T.F., 2007. Lipid rafts are triage centers for multimeric and monomeric thyrotropin receptor regulation. Endocrinol 148, 3164-3175.

Lau, S.K.P., Li, K.S.M., Huang, Y., Shek, C.-T., Tse, H., Wang, M., Choi, G.K.Y., Xu, H., Lam, C.S.F., Guo, R., Chan, K.-H., Zheng, B.-J., Woo, P.C.Y., Yuen, K.-Y.,

2010. Ecoepidemiology and complete genome comparison of different strains of severe acute respiratory syndrome-related Rhinolophus bat coronavirus in China reveal bats as a reservoir for acute, self-limiting infection that allows recombination events. J Virol 84, 2808-2819.

Le Naour, F., Rubinstein, E., Jasmin, C., Prenant, M., Boucheix, C., 2000. Severely reduced female fertility in CD9-deficient mice. Science 287, 319-321.

Leckband, D., Sivasankar, S., 2000. Mechanism of homophilic cadherin adhesion. Curr Opin Cell Biol 12, 587-592.

Lee, J., Lentz, B.R., 1998. Secretory and viral fusion may share mechanistic events with fusion between curved lipid bilayers. Proc Natl Acad Sci USA 95, 9274-9279.

Lee, J.E., Fusco, M.L., Hessell, A.J., Oswald, W.B., Burton, D.R., Saphire, E.O., 2008. Structure of the Ebola virus glycoprotein bound to an antibody from a human survivor. Nature 454, 177-182.

Leikin, S., Parsegian, V.A., Rau, D.C., 1993. Hydration forces. Annu Rev Phys Chem 44, 369-395.

Leikina, E., Chernomordik, L.V., 2000. Reversible merger of membranes at the early stage of influenza hemagglutinin-mediated fusion. Mol Biol Cell 11, 2359-2371.

Leikina, E., Mittal, A., Cho, M.S., Melikov, K., Kozlov, M.M., Chernomordik, L.V., 2004. Influenza hemagglutinins outside of the contact zone are necessary for fusion pore expansion. J Biol Chem 279, 26526-26532.

Leland, M.M., Hubbard, G.B., III, H.T.S., Soike, K.F., Hilliard, J.K., 2000. Outbreak of Orthoreovirus-induced meningoencephalomyelitis in baboons. Comp Med 50, 199-205.

Lentz, B.R., 2007. PEG as a tool to gain insight into membrane fusion. Eur Biophys J 36, 315-326.

Lescar, J., Roussel, A., Wien, M.W., Navaza, J., Fuller, S.D., Wengler, G., Wengler, G., Rey, F.A., 2001. The fusion glycoprotein shell of Semliki Forest virus: an

icosahedral assembly primed for fusogenic activation at endosomal pH. Cell 105, 137-148.

Li, W., Shi, Z., Yu, M., Ren, W., Smith, C., Epstein, J.H., Wang, H., Crameri, G., Hu, Z., Zhang, H., Zhang, J., McEachern, J., Field, H., Daszak, P., Eaton, B.T., Zhang, S., Wang, L.-F., 2005. Bats are natural reservoirs of SARS-like Coronaviruses. Science 310, 676-679.

Li, Z., Blissard, G.W., 2009. The pre-transmembrane domain of the Autographa Californica Multicapsid Nucleopolyhedrovirus GP64 protein is critical for membrane fusion and virus infectivity. J Virol 83, 10993-11004.

Lichtenberg, D., Goni, F.M., Heerklotz, H., 2005. Detergent-resistant membranes should not be identified with membrane rafts. Trends Biochem Sci 30, 430-436.

Lindau, M., Almers, W., 1995. Structure and function of fusion pores in exocytosis and ectoplasmic membrane fusion. Curr Opin Cell Biol 7, 509-517.

Lindwasser, O.W., Resh, M.D., 2001. Multimerization of Human Immunodeficiency Virus Type 1 gag promotes its localization to barges, raft-like membrane microdomains. J Virol 75, 7913-7924.

Lingwood, D., Simons, K., 2010. Lipid rafts as a membrane-organizing principle. Science 327, 46-50.

London, E., 2005. How principles of domain formation in model membranes may explain ambiguities concerning lipid raft formation in cells. Biochim Biophys Acta 1746, 203-220.

London, E., Brown, D., 2000. Insolubility of lipids in triton X-100: physical origin and relationship to sphingolipid/cholesterol membrane domains (rafts). Biochim Biophys Acta 1508, 182-195.

Lorizate, M., Huarte, N., Sáez-Cirión, A., Nieva, J.L., 2008. Interfacial pre-transmembrane domains in viral proteins promoting membrane fusion and fission. Biochim Biophys Acta 1778, 1624-1639.

Loving, R., Li, K., Wallin, M., Sjoberg, M., Garoff, H., 2008. R-Peptide cleavage potentiates fusion-controlling isomerization of the intersubunit disulfide in Moloney murine leukemia virus Env. J Virol 82, 2594-2597.

Lu, X., Silver, J., 2000. Ecotropic murine leukemia virus receptor is physically associated with caveolin and membrane rafts. Virol 276.

Lu, X., Xiong, Y., Silver, J., 2002. Asymmetric requirement for cholesterol in receptor-bearing but not envelope-bearing membranes for fusion mediated by ecotropic murine leukemia virus. J Virol 76, 6701–6709.

Madhusoodanan, M., Lazaridis, T., 2003. Investigation of pathways for the low-pH conformational transition in influenza hemagglutinin. Biophys J 84, 1926-1939.

Malinin, V.S., Lentz, B.R., 2002. Pyrene cholesterol reports the transient appearance of nonlamellar intermediate structures during fusion of model membranes. Biochem 41, 5913-5919.

Malinin, V.S., Lentz, B.R., 2004. Energetics of vesicle fusion intermediates: comparison of calculations with observed effects of osmotic and curvature stresses. Biophys J 86, 2951-2964.

Markin, V., Albanesi, J., 2002. Membrane fusion: stalk model revisited. Biophys J 82, 693-712.

Markin, V.S., Kozlov, M.M., Borovjagin, V.L., 1984. On the theory of membrane fusion: the stalk mechanism. Gen Physiol Biophys 3.

Marra, J., ., Israelachvili, J., 1985. Direct measurements of forces between phosphatidylcholine and phosphatidylethanolamine bilayers in aqueous electrolyte solutions. Biochem 24, 4608-4618.

Martens, S., Kozlov, M.M., McMahon, H.T., 2007. How synaptotagmin promotes membrane fusion. Science 316, 1205-1208.

Martens, S., McMahon, H.T., 2008. Mechanisms of membrane fusion: disparate players and common principles. Nat Rev Mol Cell Biol 9, 543-556.

Martin, I., Ruysschaert, J.-M., Epand, R.M., 1999. Role of the N-terminal peptides of viral envelope proteins in membrane fusion. Adv Drug Del Rev 38, 233–255.

Martin, I., Ruysschaert, J.M., 2000. Common properties of fusion peptides from diverse systems. Biosci Rep 20, 483-500.

Mashl, R.J., Scott, H.L., Subramaniam, S., Jakobsson, E., 2001. Molecular simulation of dioleoylphosphatidylcholine lipid bilayers at differing levels of hydration. Biophys J 81, 3005-3015.

McIntosh, T.J., Magid, A.D., Simon, S.A., 1989. Cholesterol modifies the short-range repulsive interactions between phosphatidylcholine membranes. Biochem 28, 17-25.

McMahon, H.T., Gallop, J.L., 2005. Membrane curvature and mechanisms of dynamic cell membrane remodelling. Nature 438, 590-596.

McMahon, H.T., Kozlov, M.M., Martens, S., 2010. Membrane curvature in synaptic vesicle fusion and beyond. Cell 140, 601-605.

McNew, J.A., Weber, T., Parlati, F., Johnston, R.J., Melia, T.J., Sollner, T.H., Rothman, J.E., 2000. Close is not enough: SNARE-dependent membrane fusion requires an active mechanism that transduces force to membrane anchors. J Cell Biol 150, 105-117.

Meer, G.v., Voelker, D.R., Feigenson, G.W., 2008. Membrane lipids: where they are and how they behave. Nat Rev Mol Cell Biol 9, 112-124.

Melikyan, G.B., 2008. Common principles and intermediates of viral protein-mediated fusion: the HIV-1 paradigm. Retrovirol 5, 111.

Melikyan, G.B., White, J.M., Cohen, F.S., 1995. GPI-anchored influenza hemagglutinin induces hemifusion to both red blood cell and planar bilayer membranes. J Cell Biol 131, 679-691.

Melkonian, K.A., Ostermeyer, A.G., Chen, J.Z., Roth, M.G., Brown, D.A., 1999. Role of lipid modifications in targeting proteins to detergent-resistant membrane rafts.

Many raft proteins are acylated, while few are prenylated. J Biol Chem 274, 3910-3917.

Merten, C.A., Stitz, J., Braun, G., Poeschla, E.M., Cichutek, K., Buchholz, C.J., 2005. Directed evolution of retrovirus envelope protein cytoplasmic tails guided by functional incorporation into lentivirus particles. J Virol 79, 834-840.

Mineo, C., James, G.L., Smart, E.J., Anderson, R.G., 1996. Localization of epidermal growth factor-stimulated Ras/Raf-1 interaction to caveolae membrane. J Biol Chem 271, 11930-11935.

Mittal, J., Hummer, G., 2008. Static and dynamic correlations in water at hydrophobic interfaces. Proc Natl Acad Sci USA 105, 20130-20135.

Miyado, K., Yamada, G., Yamada, S., Hasuwa, H., Nakamura, Y., Ryu, F., Suzuki, K., Kosai, K., Inoue, K., Ogura, A., Okabe, M., Mekada, E., 2000. Requirement of CD9 on the egg plasma membrane for fertilization. Science 287, 321- 324.

Modis, Y., Ogata, S., Clements, D., Harrison, S.C., 2003. A ligand-binding pocket in the dengue virus envelope glycoprotein. Proc Natl Acad Sci USA 100, 6986-6991.

Mohd Jaafar, F., Goodwin, A.E., Belhouchet, M., Merry, G., Fang, Q., Cantaloube, J.F., Biagini, P., de Micco, P., Mertens, P.P., Attoui, H., 2008. Complete characterisation of the American grass carp reovirus genome (genus Aquareovirus: family Reoviridae) reveals an evolutionary link between aquareoviruses and coltiviruses. Virol 373, 310-321.

Mohler, W.A., Shemer, G., del Campo, J.J., Valansi, C., Opoku-Serebuoh, E., Scranton, V., Assaf, N., White, J.G., Podbilewicz, B., 2002. The type I membrane protein EFF-1 is essential for developmental cell fusion. Dev Cell 2, 355-362.

Morse, S.M., 1991. Emerging viruses: defining the rules for viral traffic. Perspect Biol Med 34, 387-409.

Morse, S.M., 1995. Factors in the emergence of infectious disease. Emerg Infect Dis 1, 7-15.

Mukai, A., Hashimoto, N., 2008. Localized cyclic AMP-dependent protein kinase activity is required for myogenic cell fusion. Exp Cell Res 314, 387-397.

Mukai, A., Kurisaki, T., Sato, S.B., Kobayashi, T., Kondoh, G., Hashimoto, N., 2009. Dynamic clustering and dispersion of lipid rafts contribute to fusion competence of myogenic cells. Exp Cell Res 315, 3052-3063.

Mukherjee, S., Zha, X., Tabas, I., Maxfield, F.R., 1998. Cholesterol distribution in living cells: fluorescence imaging using dehydroergosterol as a fluorescent cholesterol analog. Biophys J 75, 1915-1925.

Muller, P., Herrmann, A., 2002. Rapid transbilayer movement of spin-labeled steroids in hman erythrocytes and in liposomes. Biophys J 82, 1418-1428.

Nayak, D.P., Hui, E.K., Barman, S., 2004. Assembly and budding of influenza virus. Virus Res 106, 147-165.

Neumann, S., Langosch, D., 2011. Conserved conformational dynamics of membrane fusion protein transmembrane domains and flanking regions indicated by sequence statistics. Proteins 79, 2418-2427.

Ni, Y., Kemp., M.C., 1995. A comparative study of avian reovirus pathogenicity: virus spread and replication and induction of lesions. Avian Dis 39, 554-566.

Nibert, M., Duncan, R., 2013. Bioinformatics of recent aqua- and orthoreovirus isolates from fish: evolutionary gain or loss of FAST and fiber proteins and taxonomic implications. PLOS ONE 8, e68607.

Niyogi, K., Hildreth, J.E., 2001. Characterization of new syncytium-inhibiting monoclonal antibodies implicates lipid rafts in human T-cell leukemia virus type 1 syncytium formation. J Virol 75.

Noguchi, H., Takasu, M., 2001. Fusion pathways of vesicles: a Brownian dynamics simulation. J Chem Phys 115.

Nowak, T., Wengler, G., 1987. Analysis of disulfides present in the membrane proteins of the West Nile flavivirus. Virology 156, 127-137.

Nusrat, A., Parkos, C.A., Verkade, P., Foley, C.S., Liang, T.W., Innis-Whitehouse, W., Eastburn, K.K., Madara, J.L., 2000. Tight junctions are membrane microdomains. J Cell Sci 113, 1771-1781.

Nussler, F., Clague, M.J., Herrmann, A., 1997. Meta-stability of the hemifusion intermediate induced by glycosyl-phosphatidylinositol-anchored influenza hemagglutinin. Biophys J 73.

Nybakken, G.E., Nelson, C.A., Chen, B.R., Diamond, M.S., Fremont, D.H., 2006. Crystal structure of the West Nile virus envelope glycoprotein. J Virol 80, 11467-11474.

O'Connor, V., Lee, A.G., 2002. Synaptic vesicle fusion and synaptotagmin: 2B or not 2B. Nat Nurosci 5, 823-824.

Odell, D., Wanas, E., Yan, J., Ghosh, H.P., 1997. Influence of membrane anchoring and cytoplasmic domains on the fusogenic activity of vesicular stomatitis virus glycoprotein G. J Virol 71, 7996-8000.

Ohvo-Rekila, H., Ramstedt, B., Leppimaki, P., Slotte, J.P., 2002. Cholesterol interactions with phospholipids in membranes. Prog lipid Res 41, 66-97.

Ono, A., Waheed, A.A., Freed, E.O., 2007. Depletion of cellular cholesterol inhibits membrane binding and higher-order multimerization of human immunodeficiency virus type 1 Gag. Virol 360, 27-35.

Ouattara, L.A., Barin, F., Barthez, M.A., Bonnaud, B., Roingeard, P., Goudeau, A., Castelnau, P., Vernet, G., Paranhos-baccalà, G., Komurian-pradel, F., 2011. Novel human Reovirus isolated from children with acute necrotizing encephalopathy. Emerg Infect Dis 17, 1436-1444.

Owens, R.J., Burke, C., Rose, J.K., 1994. Mutations in the membrane-spanning domain of the human immunodeficiency virus envelope glycoprotein that affect fusion activity. J Virol 68, 570-574.

Pabst, G., Lonez, C., Vandenbranden, M., Jestin, J., Radulescu, A., Ruysschaert, J.-M., Gutberlet, T., 2012. Stalk-free membrane fusion of cationic lipids via an interdigitated phase. Soft Matter 8, 7243-7249.

Pager, C.T., Dutch, R.E., 2005. Cathepsin L is involved in proteolytic processing of the Hendra virus fusion protein. J Virol 79, 12714-12720.

Pager, C.T., W., C.W., Patch, J., Dutch, R.E., 2006. A mature and fusogenic form of the Nipah virus fusion protein requires proteolytic processing by cathepsin L. Virol 346, 251-257.

Panchal, R.G., Ruthel, G., Kenny, T.A., Kallstrom, G.H., Lane, D., Badie, S.S., Li, L., Bavari, S., Aman, M.J., 2003. In vivo oligomerization and raft localization of Ebola virus protein VP40 during vesicular budding. Proc Natl Acad Sci USA 100, 15936-15941.

Pang, Z.P., Melicoff, E., Padgett, D., Liu, Y., Teich, A.F., Dickey, B.F., Lin, W., Adachi, R., Südhof, T.C., 2006. Synaptotagmin-2 is essential for survival and contributes to Ca2+ triggering of neurotransmitter release in central and neuromuscular synapses. J Neurosci 26, 13493-13504.

Papahadjopoulos, D., Hui, S., Vail, W.J., Poste, G., 1976a. Studies on membrane fusion. I. Interactions of pure phospholipid membranes and the effect of myristic acid, lysolecithin, proteins and dimethylsulfoxide. Biochim Biophys Acta 448, 254-264.

Papahadjopoulos, D., Vail, W.J., Newton, C., Nir, S., Jacolson, K., Poste, G., Lato, R., 1976b. Studies on membrane fusion. III. The role of Ca-induced phase changes. Biochim Biophys Acta 465, 579-598.

Patterson, G.H., Piston, D.W., Barisas, B.G., 2000. Forster distances between green fluorescent protein pairs. Anal Biochem 284, 438-440.

Pecheur, E.I., Sainte-Marie, J., Bienvenue, A., Hoekstra, D., 1999 Peptides and membrane fusion: towards an understanding of the molecular mechanisms of protein-induced fusion. J Membr Biol 167, 1–17.

Perez-Amodio, S., Beertsen, W., Everts, V., 2009. (Pre-)osteoclasts induce retraction of osteoblasts before their fusion to osteoclasts. J Bone Miner Res 19, 1722-1731.

Pidoux, G., Gerbaud, P., Cocquebert, M., Segond, N., Badet, J., Fournier, T., Guibourdenche, J., Evain-Brion, D., 2012. Human trophoblast fusion and differentiation: Lessons from trisomy 21 placenta. Placenta 33, S81-S86.

Pike, L.J., 2006. Rafts defined: a report on the Keystone Symposium on Lipid Rafts and Cell Function. J Lipid Res 47, 1597-1598.

Pike, L.J., 2009. The challenge of lipid rafts. J Lipid Res 50, S323-S328.

Pike, L.J., Han, X., Chung, K.N., Gross, R.W., 2002. Lipid rafts are enriched in arachidonic acid and plasmenylethanolamine and their composition is independent of caveolin-1 expression: a quantitative electrospray ionization/mass spectrometric analysis. Biochem 41, 2075-2088.

Podbilewicz, B., Leikina, E., Sapir, A., Valansi, C., Suissa, M., Shemer, G., Chernomordik, L.V., 2006. The C. elegans developmental fusogen EFF-1 mediates homotypic fusion in heterologous cells and in vivo. Dev Cell 11, 471-481.

Poschner, B.C., Fischer, K., Herrmann, J.R., Hofmann, M.W., Langosch, D., 2010. Structural features of fusogenic model transmembrane domains that differentially regulate inner and outer leaflet mixing in membrane fusion. Mol Membr Biol 27, 1-10.

Pötgens, A.J.G., Drewlo, S., Kokozidou, M., Kaufmann, P., 2004. Syncytin: the major regulator of trophoblast fusion? Recent developments and hypotheses on its action. Hum Reprod Update 10, 487-496.

Predescu, S.A., Predescu, D.N., Shimizu, K., Klein, I.K., Malik, A.B., 2005. Cholesterol-dependent Syntaxin-4 and SNAP-23 clustering regulates caveolar fusion with the endothelial plasma membrane. J Biol Chem 280, 37130-37138.

Prives, J., Shinitzky, M., 1977. Increased membrane fluidity precedes fusion of muscle cells. Nature 268, 761-763.

Qiao, H., Armstrong, R.T., Melikyan, G.B., Cohen, F.S., White, J.M., 1999. A specific point mutant at position 1 of the influenza hemagglutinin fusion peptide displays a hemifusion phenotype. Mol Biol Cell 10, 2759-2769.

Racine, T., Hurst, T., Barry, C., Shou, J., Kibenge, F., Duncan, R., 2009. Aquareovirus effects syncytiogenesis by using a novel member of the FAST protein family translated from a noncanonical translation start site. J Virol 83, 5951-5955.

Rand, R.P., Parsegian, V.A., 1989. Hydration forces between phospholipids bilayers. Biochim Biophys Acta 988, 351-376.

Rawat, S.S., Viard, M., Gallo, S.A., Rein, A., Blumenthal, R., Puri, A., 2003. Modulation of entry of enveloped viruses by cholesterol and sphingolipids. Mol Membr Biol 20, 243-254.

Reuven, E.M., Dadon, Y., Viard, M., Manukovsky, N., Blumenthal, R., Shaia, Y., 2012. HIV-1 gp41 transmembrane domain interacts with the fusion peptide: implication in lipid mixing and inhibition of virus-cell fusion. Biochem 51, 2867-2878.

Rey, F.A., Heinz, F.X., Mandl, C., Kunz, C., Harrison, S.C., 1995a. The envelope glycoprotein from tick-borne encephalitis virus at 2 A resolution. Nature 375, 291-298.

Rey, F.A., Heinz, F.X., Mandl, C., Kunz, C., Harrison, S.C., 1995b. The envelope glycoprotein from tick-borne encephalitis virus at 2 A resolution. Nature 375, 291-298.

Risselada, H.J., Marrink, S.J., 2009. Curvature effects on lipid packing and dynamics in liposomes revealed by coarse grained molecular dynamics simulations. Phys Chem Chem Phys 11, 2056-2067.

Roche, S., Bressanelli, S., Rey, F.A., Gaudin, Y., 2006. Crystal structure of the low-pH form of the vesicular stomatitis virus glycoprotein G. Science 313.

Roche, S., Rey, F.A., Gaudin, Y., Bressanelli, S., 2007. Structure of the prefusion form of the vesicular stomatitis virus glycoprotein G. Science 315, 843-848.

Rothman, J.E., 1994. Mechanisms of intracellular protein transport. Nature 372, 55-63.

Ruebner, M., Strissel, P.L., Ekici, A.B., Stiegler, E., Dammer, U., Goecke, T.W., Faschingbauer, F., Fahlbusch, F.B., Beckmann, M.W., Strick, R., 2013. Reduced

Syncytin-1 Expression Levels in Placental Syndromes Correlates with Epigenetic Hypermethylation of the ERVW-1 Promoter Region. PLOS ONE 8, e56145.

Russell, C.J., Jardetzky, T.S., Lamb, R.A., 2001. Membrane fusion machines of paramyxoviruses: capture of intermediates of fusion. EMBO J 20, 4024-4034.

Sackett, K., Nethercott, M.J., Epand, R.F., Epand, R.M., Kindra, D.R., Shai, Y., Weliky, D.P., 2010. Comparative analysis of membrane-associated fusion peptide secondary structure and lipid mixing function of HIV gp41 constructs that model the early pre-hairpin intermediate and final hairpin conformations. J Mol Biol 397, 301-315.

Saez-Cirion, A., Gomara, M.J., Agirre, A., Nieva, J.L., 2003. Pre-transmembrane sequence of Ebola glycoprotein. Interfacial hydrophobicity distribution and interaction with membranes. FEBS Lett 533, 47-53.

Saez-Cirion, A., Nir, S., Lorizate, M., Agirre, A., Cruz, A., Perez-Gil, J., Nieva, J.L., 2002. Sphingomyelin and cholesterol promote HIV-1 gp41 pretransmembrane sequence surface aggregation and membrane restructuring. J Biol Chem 277, 21776-21785.

Saginario, C., Sterling, H., Beckers, C., Kobayashi, R., Solimena, M., Ullu, E., Vignery, A., 1998. MFR, a putative receptor mediating the fusion of macrophages. Mol Cell Biol 18, 6213-6223.

Sakai, T., Ohuchi, R., Ohuchi, M., 2002. Fatty acids on the A/USSR/77 influenza virus hemagglutinin facilitate the transition from hemifusion to fusion pore formation. J Virol 76, 4603-4611.

Sal-Man, N., Gerber, D., Bloch, I., Y. Shai, 2007. Specificity in transmembrane helix–helix interactions mediated by aromatic residues. J Biol Chem 282, 19753-19761.

Salsman, J., Top, D., Barry, C., Duncan, R., 2008a. A virus-encoded cell-cell fusion machine dependent on surrogate adhesins. PLoS Pathog 4, e1000016.

Salsman, J., Top, D., Barry, C., Duncan, R., 2008b. A virus-encoded cell-cell fusion machine dependent on surrogate adhesins. PLoS Pathog 4, e1000016.

Salsman, J., Top, D., Boutilier, J., Duncan, R., 2005. Extensive syncytium formation mediated by the Reovirus FAST proteins triggers apoptosis-induced membrane instability J Virol 79, 8090-8100.

Salzwedel, K., West, J.T., Hunter, E., 1999. A conserved tryptophan-rich motif in the membrane-proximal region of the human immunodeficiency virus type 1 gp41 ectodomain is important for Env-mediated fusion and virus infectivity. J Virol 73, 2469-2480.

Sanchez-San Martin, C., Liu, C.Y., Kielian, M., 2009. Dealing with low pH: entry and exit of alphaviruses and flaviviruses. Trend Microbiol 17, 514-521.

Sapir, A., Avinoam, O., Podbilewicz, B., Chernomordik, L.V., 2008. Viral and developmental cell fusion mechanisms: conservation and divergence. Dev Cell 14, 11-21.

Satcher, D., 1995. Emerging infections: getting ahead of the curve. Emerg Infect Dis 1, 1-6.

Scheiffele, P., G.Roth, M., Simons, K., 1997. Interaction of influenza virus haemagglutinin with sphingolipid–cholesterol membrane domains via its transmembrane domain. EMBO J 16, 5501-5508.

Schibli, D.J., Montelaro, R.C., Vogel, H.J., 2001. The membrane-proximal tryptophan-rich region of the HIV glycoprotein, gp41, forms a well-defined helix in dodecylphosphocholine micelles. Biochem 40, 9570-9578.

Schriff, L., Nibert, M., Tyler, K., 2007. Orthoreoviruses and their replication, in: Knipe, D., Griffin, D., Lamb, R., Straus, S., Howley, P., Martin, M., Roizman, B. (Eds.), Fields Virology. Lippincott Williams & Wilkins, Philadelphia, pp. 1853–1915.

Schroeder, R., London, E., Brown, D., 1994. Interactions between saturated acyl chains confer detergent resistance on lipids and glycosylphosphatidylinositol (GPI)-anchored proteins: GPI-anchored proteins in liposomes and cells show similar behavior. Proc Natl Acad Sci USA 91, 12130-12134.

Sekar, R.B., Periasamy, A., 2003. Fluorescence resonance energy transfer (FRET) microscopy imaging of live cell protein localizations. J Cell Biol 160, 629-633.

Sen, A., Hui, S.W., 1988. Direct measurement of headgroup hydration of polar lipids in inverted micelles. Chem Phys Lipids 49, 179-184.

Sevier, C.S., Kaiser, C.A., 2006. Conservation and diversity of the cellular disulfide bond formation pathways. Antioxid Redox Sign 8, 797-811.

Shang, L., Yue, L., Hunter, E., 2008. Role of the membrane-spanning domain of human immunodeficiency virus type 1 envelope glycoprotein in cell-cell fusion and virus infection. J Virol 82, 5417-5428.

Shemer, G., Podbilewicz, B., 2002. LIN-39/Hox triggers cell division and represses EFF-1/Fusogen-dependent vulval cell fusion. Genes Dev 16, 3136-3141.

Shemer, G., Suissa, M., Kolotuev, I., Nguyen, K.C., Hall, D.H., Podbilewicz, B., 2004. EFF-1 is sufficient to initiate and execute tissue- specific cell fusion in C. elegans. Curr Biol 14, 1587-1591.

Shillcock, J.C., Lipowsky, R., 2005. Tension-induced fusion of bilayer membranes and vesicles. Nat Mater 4, 225-228.

Shmulevitz, M., and R. Duncan, 2000. A new class of fusion-associated small transmembrane (FAST) proteins encoded by the non-enveloped fusogenic reoviruses. EMBO J 19, 902-912.

Shmulevitz, M., Corcoran, J., Salsman, J., Duncan, R., 2004a. Cell-cell fusion induced by the Avian Reovirus membrane fusion protein is regulated by protein degradation. J Virol 78, 5996-6004.

Shmulevitz, M., Epand, R.F., Epand, R.M., Duncan, R., 2004b. Structural and functional properties of an unusual internal fusion peptide in a nonenveloped virus membrane fusion protein. J Virol 78, 2808-2818.

Shmulevitz, M., Salsman, J., Duncan, R., 2003. Palmitoylation, membrane-proximal basic residues, and transmembrane glycine residues in the Reovirus p10 protein are essential for syncytium formation. J Virol 77, 9769-9779.

Siegel, D.P., 1993. Energetics of intermediates in membrane fusion: comparison of stalk and inverted micellar intermediate mechanisms. Biophys J 65, 2124-2140.

Siegel, D.P., Epand, R.M., 1997. The mechanism of lamellar-to-inverted hexagonal phase transitions in phosphatidylethanolamine: implications for membrane fusion mechanisms. Biophys J 73, 3089-3111.

Siegel, D.P., Epand, R.M., 2000. Effect of influenza hemagglutinin fusion peptide on lamellar/inverted phase transitions in dipalmitoleoylphosphatidylethanolamine: implications for membrane fusion mechanisms. Biochim Biophys Acta 1468, 87-98.

Simon, S.A., McIntosh, T.J., 1989. Magnitude of the solvation pressure depends on dipole potential. Proc Natl Acad Sci USA 86, 9263-9267.

Singer, S.J., Nicolson, G.L., 1972. The fluid mosaic model of the structure of cell membranes. Science 175, 720-731.

Sjoberg, M., Garoff, H., 2003. Interactions between the transmembrane segments of the alphavirus E1 and E2 proteins play a role in virus budding and fusion. J Virol 77, 3441-3450.

Skehel, J.J., Bayley, P.M., Brown, E.B., Martin, S.R., Waterfield, M.D., White, J.M., Wilson, I.A., Wiley, D.C., 1982a. Changes in the conformation of influenza virus hemagglutinin at the pH optimum of virus-mediated membrane fusion. Proc Natl Acad Sci USA 79, 968-972.

Skehel, J.J., Bayley, P.M., Brown, E.B., Martin, S.R., Waterfield, M.D., White, J.M., Wilson, I.A., Wiley., D.C., 1982b. Changes in the conformation of influenza virus hemagglutinin at the pH optimum of virus-mediated membrane fusion. Proc Natl Acad Sci USA 79, 968-972.

Skehel, J.J., Cross, K., Steinhauer, D., Wiley, D.C., 2001. Influenzafusion peptides. Biochem. Soc. Trans. 29, 623-626.

Skehel, J.J., Wiley, D.C., 2000. Receptor binding and membrane fusion in virus entry: the influenza hemagglutinin. Annu Rev Biochem 69, 531-569.

Smith, E.C., Culler, M.R., Hellman, L.M., Fried, M.G., Creamer, T.P., Dutch, R.E., 2012a. Beyond anchoring: the expanding role of the hendra virus fusion protein

transmembrane domain in protein folding, stability, and function. J Virol 86, 3003-3013.

Smith, E.C., Gregory, S.M., Tamm, L.K., Creamer, T.P., Dutch, R.E., 2012b. Role of sequence and structure of the Hendra fusion protein fusion peptide in membrane fusion. J Biol Chem 287, 30035-30048.

Sollner, T.H., 2004. Intracellular and viral membrane fusion: a uniting mechanism. Curr Opin Cell Biol 16, 429-435.

Sollner, T.H., Bennett, M.K., Whiteheart, S.W., Scheller, R.H., Rothman, J.E., 1993. A protein assembly-disassembly pathway in vitro that may correspond to sequential steps of synaptic vesicle docking, activation, and fusion. Cell 75, 409-418.

Stadler, K., Allison, S.L., Schalich, J., Heinz, F.X., 1997. Proteolytic activation of tick-borne encephalitis virus by furin. J Virol 71, 8475-8481.

Steck, T.L., Ye, J., Lange, Y., 2002. Probing red cell membrane cholesterol movement with cyclodextrin. Biophys J 83, 2118-2125.

Stein, A., Weber, G., Wahl, M.C., Jahn, R., 2009. Helical extension of the neuronal SNARE complex into the membrane. Nature 460, 525-528.

Stein, K.K., Primakoff, P., Myles, D., 2004. Sperm-egg fusion: events at the plasma membrane. J Cell Sci 117, 6269-6274.

Steinbauer, B., Mehnert, T., Beyer, K., 2003. Hydration and lateral organization in phospholipid bilayers containing sphingomyelin: A 2H-NMR study. Biophys J 85, 1013-1024.

Steinhauer, D.A., Wharton, S.A., Skehel, J.J., Wiley, D.C., 1995. Studies of the membrane fusion activities of fusion peptide mutants of influenza virus hemagglutinin. J Virol 69, 6643-6651.

Stiasny, K., Allison, S.L., Mandl, C.W., Heinz, F.X., 2001. Role of metastability and acidic pH in membrane fusion by tick-borne encephalitis virus. J Virol 75, 7392-7398.

Stiasny, K., Allison, S.L., Marchler-Bauer, A., Kunz, C., Heinz, F.X., 1996. Structural requirements for low-pH-induced rearrangements in the envelope glycoprotein of tick-borne encephalitis virus. J Virol 70, 8142-8147.

Stieneke-Grober, A., Vey, M., Angliker, H., Shaw, E., Thomas, G., Roberts, C., Klenk, H.D., Garten, W., 1992. Influenza virus hemagglutinin with multibasic cleavage site is activated by furin, a subtilisin-like endoprotease. EMBO J 11, 2407-2414.

Struck, D.K., Hoekstra, D., Pagano, R.E., 1981. Use of resonance energy transfer to monitor membrane fusion. Biochem 20, 4093-4099.

Suarez, T., Gallaher, W.R., Agirre, A., Goni, F.M., Nieva, J.L., 2000. Membrane interface-interacting sequences within the ectodomain of the human immunodeficiency virus type 1 envelope glycoprotein: putative role during viral fusion. J Virol 74, 8038-8047.

Supekar, V.M., Bruckmann, C., Ingallinella, P., Bianchi, E., Pessi, A., Carfi, A., 2004. Structure of a proteolytically resistant core from the severe acute respiratory syndrome coronavirus S2 fusion protein. Proc Natl Acad Sci USA 101, 17958-17963.

Sutton, R.B., Ernst, J.A., Brunger, A.T., 1999. Crystal structure of the cytosolic C2A-C2B domains of synaptotagmin III. Implications for Ca2+-independent SNARE complex interaction. J Cell Biol 147, 589-598.

Szule, J.A., Fuller, N.L., Rand, R.P., 2002. The effects of acyl chain length and saturation of diacylglycerols and phosphatidylcholines on membrane monolayer curvature. Biophys J 83, 977-984.

Takeda, M., Leser, G.P., Russell, C.J., Lamb, R.A., 2003. Influenza virus hemagglutinin concentrates in lipid raft microdomains for efficient viral fusion. Proc Natl Acad Sci USA 100, 14610-14617.

Talbot, P., Shur, B.D., Myles, D.G., 2003. Cell adhesion and fertilization: Steps in oocyte transport, sperm-zona pellucida interactions, and sperm-egg fusion. Biol Reprod 68, 1-9.

Tamm, L.K., Han, X., 2000. Viral fusion peptides: a tool set to disrupt and connect biological membranes. Biosci Rep 20, 501-518.

Tamm, L.K., Han, X., Li, Y., Lai, A.L., 2002. Structure and function of membrane fusion peptides. Biopolymers 66, 249–260.

Taylor, M.V., 2002. Muscle differentiation: how two cells become one. Curr Biol 12, R224-228.

Thalmann, C.M., Cummins, D.M., Yu, M., Lunt, R., Pritchard, L.I., Hansson, E., Crameri, S., Hyatt, A., Wang, L.-F., 2010. Broome virus, a new fusogenic Orthoreovirus species isolated from an Australian fruit bat. Virol 402, 26-40.

Tong, S., Yi, F., Martin, A., Yao, Q., Li, M., Compans, R.W., 2001. Three membrane-proximal amino acids in the Human Parainfluenza Type 2 (HPIV 2) F protein are critical for fusogenic activity. Virol 280, 52-61.

Top, D., de Antueno, R., Salsman, J., Corcoran, J., Mader, J., Hoskin, D., Touhami, A., Jericho, M.H., Duncan, R., 2005. Liposome reconstitution of a minimal protein-mediated membrane fusion machine. EMBO J 24, 2980-2988.

Top, D., Read, J., Dawe, S., Syvitski, R., Duncan, R., 2012. Cell-cell membrane fusion induced by the p15 FAST protein requires a novel fusion peptide motif containing a myristoylated polyproline type II helix. J Biol Chem 287, 3403-3414.

Tremblay, M.L., Banks, A.W., Rainey, J.K., 2010. The predictive accuracy of secondary chemical shifts is more affected by protein secondary structure than solvent environment. J Biomol NMR 46, 257-270.

Ungar, D., Hughson, F.M., 2003. SNARE protein structure and function. Annu Rev Cell Dev Biol 19, 493-517.

Ungermann, C., Lanosch, D., 2005. Functions of SNAREs in intracellular membrane fusion and lipid bilayer mixing. J Cell Sci 118, 3819-3828.

Vaidya, N.K., Huang, H., Takagi, S., 2007. Modelling HA protein-mediated interaction between an influenza virus and a healthy cell: pre-fusion membrane deformation. Math Med Biol 24, 251-270.

Veronese, F.D., DeVico, A.L., Copeland, T.D., Oroszlan, S., Gallo, R.C., Sarngadharan, M.G., 1985. Characterization of gp41 as the transmembrane protein coded by the HTLV-III/LAV envelope gene. Science 229, 1402-1405.

Vieler, E., Baumgartner, W., Herbst, W., Kohler, G., 1994. Characterization of a reovirus isolate from a rattle snake, Crotalus viridis, with neurological dysfunction. Arch Virol 138, 341-344.

Vignery, A., 2000. Osteoclasts and giant cells: macrophage-macrophage fusion mechanism. Int J Exp Pathol 81, 291-304.

Vignery, A., 2005. Macrophage fusion : the making of osteoclasts and giant cells. J Exp. Med. 202, 337-340.

Vishwanathan, S.A., Hunter, E., 2008. Importance of the membrane-perturbing properties of the membrane-proximal external region of human immunodeficiency virus type 1 gp41 to viral fusion. J Virol 82, 5118-5126.

Voet, D., Voet, J.G., 2004a. Amino Acids, in: Harris, D., Fitzgerald, P. (Eds.), Biochemistry, 3 ed. John Wiley & Sons, Hoboken, NJ, p. 67.

Voet, D., Voet, J.G., 2004b. Lipids and membranes, in: Harris, D., Fitzgerald, P. (Eds.), Biochemistry, 3 ed. John Wiley & Sons, Hoboken, NJ, pp. 386-388.

Volke, F., Eisenblatter, S., Galle, J., Klose, G., 1994. Dynamic properties of water at phosphatidylcholine lipid-bilayer surfaces as seen by deuterium and pulse field gradient proton NMR. Chem Phys Lipids 70, 121-131.

Volke, F., Pampel, A., 1995. Membrane hydration and structure on a subnanometer scale as seen by high resolution solid state nuclear magnetic resonance: POPC and POPC/C12EO4 model membranes. Biophys J 68, 1960-1965.

Wahlberg, J.M., Boere, W.A., Garoff, H., 1989. The heterodimeric association between the membrane proteins of Semliki Forest virus changes its sensitivity to low pH during virus maturation. J Virol 63, 4991-4997.

Wahlberg, J.M., Garoff, H., 1992. Membrane fusion process of Semliki Forest virus. I: Low pH-induced rearrangement in spike protein quaternary structure precedes virus penetration into cells. J Cell Biol 116, 339-348.

Wakelam, M.J., 1985. The fusion of myoblasts. Biochem J 228, 1-12.

Weber, T., Zemelman, B.V., McNew, J.A., Westermann, B., Gmachl, M., Parlati, F., Sollner, T.H., Rothman, J.E., 1998. SNAREpins: minimal machinery for membrane fusion. Cell 92, 759-772.

Weinstein, D.B., 1968. The lipid composition of the surface membrane of the L cell. Wistar Inst Symp Monogr 8, 17-21.

Weissenhorn, W., Carfi, A., Lee, K.H., Skehel, J.J., Wiley, D.C., 1998. Crystal structure of the Ebola virus membrane fusion subunit, GP2, from the envelope glycoprotein ectodomain. Mol Cell 2, 605-616.

Weissenhorn, W., Dessen, A., Harrison, S.C., Skehel, J.J., Wiley, D.C., 1997. Atomic structure of the ectodomain from HIV-1 gp41. Nature 387, 426-430.

Weissenhorn, W., Hinz, A., Gaudin, Y., 2007. Virus membrane fusion. FEBS Lett 581, 2150-2155.

West, J.T., Johnston, P.B., Dubay, S.R., Hunter, E., 2001. Mutations within the putative membrane-spanning domain of the simian immunodeficiency virus transmembrane glycoprotein define the minimal requirements for fusion, incorporation, and infectivity. J Virol 75, 9601-9612.

White, J.M., Delos, S.E., Brecher, M., Schornberg, K., 2008. Structures and mechanisms of viral membrane fusion proteins: multiple variations on a common theme. Crit Rev Biochem Mol Biol 43, 189-219.

White, J.M., J. Kartenbeck, Helenius., A., 1982. Membrane fusion activity of influenza virus. EMBO J 1, 217-222.

White, S.H., Ladokhin, A.S., Jayasinghe, S., Hristova, K., 2001. How membranes shape protein structure. J Biol Chem 276, 32395-32398.

Wiley, D.C., Skehel, J.J., 1987. The structure and function of the hemagglutinin membrane glycoprotein of influenza virus. Annu Rev Biochem 56, 365-394.

Wilschut, J., Duzgunes, N., Hoekstra, D., Papahadjopoulos, D., 1985. Modulation of membrane fusion by membrane fluidity: temperature dependence of divalent cation induced fusion of phosphatidylserine vesicles. Biochem 24, 8-14.

Wilson, I.A., Skehel, J.J., Wiley, D.C., 1981. Structure of the haemagglutinin membrane glycoprotein of influenza virus at 3 A resolution. Nature 289, 366-373.

Wishart, D.S., Sykes, B.D., Richards, F.M., 1992. The chemical shift index- a fast and simple method for the assignment of protein secondary structure through NMR-spectroscopy. Biochem 31, 1647-1651.

Wong, A.H., Cheng, P.K.C., Lai, M.Y.Y., Leung, P.C.K., Wong, K.K.Y., Lee, W.Y., Lim, W.W.L., 2012. Virulence potential of fusogenic orthoreoviruses. Emerg Infect Dis 18, 944-948.

Wong, S., Lau, S., Woo, P., Yuen, K.-Y., 2007. Bats as a continuing source of emerging infections in humans. Rev Med Virol 17, 67-91.

Wong, S.W., Kwon, M.J., Choi, A.M., Kim, H.P., Nakahira, K., Hwang, D.H., 2009. Fatty acids modulate Toll-like receptor 4 activation through regulation of receptor dimerization and recruitment into lipid rafts in a reactive oxygen species-dependent manner. J Biol Chem 284, 27384-27392.

Woolhouse, M.E.J., Gowtage-Sequeria, S., 2005. Host range and emerging and reemerging pathogens. Emerg Infect Dis 11, 1842-1847.

Woolhouse, M.E.J., Howey, R., Gaunt, E., Reilly, L., Chase-Topping, M., Savill, N., 2008. Temporal trends in the discovery of human viruses. Proc Biol Sci 275, 2111-2115.

Wu, H., Zheng, L., Lentz, B.R., 1996. A slight asymmetry in the transbilayer distribution of lysophosphatidylcholine alters the surface properties and poly(ethylene glycol)-mediated fusion of dipalmitoylphosphatidylcholine large unilamellar vesicles. Biochem 35, 12602-12611.

Xu, Y., Liu, Y., Lou, Z., Qin, L., Li, X., Bai, Z., Pang, H., Tien, P., Gao, G.F., Rao, Z., 2004. Structural basis for coronavirus-mediated membrane fusion: Crystal structure of mouse hepatitis virus spike protein fusion core. J Biol Chem 279, 30514-30522.

Yancey, P.G., Rodrigueza, W.V., Kilsdonk, E.P.C., Stoudt, G.W., Johnson, W.J., Phillips, M.C., Rothblat, G.H., 1996. Cellular cholesterol efflux mediated by cyclodextrins. J Biol Chem 271, 16026-16034.

Yang, Q.L., Guo, Y., Li, L., Hui, S.W., 1997. Effects of lipid headgroup and packing stress on poly(ethylene glycol)-induced phospholipid vesicle aggregation and fusion. Biophys J 73, 277-282.

Yin, H.S., Paterson, R.G., Wen, X., Lamb, R.A., Jardetzky, T.S., 2005. Structure of the uncleaved ectodomain of the paramyxovirus (hPIV3) fusion protein. Proc Natl Acad Sci USA 102, 9288-9293.

Yin, H.S., Wen, X., Paterson, R.G., Lamb, R.A., Jardetzky, T.S., 2006. Structure of the parainfluenza virus 5 F protein in its metastable, prefusion conformation. Nature 439, 38-44.

Zhang, R.M., Snyder, G.H., 1989. Dependence of formation of small disulfide loops in two-cysteine peptides on the number and types of intervening amino acids. J Biol Chem 264, 18472-18479.

Zhang, X., Fugere, M., Day, R., Kielian, M., 2003. Furin processing and proteolytic activation of Semliki Forest virus. J Virol 77, 2981-2989.

Zhu, B., Chappuis-Flament, S., Wong, E., Jensen, I.E., Gumbiner, B.M., Leckband, D., 2003. Functional analysis of the structural basis of homophilic cadherin adhesion. Biophys J 84, 4033-4042.

Zidovetzki, R., Levitan, I., 2007. Use of cyclodextrins to manipulate plasma membrane cholesterol content: evidence, misconceptions and control strategies. Biochim Biophys Acta 1768, 1311-1324.

Zimmerberg, J., Kozlov, M.M., 2006. How proteins produce cellular membrane curvature. Nat Rev Mol Cell Biol 7, 9-19.